

Assessment of Wind Turbines Generators Influence in Aeronautical Navigation Systems

Joana de Albuquerque Fernandes

Thesis to obtain the Master of Science Degree in
Electrical and Computer Engineering

Examination Committee

Chairperson: Prof. Fernando Duarte Nunes

Supervisor: Prof. Luís Manuel de Jesus Sousa Correia

Member of Committee: Prof. António Manuel Restani Graça Alves Moreira

Member of Committee: Eng. Carlos Alves

October 2013

To my parents and Alexandre

Acknowledgements

First of all, I want to thank Prof. Luís M. Correia, who gave me the opportunity to write this thesis. I will never forget his professionalism, discipline, patience and guidelines in our weekly meetings, so important to the development of the work, always sharing his knowledge about technical subjects and about his life experience.

My second dedication is to NAV Portugal, more specifically to Eng. Luís Pissarro, Eng. Márcio Teixeira, and Eng. Carlos Alves, whose contribution in regular feedback meetings to this work and clarification of my doubts were crucial for the development of this thesis.

I want to express my gratitude for being part of GROW, in which I learnt more about telecommunications with the other members and improved my presentation skills in the GROWing meetings. I also would like to thank Michal Mackowiak for the helpful comments on the preparation of the final version of my thesis.

A special thanks to Prof. Sofia Costa, for her availability for several hours of support and contribution for the improvement of my English and my work.

To my “office” colleagues and friends, especially to Dinis Rocha, Diogo X. Almeida and Ricardo Santos, sincere thanks for their friendship, support and help with my numerous doubts, and for the knowledge and experience sharing and the amusing moments. To all my other friends for the time spent outside the work environment and for the relaxing and amusing moments.

And last, but not least, my deep gratitude to my parents and my brother, for their unconditional support, encouragement and effort so I could get a good education, and for teaching me that with effort and dedication everything is possible. And, to the love of my life, Alexandre, for his love, care, friendship and support in the critical phases of this journey when I felt I was reaching a dead end. Thank you for being always by my side.

Abstract

The main objective of this Thesis was to study and quantify the influence of wind turbine generators on the omnidirectional range systems of very high frequency (VOR) installed in Portugal, as well as to define exclusion regions around the aforesaid systems. These goals were accomplished through the development and implementation of several models: tower and blades structures, determination of the losses introduced by obstacles, and definition of flight routes. In order to verify the influence caused by wind turbines, simulations were performed for the flight levels 55 and 450, and for several previously defined flight routes. In Nisa, where there is nearby in a wind farm at Serra da Amêndoa, the received power of the diffracted signal presents significant values compared to the receiver sensitivity, which may originate a carrier-to-interference ratio lower than the acceptable minimum. The minimum distance at which the nearest wind turbine should be installed is 10.3 km, in order to guarantee an acceptable carrier-to-interference ratio.

Keywords

VOR, Aircraft Navigation, Interference, Wind Turbines, Exclusion Regions.

Resumo

O principal objetivo desta tese foi o de estudar e quantificar a influência de turbinas eólicas nos vários sistemas de navegação omnidireccional em VHF (VOR) instalados por Portugal, e definir regiões de exclusão em torno dos referidos sistemas. Estes objetivos foram alcançados através do desenvolvimento e implementação de vários modelos: estrutura da torre e das pás das turbinas, determinação da atenuação de possíveis obstáculos, e definição de rotas de voo. A fim de verificar a interferência provocada pelas turbinas, as simulações foram realizadas para os níveis de voo 55 e 450, para várias rotas previamente definidas. Em Nisa, para o parque eólico da Serra da Amêndoa, a potência recebida do sinal difratado apresenta valores significativos em comparação com a sensibilidade do recetor, o que leva a uma relação portadora-interferência menor do que o mínimo aceitável. A distância mínima à qual a turbina mais próxima deve ser colocada do VOR é de 10.3 km, para garantir uma relação portadora-interferência aceitável.

Palavras-chave

VOR, Navegação Aérea, Interferência, Turbinas Eólicas, Regiões de Exclusão.

Table of Contents

Acknowledgements	v
Abstract.....	vii
Resumo	viii
Table of Contents.....	ix
List of Figures	xi
List of Tables.....	xiii
List of Acronyms	xiv
List of Symbols.....	xvi
List of Software	xix
1 Introduction	2
1.1 Overview.....	3
1.2 Motivation and Contents	5
2 Fundamental Aspects.....	8
2.1 Aeronautical Navigation Systems	9
2.1.1 Features of VOR.....	9
2.1.2 VOR's Operation Mode	11
2.1.3 Radio Interface	12
2.2 Wind Turbines Generators.....	14
2.2.1 Features of Wind Turbines	14
2.2.2 Wind Turbine's Operation Mode.....	16
2.3 Wind Turbines' Effects on VOR	17
2.3.1 Problem Definition	17
2.3.2 Interference Effects on VOR.....	19
2.4 State of The Art	21

3	Model Development and Implementation	24
3.1	Exclusion Regions Criteria.....	25
3.1.1	DVOR Interference Zone	25
3.1.2	Shadow Height and Flight Altitude Determination.....	27
3.1.3	Exclusion Regions Determination.....	30
3.2	Wind Turbines Modelling	32
3.2.1	Tower RCS Model	32
3.2.2	Blades Model	35
3.2.3	Power Calculation.....	36
3.3	Flight Routes	41
3.4	Implementation in a Simulator	42
3.5	Simulator Assessment.....	45
4	Results and Data Analysis.....	52
4.1	Scenarios Definition.....	53
4.1.1	Lisbon Region Scenario	56
4.1.2	Centre and Algarve Regions Scenarios	57
4.1.3	Autonomous Regions Scenarios	59
4.2	Simulator Results and Analysis	60
4.2.1	Lisbon Region Scenario	61
4.2.2	Centre and Algarve Regions Scenarios	64
4.2.3	Autonomous Regions Scenarios	67
4.3	Exclusion Regions Definition	68
5	Conclusions.....	72
Annex A.	Usage of Wind Generators in Portugal.....	78
Annex B.	Shadow Height and Flight Altitude Details	84
Annex C.	Exclusion Zones Details.....	88
Annex D.	Gain of the Transmitting Antenna.....	90
Annex E.	Diffraction Coefficient Details	94
Annex F.	Test Routes	98
References	102

List of Figures

Figure 1.1 - Size and power evolution of wind turbines over time (adapted from [GWGT13]).	4
Figure 1.2 - Installed capacity in Portugal (adapted from [Eoli13]).	5
Figure 2.1 - DVOR ground beacon (extracted from [WiCo12]).	10
Figure 2.2 - Polar diagram (extracted from [NAV12a]).	13
Figure 2.3 - Frequency spectrum of the DVOR (VOR) (extracted from [NAV12a]).	13
Figure 2.4 - Wind turbine's main sections (adapted from [WiEn12]).	15
Figure 2.5 - Axis orientation and rotor hub position (extracted from [Rene12]).	15
Figure 2.6 - Control mechanisms (extracted from [Rene12]).	16
Figure 2.7 - Wind turbine siting in a wind farm and its wake effect (adapted from [IWAG12]).	18
Figure 2.8 - Reflection/Scattered.	20
Figure 2.9 - Second Fresnel zone obstructed by wind turbine (adapted from [Rais12]).	20
Figure 2.10 - Shadow region (adapted from [Rais12]).	21
Figure 3.1 - Definition of BRA in side elevation view (adapted from [ICAO09]).	25
Figure 3.2 - Guidance process (adapted from [ICAO09]).	26
Figure 3.3 - Subtended angle by wind turbine.	27
Figure 3.4 - Shadow height cast by the wind turbine diagram (adapted from [Rais12]).	29
Figure 3.5 - Fresnel zone clearance diagram (extracted from [Rais12]).	30
Figure 3.6 - Earth dip's effect on distance between DVOR antenna and wind turbine (adapted from [Rais12]).	31
Figure 3.7 - Segmented tower geometry (extracted from [RaBr07a]).	33
Figure 3.8 - Bi-static RCS layout (adapted from [RaBr07b]).	34
Figure 3.9 - Blades scheme (adapted from [Elec13]).	36
Figure 3.10 - Scenario with water.	39
Figure 3.11 - General structure of the simulator.	44
Figure 3.12 - Scenario for the DVOR in Porto Santo.	45
Figure 3.13 - Terrain profile and Fresnel ellipsoid for the Porto Santo scenario.	46
Figure 3.14 - Received and interfering powers in the Porto Santo Island scenario.	46
Figure 3.15 - Carrier to Interference Ratio in the Porto Santo Island scenario.	47
Figure 3.16 - Scenario for the DVOR in Horta.	48
Figure 3.17 - Terrain profile and Fresnel ellipsoid for the Porto Santo scenario.	49
Figure 3.18 – Received and interfering powers in the Horta Island scenario.	49
Figure 3.19 - Carrier to Interference Ratio in the Horta Island scenario.	50
Figure 4.1 - DVOR and wind turbines location in Madeira Archipelago.	54
Figure 4.2 - CVOR or DVOR and wind turbines location in Azores Archipelago.	54
Figure 4.3 - DVOR and wind turbines location in mainland Portugal.	55
Figure 4.4 - Flight routes for the Lisbon scenario (adapted from [NAV12c]).	57
Figure 4.5 - Flight routes for Fátima scenario (adapted from [NAV12c]).	58
Figure 4.6 - Flight routes for Nisa scenario (adapted from [NAV12c]).	58
Figure 4.7 - Flight routes for Sagres scenario (adapted from [NAV12c]).	59
Figure 4.8 - Flight routes for Porto Santo scenario (adapted from [NAV12c]).	60
Figure 4.9 - Flight routes for Flores, Horta and Santa Maria scenarios (adapted from [NAV12c]).	60

Figure 4.10 - Variation of the diffraction coefficient for the rotation of the blades' rotor.	61
Figure 4.11 - Variation of the diffraction coefficient for the rotation of the blades.....	62
Figure 4.12 - Received and interfering powers for Lisbon scenario and Sobral wind farm.	63
Figure 4.13 - Carrier to Interference Ratio for Lisbon scenario and Sobral wind farm.	63
Figure 4.14 – Received and interfering powers for Nisa scenario and Serra da Amêndoa wind farm.....	65
Figure 4.15 - Carrier to Interference Ratio for Nisa scenario and Serra da Amêndoa wind farm.....	66
Figure B.1 - Generic oblique triangle (extracted from [Math13]).	85
Figure D.1 - Horizontal pattern of a DVOR loop antenna.....	91
Figure D.2 - Vertical pattern of a DVOR loop antenna.	92

List of Tables

Table 2.1 - Navigation aid classifications (extracted from [ToWy07]).	11
Table 3.1 - BRA parameter values (adapted from [ICAO09]).	26
Table 3.2 - Flight levels (in [NAV12c]).	32
Table 4.1 - Characteristics of CVOR and DVORs located in Portugal (in [NAV12c]).	53
Table 4.2 - Characterisation of each scenario.	56
Table 4.3 - Interference distance for Nisa DVOR beacon.	65
Table 4.4 - Boundary distance of the exclusion zone for the simulations.	69
Table 4.5 - Boundary distance of the exclusion zone for the three criteria.	71
Table A.1 - Wind generators' usage in Lisbon district (in [WFiP12] and [NAV12c]).	79
Table A.2 - Wind generators' usage in Santarém district (in [NAV12c]).	80
Table A.3 - Wind generators' usage in Santarém district (in [NAV12c]).	80
Table A.4 - Wind generators' usage in Faro district (in [WFiP12] and [NAVA12]).	81
Table A.5 - Wind generators' usage in Azores and Madeira (in [WFiP12] and [NAVA12]).	82
Table F.1 - Input files for Lisbon scenario.	99
Table F.2 - Input files for Fátima scenario.	99
Table F.3 - Input files for Nisa scenario.	99
Table F.4 - Input files for Sagres scenario.	100
Table F.5 - Input files for Porto Santo scenario.	100
Table F.6 - Input files for Flores, Horta and Santa Maria scenario.	100

List of Acronyms

AC	Alternate Current
AGL	Above Ground Level
AM	Amplitude Modulated
AWO	All Weather Operation
BRA	Building Restricted Area
CDI	Course Deviation Indicator
CIR	Carrier-to-Interference Ratio
CNS	Communication, Navigation and Surveillance
CVOR	Conventional Doppler VHF- Omnidirectional Radio range
DME	Distance Measuring Equipment
DVOR	Doppler VHF - Omnidirectional Radio range
E	East
ECEF	Earth-Centred, Earth-Fixed
FAA	Federal Aviation Authority
FL	Flight Level
FM	Frequency Modulated
HAWT	Horizontal Axis Wind Turbine
ILS	Instrument Landing System
LoS	Line-of-Sight
MSA	Minimum Safe Altitude
MSL	Mean Sea Level
N	North
NAV Portugal, E.P.E	Navegação Aérea de Portugal
NE	North-East
NLoS	Non-Line-of-Sight
NW	North-West
OBI	Omni-Bearing Indicator
OBS	Omni-Bearing Selector
OGA	Official Airline Guide
RCS	Radar Cross Section
RF	Radio Frequency
RPS	Rotation per Second
S	South
SE	South-East

SSV	Standard Service Volume
SW	South-West
TMA	Terminal Manoeuvring Area
VAWT	Vertical Axis Wind Turbine
VHF	Very High Frequency
VOR	VHF - Omnidirectional radio Range
W	West
WGS-84	World Geodetic System 1984

List of Symbols

α	Subtend vertical angle
α_d	Angle between the incident ray and the normal to the blade
α_{dec}	Declination angle relative to West
α_{mag}	Magnetic angle of the route
α_{true}	True angle of the route
β	Angle between the vertical axis of the VOR beacon and the wind turbine
β_e	Angle between the incident ray and the edge
Δf	Bandwidth
φ	Angle between the beam direction and the wind turbine measured horizontally
φ_i	Latitude in point i
φ_n	Incidence angle
φ_T	Latitude of the wind turbine
λ	Wavelength
λ_i	Longitude in point i
λ_T	Longitude of the wind turbine
ω_{rot}	Number of rotations per second
σ	Radar Cross Section
σ_b	Bi-static Radar Cross Section
$\sum L_i$	Vertical spacing of the parallel of the latitude in point i
θ	Bi-static scattering angle
θ_d	Angle between the diffracted ray and the normal to the blade
θ_v	Angle between the beam direction and the wind turbine measured vertically
v	Dimensionless parameter
(C/I)	Signal-to-interference ratio
$(C/I)_{min}$	Signal-to-interference ratio minimum
a	Length for semi-major axis
b	Length for semi-minor axis
C_m	Excitation of m^{th} mode

d_{amax}	Largest dimension of the antennas
d_{BO}	Distance from VOR beacon to the obstacle
d_{BT}	Distance from VOR beacon to the wind turbine
d_{BTmin}	Boundary distance of the exclusion zone
d_{int}	Interference distance
d_{inter}	Distance between fixed intervals
d_{min}	Minimum valid distance
d_{OT}	Distance from obstacle to the wind turbine
d_{path}	Path length
d_T	Total distance from the VOR beacon to an aircraft
d_{TP}	Distance from the wind turbine to an aircraft
D_a	Diameter of array
D_e	Diffraction coefficient for one edge
D_i	Diffraction coefficient for each blade
D_m	Normalised directional pattern in the horizontal plane
D_{rotor}	Diameter of rotor blades
E^s	Scattered complex field strength
E^i	Incident complex field strength
f_{Dbla}	Frequency deviation for wind turbine's blades
f_{Dvor}	Frequency deviation for DVOR
F	Noise figure of the receiver equipment
F_{BT}	Terrain induced attenuation factor between the VOR beacon and the wind turbine
F_{TP}	Terrain induced attenuation factor between the wind turbine and the aircraft
G_H	Gain of horizontal component
G_{max}	Gain of the transmitting antenna in the maximum direction
G_r	Gain of the received antenna
G_t	Gain of the transmitting antenna
G_V	Gain of vertical component
h	Tower's height
h_B	VOR beacon's height
h_{dip}	Earth dip
h_F	Flight altitude for the first Fresnel zone clearance
h_i	Height of the point i
h_S	Shadow height cast by the wind turbine
h_T	Wind turbine's height
h'_T	Equivalent wind turbine's height
i	Current position

$J_m(kr)$	Bessel function
k	Wavenumber
kr	Modulation index
K	Average refractive index of the Earth
L_i	Parallel of latitude in point i
L_o	Path loss in free space propagation
L_{ob}	Obstacle's losses
n	Number of the Fresnel zone
N_{points}	Number of points to test in the path
n_t	Total number of elements in the array
N_t	Number of wind turbines in a wind farm
P_N	Average noise power
P_r	Received power from the direct ray
P_{ri}	Received power for an i^{th} wind turbine
P_{riD}	Received power for the signal diffracted by the blades
P_{riRCS}	Received power for the signal reflected by the tower
P_{rt}	Total received power
P_t	Transmitted power
r	Radius of the array
r_a	Average radius of section
r_b	Distance from the blade
r_{eq}	Equivalent Earth's radius
r_{max}	Maximum radius of the tower
r_{min}	Minimum radius of the tower
r_{ne}	Radius of the n^{th} Fresnel zone
r_o	Radius of the Earth
r_{1e}	Radius of the first Fresnel zone
r'_{1e}	Radius of the first Fresnel zone for d_{TP}
R	Range
u_e	Diffracted field
u_i	Incident field
\bar{x}	Obstacle height above or below of the direct ray between the transmitting and receiving antennas

List of Software

Google Earth

Mathworks Matlab r2013a

Microsoft Excel 2010

Microsoft Power Point 2010

Microsoft Visio 2010

Microsoft Word 2007

Paint

Geographical Information system

Numerical computing software

Calculation and chart tool software

Presentation software

Scheme design software

Text editor software

Image editing software

Chapter 1

Introduction

In this chapter one introduces the theme of this dissertation, in a contextual and motivational perspective, while simultaneously giving a brief overview of the developed work. Before establishing work targets, the scope and the main contributions are brought up. At the end of the chapter, a detailed presentation of the work's structure is provided.

1.1 Overview

Since the middle of the XIX century, when the first aircraft was built and tried for the first time, this means of transportation has been intensely explored, and the number of aircrafts that fly every day has been significantly increasing. A report of the Official Airline Guide (OGA) states that, in 2007, the number of schedule airline flights that took place worldwide has been presented a record increase of 4.7% relative to the previous year [OAGR13]. In Portugal, in July this year, compared to the same month of 2012, air traffic increased 1.4% in Lisbon's airport, and average daily flights grew 1.2% [Hard13]. The aforesaid presented values give a brief overview of the increase in flights since the dawn of aviation.

In the beginning of the XX century, pilots began to fly at night and in all weather conditions, therefore, navigation aids were developed for use inside the aircraft, to guide pilots from the ground, and help them to maintain aircraft altitude. After these simple systems, a successful system of two ways radio communication air-to-ground at low frequency was developed, and subsequently, after World War II, a higher frequency transmitter, called Very high frequency Omni-directional radio Range (VOR), was developed allowing pilots to fly in- or outbound along a certain quadrant on a radial line. VOR systems provide ground transmitter locations to pilots, their frequencies and identifying Morse codes [Prin13].

NAV Portugal is responsible for providing air traffic services in the Portuguese airspace, in accordance to national and international standards. For the provision of airspace control, just as radars, radios or communication stations, a lot of equipment is required, which involves a significant investment for its deployment and maintenance. Among these, new radiocommunications technologies appeared in aeronautical navigation aid, the VOR systems, later substituted by Doppler VOR (DVOR), which are the main focus of this Thesis. With these systems, it was possible to know the aircraft's location in the airspace and its identification, as well as setting its course and controlling it [NAV12d].

Wind turbines are structures that are being increasingly used and installed over the years, to generate electricity from the wind energy, as this is considered a clean and profitable energy. The first historical record remotes to the 200 BC, when the first windmills were used to extracted water and grinding seeds in a province of Persia. All over Europe, until to the end of the XIX century, rustic wind turbines were used for several purposes, such as water pumping, vegetables oils production, paper manufacturing, and so on. The early adaptation of rustic wind turbines, with small size, for electrical power generation from the wind energy began in the late of XIX century. In consequence of this evolution on the purpose given to the usage of the wind turbine, structures with increasing dimensions and more efficient emerged over the years, as portrayed in Figure 1.1, according to the needs of each location of installation of the turbines [Hist13].

Since the emergence of the first wind turbines, at about 1985s, capable of converting energy into electrical power, that the diameter of the their rotors has doubled each decade, as shown in Figure 1.1, and therefore increased the height of the turbine. Each generation of wind turbines was predicted to be the biggest; however, turbines keep growing, in an effort to capture the stronger winds accessible at higher elevations, and improve performance.

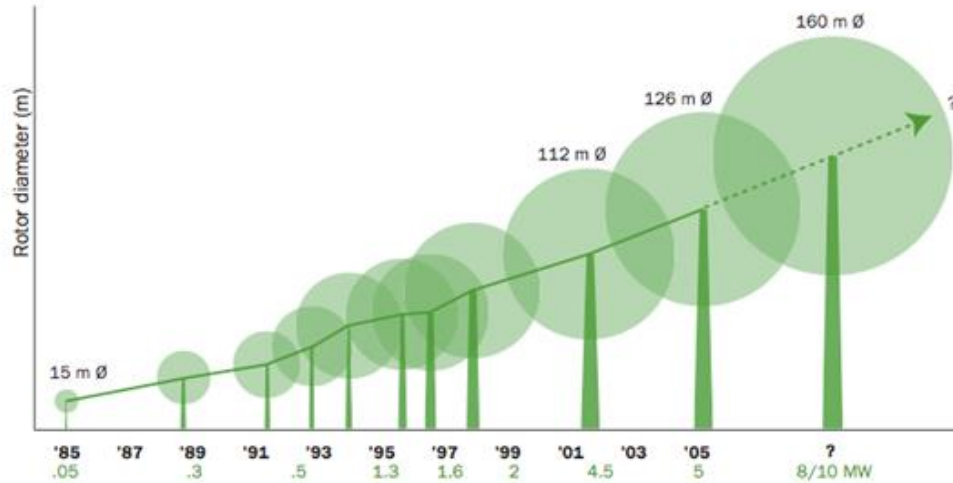


Figure 1.1 - Size and power evolution of wind turbines over time (adapted from [GWGT13]).

Wind turbines placement at the top of hills and coastal areas is the most used, since it is the simplest and the one that leads to better results for higher powers. In these locations, the efforts to manoeuvre the structure are smaller and there is better stability. Therefore, the turbines' blades must be always oriented according to the direction of the wind.

All over the world, the use of wind energy for electricity producing has been increasing; the largest amount of the installed wind capacity is in Europe, in which this form of energy had an extremely fast growth in the last decade. Since 2002, the implementation of a specific and stable legislative framework for renewable energy sources has allowed a significant growth of the installation of structures to use wind energy, in order to achieve more than 4 500 MW, which corresponds to the production of about 15% of the electricity consumed in Portugal [Eoli13]. Figure 1.2 presents, in general, the evolution of the installed capacity in Portugal, in which it is noticeable the aforementioned increasing of this capacity, in MW, from year to year. In this case, wind turbines are mostly installed inland, and in sparsely populated coastal areas.

The main goal of this Thesis was to assess the influence of wind turbines generators in the DVOR systems owned by NAV Portugal, when a group of these turbines, i.e., a wind farm, was installed in its vicinity. Also, one intended to define exclusions regions around the location of the beacons where no turbines can be installed. So, considering the locations of the DVOR systems and the wind farms, it is important to study the interference problems caused on DVOR systems by wind turbines while operating, because the communication between the aircraft and the DVOR beacon should be absolutely precise, free from any kind of Radio Frequency (RF) signal disturbances. To this end, it is necessary to understand how wind turbines and VOR systems operate. In order to achieve these goals, one simulator was developed, to analyse the influence of wind turbines in DVOR beacons and, subsequently, to estimate the boundary distance of the exclusion regions around the beacon for each of the different scenarios under study. Finally, these distances obtained by the simulator were compared to the distances given by theoretical equations, to verify if the results of the simulator are in accordance in between them.

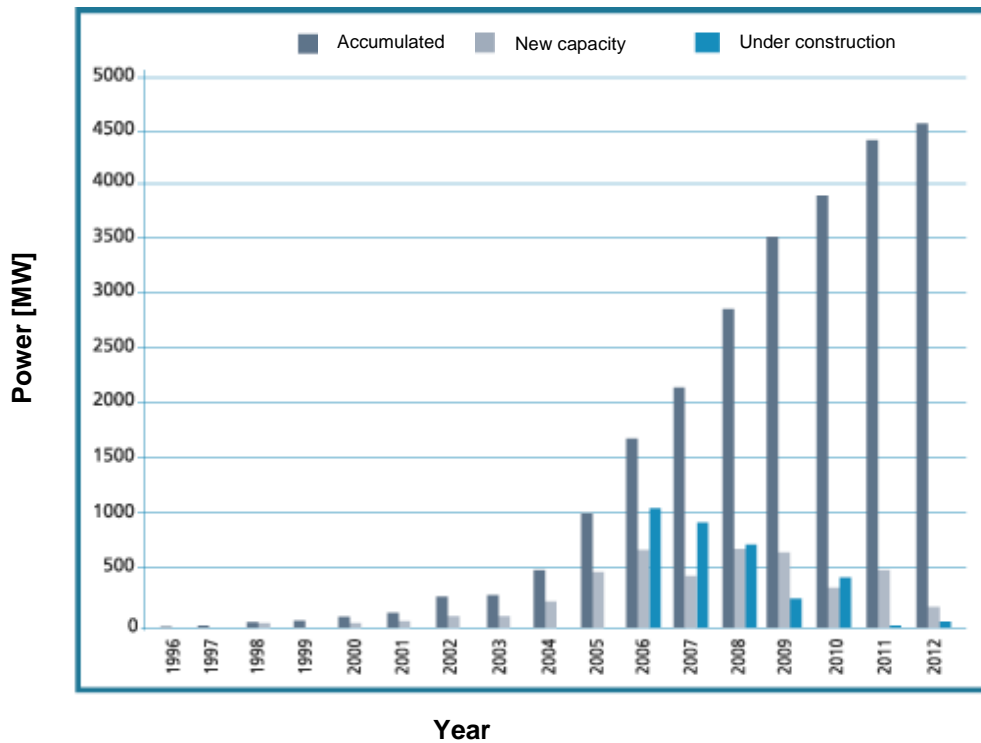


Figure 1.2 - Installed capacity in Portugal (adapted from [Eoli13]).

There are many papers concerning this theme but the studies developed taking into account different approaches of the problem of the interference caused by the wind turbines regarding the one considered in this Thesis. Its innovation is related to the approach that is made of the problem under study. So, the analysis of the problem is done through the analysis of the powers received by the aircraft, that is, the power of the direct signal and the interfering power due to the presence of the wind turbine, and from this analysis is that one gets the best solution to the problem.

1.2 Motivation and Contents

Despite the wide utilisation of wind turbines to produce electricity, as well as the regular use to the aeronautical navigation aids, there are not enough studies and conclusions about the exclusion regions around the aids, in which a infrastructure cannot be installed, so it is important to have a more detailed study.

The present work is focused on assessing the performance of the DVOR systems installed by NAV in Portugal, when they are in communication with the aircraft, and also to study the influence of the wind farms on these systems. In order to assess this communication, two aspects were analysed, i.e., the profile of the terrain between the DVOR beacon and the wind turbine, and the interfering power of the signal diffracted/reflected by the structure of the turbine. The final main subject of the Thesis is to make a proposal for the boundary distance of exclusion regions to the scenarios in which interference problems are noticeable.

This Thesis was made in collaboration with NAV Portugal, E.P.E, a company responsible for the provision of air traffic services. Besides the scope establishment, the company was also helpful in providing essential information required to the development of the work.

This work is composed of 5 Chapters, including the present one, followed by 6 annexes to complement the content of the Thesis:

- In Chapter 2, one presents the fundamental concepts of the aeronautical navigation aids, focusing on the DVOR systems, as well as its operation mode. Afterwards, a detailed description of the basic aspects of the wind turbines are presented, and its interference effects on DVOR systems. Finally, a brief state of the art about the problem under study is presented.
- In Chapter 3, the theoretical equations based on specific criteria to determine the boundary distances of the exclusion regions, and the developed models for the structure of the wind turbines, the characterisation of the terrain profile, and the definition of the flight routes are presented. A detailed description of the implementation of the models in a simulator is also presented. And, finally, one shows an assessment of the performance of the simulator and its requirements.
- In Chapter 4, one presents the results from several simulations. This chapter includes the results obtained by the theoretical equations for the exclusion regions defined from specific criteria and by the simulator, which gives the boundary of the exclusion regions through several simulations. Finally, a comparison between the results of both methods is done, and the optimum solution is presented.
- Chapter 5 summarises the work developed in this Thesis, draws the conclusions, and finally discusses the future work that could be done in this area.

At the end of this Thesis, a set of annexes with auxiliary information are included. In Annex A, one presents the location of all wind turbines of each wind farm to study. In Annex B, some intermediate steps required to the determination of the shadow height created by the wind turbines and of the flight altitude for an aircraft are detailed. In Annex C, some intermediate steps required to the determination of the equations established by the criteria into consideration are detailed. In Annex D, one presents the methodology and expressions used to estimate the gain of the transmitting antenna. In Annex E, the steps followed for the estimation of the diffraction coefficient in the simulator are detailed. Finally, in Annex F, one presents the initial and final points of each section of a flight route, which compose one of the input files of the simulator.

Chapter 2

Fundamental Aspects

This chapter provides an overview of the fundamental theoretical concepts to understand the operation mode of the aeronautical navigation system, wind turbines and their influence on the mentioned navigation systems, mainly focussing on exclusion regions, and concluding with a brief state of the art.

2.1 Aeronautical Navigation Systems

This section presents the fundamental concepts about the aeronautical navigation system, namely its main features, operation mode and radio interface.

2.1.1 Features of VOR

VOR systems are a type of short range radio navigation system operating in the VHF band, installed at a reference point on an airway or an airport. Currently, VOR is widely used, as it practically is not affected by static effects and is detectable during either day or night, providing magnetic bearing in form of radials, throughout 360° of the ground transmitter, regarding the location of an aircraft to a reference point [NAV12a]. The radials are a set of lines indicating the direction of the aircraft relative to the VOR ground beacon, being numbered from 1° to 360°. The 360° radial is the track leaving the VOR station towards the magnetic north – the normal reference for the radials.

The VOR indicator on board is named Omni-Bearing Indicator (OBI). This indicator has a vertical bar named Course Deviation Indicator (CDI), which travels to the left or right according to the aircraft's position to the radial set by the pilot in the Omni-Bearing Selector (OBS), so it indicates which side the aircraft should travel in order to find the required radial. The OBI is also composed of a TO/FROM indicator that, together with an active navigation system, indicates the flight direction relative to the ground beacon.

The VOR alone just provides information on the aircraft's direction regarding the ground beacon without considering the flight direction, thus, several VORs are equipped with an active navigation system, the Distance Measuring Equipment (DME), also called VOR/DME. Those are ground stations that provide indication of distance between the aircraft and the aforesaid ground station through the calculation of the time elapsed between the pulse sending (i.e., DME interrogator) and reception (i.e., DME transponder). This system is in constant communication with the aircraft from the moment it enters its operating range. The DME system is a very useful addition to VOR, as it allows the pilot to know the distance to the station and also the flight direction relatively to it, checking only if the distance increases or decreases [Sant12].

Besides VORs equipped with the DME, there are still other types of VOR stations worth mentioning, considering those that are not detailed further in this Thesis [NAV12a].

- Doppler VOR (DVOR): it has a lower site error, being based on the Doppler principle.
- Test VOR (VOT): transmitter for pre-flight checks of airborne equipment requiring tuning the frequency and centralising CDI, so that the reading should be within $\pm 4^\circ$ of 0° FROM or 180° TO, anywhere on the aerodrome; of course, it is not for navigational information purposes.
- Terminal VOR (TVOR): usually used at major aerodromes, being low powered transmitters, for arrival and departure navigation.

- Weather Broadcast VOR (BVOR): it is intended to transmit in voice weather information of some specific aerodromes in between the identification signals.
- VORTAC: a VOR and TACAN - military navigation aid - joining bearing and distance information compatible to civil DME.
- DB VORTAC: combination of a weather broadcasting Doppler VOR with a TACAN.
- PVOR: a precision VOR.

This Thesis focuses on the DVOR type, Figure 2.1, and its operating mode is detailed at Subsection 2.1.2. The DVOR is a VOR system based on the Doppler effect for bearing information signals, being composed of an array of 48 sideband antennas sending a variable phase signal, and also an omnidirectional, central carrier antenna sending a reference phase signal, mounted on a suitable levelled ground [ToWy07]. This system might be implemented in airports and airways, and may be located in the same place as DME, just as the VOR system.



Figure 2.1 - DVOR ground beacon (extracted from [WiCo12]).

The VOR receiver does not distinguish between a signal from a Conventional VOR (CVOR) or from a DVOR, and the pilot treats both types in the same way.

Ground transmitters radiate signals up to 60° to 80° elevation above the horizon. Between both elevations, there is an area with no or weak radiation, in the form of an inverted cone. In this area the indications in the airborne equipment are inaccurate. The indications are accurate and stable again, after passing the station [NAV12a].

Usually, the transmitting power of a VOR station is about 200 W, receivable at ranges around 200 nmi in the case of the enroute VORs transmitting, or about 50 W in the case of Terminal VOR. The DVOR has an adjustable transmitting power between 25 W and 100 W.

Given the fact that VOR transmitters are in VHF, the receiver and transmitter's heights define the Line of Sight (LoS) range, as it depends of possible ground obstacles and the flight altitude [NAV12a]. At higher altitudes, it is possible to receive more distant VOR signals, but with reduced signal integrity. The range depends basically on the transmitter power and the receiver sensitivity. In practice, navigations' aids have a designated Standard Service Volume (SSV) that defines the reception limits within altitude envelope as show in Table 2.1. It is an altitude above ground level (AGL), assuming the ground is flat, in which AGL is the measured altitude with respect to the underlying ground surface.

Table 2.1 - Navigation aid classifications (extracted from [ToWy07]).

Classification	Flight Altitude [ft]	Range [nmi]
Terminal	1 000-12 000	25
Low altitude	1 000-18 000	40
High altitude	1 000-14 500	40
	14 500-60 000	100
	18 000-45 000	130

The accuracy of transmission system for VORs is less than $\pm 3^\circ$. However, in presence of all combined errors, including airborne equipment, the accuracy will be within $\pm 5^\circ$. In the case of DVOR, the bearing accuracy is $\pm 0.5^\circ$, for all elevation angles from 0° to 40° , and the bearing stability is typically $\pm 0.1^\circ$ [Hult08].

CVORs are quite error prone, which may harm signal's quality and accuracy; therefore, they have been gradually replaced by DVORs. The most serious errors limiting VORs performance may be originated by: signal generation error and defective 360° radial alignment with local magnetic north induce signal inaccuracy (beacon alignment or ground beacon error); physical obstacles and uneven terrain (site error); occasional signals reflected by uneven terrain or other physical obstacles during propagation may distort the sending signals (propagation error); airborne equipment malfunctions due to manufacturing problems (airborne equipment error); and pilotage error [NAV12a].

2.1.2 VOR's Operation Mode

The basic operation principle lies in bearing measurement by phase difference comparison. This means that the transmitter on the ground produces and transmits two separate signals, which make it possible for the receiver to determine its position relative to the ground beacon by comparing the phase difference of these two signals.

In order for an aircraft to recognise its own magnetic bearing, VOR radiates both a reference phase signal and variable phase one, where the phase of the former depends on the bearing of radiation, while that of the latter is constant regardless of the bearing. The second signal is produced by transmissions from a rotating loop at 30 Rotations Per Second (RPS) along with a non-directional transmitter. By virtue of rotation, a combined signal transmission at 30 Hz Amplitude Modulated (AM) is radiated. The transmission is arranged such that the phase difference between two signals oriented to the magnetic north is zero and, in all other directions, equals the value of the radial. At the airborne receiver both signals are received and their phase difference, which corresponds to the magnetic direction from the VOR station, is displayed on different indicators appropriately as magnetic bearing to or from the VOR station. The above mentioned signals are identical when they are received at a position located in the direction of magnetic north taking the VOR as reference. If the receiving point changes clockwise around VOR, the phase of variable phase signal is delayed relatively to the reference phase signal, and the delay comes in the 360° , when the point makes a clockwise full turn about the VOR.

Assuming that there is no error on the information from the VOR station, the angular difference of the receiving point corresponds to the delay in phase, thus, accuracy bearing information can be provided to the aircraft.

In the DVOR, the change of Frequency Modulated (FM) and AM for the reference phase signal and variable phase signals, as compared to conventional VOR, is compensated by rotating the DVOR antenna pattern in the opposite way of the VOR. DVOR transmits two signals, just as the VOR, and in addition to bearing information signals, identity code and voice signals in Morse code are also transmitted to the aircraft [ToWy07] and [NAV12a].

DVOR uses two rotating patterns (diagonally opposite each other) at 30 RPS:

- 9 960 Hz above the reference frequency;
- 9 960 Hz below the reference frequency.

The diameter of the array, together with the pattern rotation speed, creates a Doppler shift of 480 Hz (at VOR frequencies), which creates an FM signal in the aircraft receiver over a range $9\,960\text{ Hz} \pm 480\text{ Hz}$ varying at 30 Hz in a sine wave [ToWy07] and [Hult08].

2.1.3 Radio Interface

The VOR antenna is a horizontally polarised one, with omnidirectional characteristics and operates in the [108, 118] MHz range, the same range of frequencies for the DVOR. In this range, even tenths of each 0.5 MHz increment are allocated to VOR frequencies, because the odd tenths are allocated for Instrument Landing System (ILS) frequencies, in order to distinguish both systems, as both share the same receiver.

It was previously mentioned that VOR sends two signals, in which the reference phase signal is FM at 30 Hz sine wave, with a constant phase relative to all VOR directions, and the variable phase signal is AM at 30 Hz sine wave, a signal with a specific phase difference in reference to the reference phase signal depending on the receiver direction, Figure 2.2 [ToWy07].

The reference phase signal frequency modulates a subcarrier of $f_0 \pm 9\,960\text{ Hz}$ with a frequency shift of $\pm 480\text{ Hz}$. Then the subcarrier is radiated as amplitude modulation of the carrier f_0 with 30% modulation depth. The modulation of the carrier f_0 is allocated an identity code (1 020 Hz) and voice (300 to 3 000 Hz).

Two crossed omnidirectional dipoles radiate the variable phase signal. These dipoles receive sideband signals, which carrier is suppressed, from two sideband transmitters with 90° phase difference in the envelope.

An omnidirectional antenna radiates the carrier f_0 , thus, producing a pure AM, due to the superposition of the carrier and the 30 Hz sidebands in the field, if the phase is correctly set. Then the phase of the resulting 30 Hz signal depends on the azimuth (the geographical angle between North and the direction of the aircraft relative to the ground beacon), related to the 30 Hz reference signal [NAV12b].

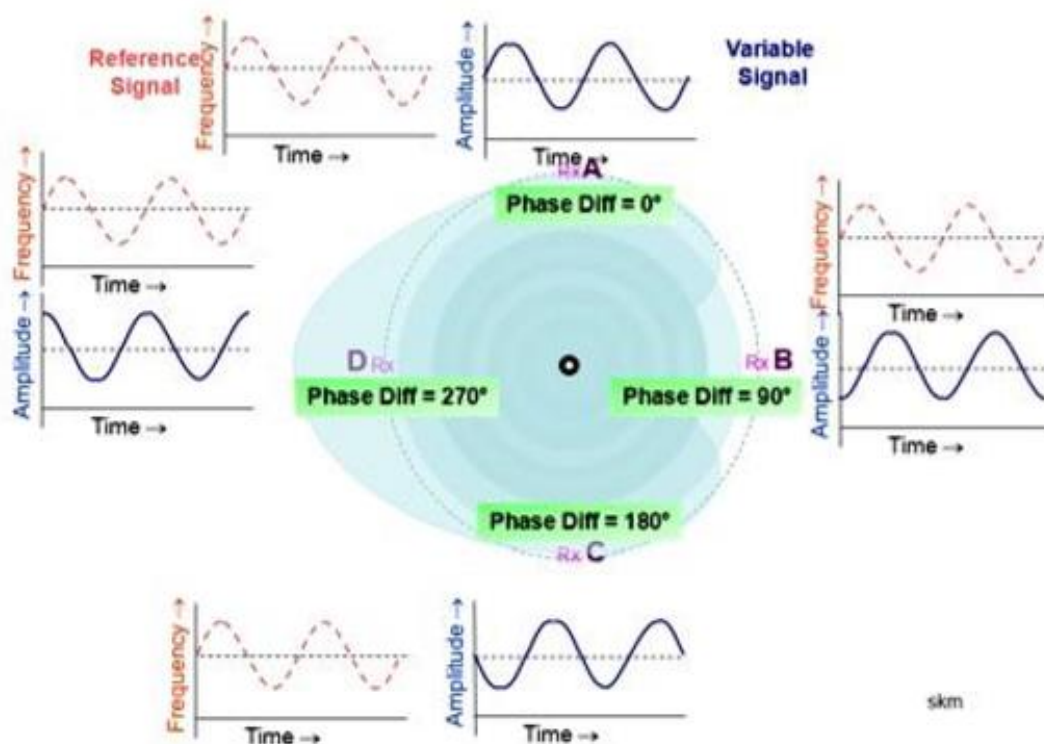


Figure 2.2 - Polar diagram (extracted from [NAV12a]).

In a DVOR system, the variable phase signal and the reference phase signal are transmitted by FM and AM, respectively. That is, the modulations are opposite as compared to the conventional VORs. It benefits from a much larger antenna aperture in a conventional VOR, thus, reducing the pointing error up to 10 times.

A stationary centre antenna transmits omnidirectionally the modulated carrier signal, which is AM, with the voice and the identity code in addition to the 30 Hz reference signal.

The variable signal of the DVOR, Figure 2.3, is located on the subcarrier $f_1 = 9\,960$ Hz. To this end the DVOR transmitter generates separately the two sidebands ($f_0 - f_1$) and ($f_0 + f_1$), which are radiated by rotating outer antennas.

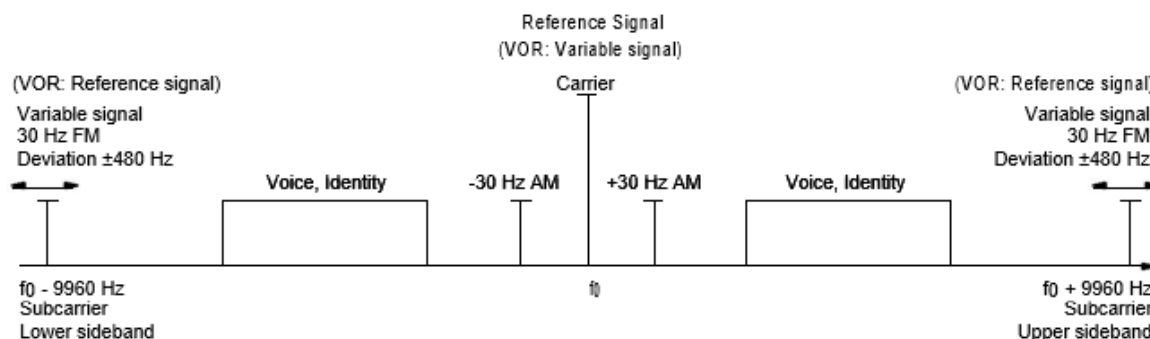


Figure 2.3 - Frequency spectrum of the DVOR (VOR) (extracted from [NAV12a]).

The modulation depth of the each frequency can be adjusted within a certain range. The typical values are [NAV12a]:

- 30 Hz navigation signal: 30%.
- 9 960 Hz auxiliary carrier: 30%.
- Voice: 30%.
- Identity code: 10%.

2.2 Wind Turbines Generators

This section approaches the main wind turbines types, focussing on the most usual one for a detailed description of its features and operating mode. Finally, wind farms are also briefly mentioned, being further detailed in a later section.

2.2.1 Features of Wind Turbines

A wind turbine is a device for converting the wind's kinetic energy, also called wind energy, into mechanical one. The wind energy depends on the environmental conditions where the turbines are built. In Portugal, by the western shoreline, especially in the central area or some places in northern inland, the wind's year medium speed is high, about 6 to 7 m/s at 60 m height [Cast11].

Wind turbines are classified into two general types:

- Horizontal Axis Wind Turbine (HAWT);
- Vertical Axis Wind Turbine (VAWT).

Since the latter takes no advantage from the high wind speed for higher elevations above ground, the turbine mentioned in the first place is more often used. Considering this, there is no need to detail the main features and characteristics of the VAWT. On the other hand, the HAWT has a design similar to a windmill, where helix shaped blades turn around a horizontal axis, parallel to the ground.

Figure 2.4 shows the wind energy converting system, which divides in three main sections: rotor, nacelle and tower.

The rotor might be placed up- or downwind of the tower, Figure 2.5. The upwind option, in which the rotor is before the tower, is preferred so that the tower will not disturb the wind. If the rotor is installed downwind the tower, it allows the rotor's self-alignment with the wind direction; however, the disturbance caused by the tower in the wind's flow before it hits the tower is considered a disadvantage. On the other hand, it is necessary that the point where the blades are set – rotor hub – is allowed to swivel, that is, it must present tilt to the vertical in order to hold unbalances resulting from the blades passage before the tower.

Current large wind turbines are composed of three blades rotors, as these present better efficiency and less air resistance, with a diameter between 20 and 90 m, and its rotational angular speed ranging from 20 to 150 rpm.



Figure 2.4 - Wind turbine's main sections (adapted from [WiEn12]).

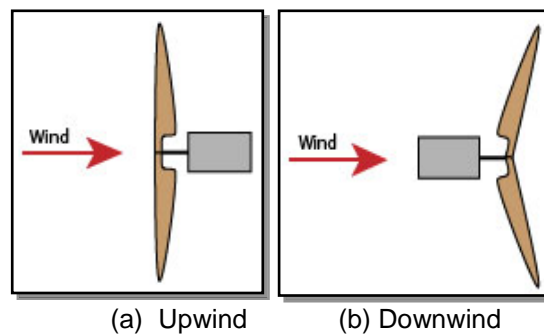


Figure 2.5 - Axis orientation and rotor hub position (extracted from [Rene12]).

Another section of wind turbines is the nacelle that holds, among other equipment, the main shaft, gearbox (if existing), the generator, and the directional orientation mechanism. If existing, gearbox allows adapting the turbine's rotor frequency, typically ranging from 0.33 Hz – 20 rpm – or 0.5 Hz – 30 rpm – to the generator frequency that is of the mains of 50 Hz. It is also necessary to align the rotor with the wind direction, in order to get as much energy as possible, performed by the directional orientation mechanism, which taking the information received from a wind direction sensor, turns the nacelle and rotor until the turbine stays in the proper position. On top of the nacelle seats an anemometer and its direction sensor. The anemometer main purpose is to measure wind speed, thus, allowing to control the turbine, namely its starting, that is cut-in wind speed from 5 m/s, and cut-out speed in case of wind speeds over 25 m/s [Cast11].

The turbine tower supports nacelle and elevates the rotor to a height with higher wind speed and less disturbance regarding the ground. Current towers are of tubular type and rise to heights around 100 m, depending on the planned wind energy power, so the structure must be designed to stand significant loads, and endure weather exposure throughout its life-span, about 20 years. The turbine's expected life-span should consider that the wind's floating component might include significant energy at frequencies close to the turbine's structure oscillating frequencies, which shall reduce this period.

Occasionally, for wind speeds above the rated wind speed, it is necessary to limit the wind generator supplied power, as there is no economic advantage in its rise. This regulation might be affected by stalling or pitch control, which operational mode is detailed in Subsection 2.2.2 [Cast11].

2.2.2 Wind Turbine's Operation Mode

In a typical design of turbine, the rotor blades are connected to an axis linking to a gearbox, which will allow raising the blades' rotating speed, in a range mentioned in Subsection 2.2.1. The rotating shaft turns inside the generator producing the AC (alternate current) power. This power must be produced at the right frequency and voltage, compatible to the mains.

The wind speed hits the rotors influencing the energy amount received by the turbine, therefore, current wind turbines are designed to operate more effectively at wind speeds between 13 to 16 m/s, corresponding to the rated wind speed. As sometimes the wind speed is above these values, a wind turbine should be able to adapt to its dominating speed to operate more efficiently. There are two basic approaches, above mentioned in Subsection 2.2.1 (Figure 2.6), to control and protect the turbine:

- Pitch control, in which an anemometer is installed on top of the nacelle and permanently checks the wind speed sending signals to a pitch actuator, which adjusts the blades' angles to catch more efficiently wind energy.
- Stalling, in which the blades are blocked and there is no adjustment during the operation.

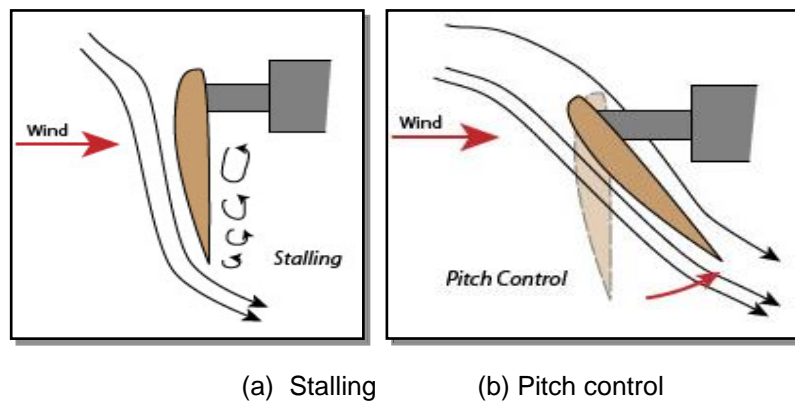


Figure 2.6 - Control mechanisms (extracted from [Rene12]).

Both design approaches have relative advantages. A pitch controlled turbine is considered slightly more effective than a stalling design. On the other hand, a stalling turbine is frequently considered more reliable, because they are more simple from a mechanical and operational point of view than pitch control ones. Furthermore, the blades are designed and shaped to increasingly reduce wind charge angle to the blade so to maximise the output power and protect the turbine from excessive wind speed [Cast11] and [Rene12].

To get the most from the wind speed and generate larger amount of energy, wind generators are typically grouped in wind farms. These are built by turbine groups set in rows or perpendicular formations to the dominant wind direction, see Section 2.3.

The building of wind farms must take into consideration the land conditions intended to build the wind generators, namely land unlevelled, obstacles, and areas orography to get the best yield possible. Land unlevelled diminishes wind speed, and obstacles and unlevelled surfaces cause turbulence with

a negative impact in wind efficiency. These above mentioned factors also cause huge wear on wind generators [Cast11].

2.3 Wind Turbines' Effects on VOR

This section approaches the main phenomena causing disturbances in the RF signal, referring some relevant aspects allowing one to better understand the origin of the above phenomena, such as wind turbines' distribution, its wake effect and Radar Cross Section (RCS), etc. Subsequently, the referred signal degradation causing phenomena is detailed to contribute for a later numerical analysis, in Chapter 4, as well as its mathematical concepts, Chapter 3, of each one and an assessment of the impact of each disturbance in RF signal.

2.3.1 Problem Definition

Wind turbines are the main sources of interference analysed in this Thesis. Therefore, besides theoretical aspects referred in Subsection 2.2.2 regarding it, it is necessary to include some new concepts essential to understand the main phenomena responsible for the RF signal degradation and caused by turbine or wind farm presence close to DVOR antennas.

Considering the aforesaid regarding aeronautical navigation systems, in Subsection 2.1.1, it is relevant to address the Doppler Effect concept. So, if VOR beacons are installed close to obstructions, or when an aircraft using VOR signals flies over mountainous terrain, the bearing accuracy is deteriorated by reflections (site errors). The DVOR solves this problem with the Doppler Effect for determination of the bearing. In general, this effect is the change in the frequency of a wave observed at a receiver whenever the source or the receiver of the wave is moving relative to the other, or to the carrier of the wave (the medium). By applying this effect, one can overcome these limitations.

The maximum resulting Doppler Effect by a dipole rotating eccentrically on a periodical orbit, that changes the distance between transmitter and receiver, produces a sinusoidal frequency modulation of the carrier, which phase contains the bearing information, by a deviation calculated by the following equation [Hill04]:

$$f_{Dvor[Hz]} = \frac{\pi \cdot D_{a[m]} \cdot \omega_{rot[rps]}}{\lambda_{[m]}} \quad (2.1)$$

where:

- f_{Dvor} : frequency deviation for DVOR;
- D_a : diameter of array (set of antennas that build the DVOR);
- ω_{rot} : number of rotations per second;
- λ : wavelength of the electromagnetic signal.

The above mentioned DVOR, see Subsection 2.1.1, reduces the bearings errors caused by the RF

energy reflection from objects near the ground [Hill04].

Wind turbines are rarely found isolated, but gathered in wind farms, so it is necessary to carefully plan the siting of wind turbines in the farm, as its close proximity to a navigation aid may result in an effect on the coverage of the radiated signals. The effect of wind farms on aeronautical navigation systems is influenced by the physical characteristics, operational parameters, and siting of the wind turbines.

The capability of an object to intercept and return radio energy depends upon the size, shape, orientation, and reflectivity of the object. The reflectivity of a wind turbine's rotor blades depends on the materials it is composed of, assuming they are composed of non-metallic materials, usually light weight carbon fibre. In general, this ability to reflect increases with the size of an object, such that a large wind turbine may be expected to reflect more signal. In a similar manner, the ability of an object to create blockage between a signal source and the reception point also depends largely on the size and shape of the object.

Considering that the wind turbine generates mechanical energy from the incident wind energy, the "outgoing" wind holds much lower energy regarding the "entry" one. Effectively, in the back of the turbine, a turbulent wake effect takes place, much slower regarding the incident wind speed. That is why the turbines in a wind farm must be sited rigorously. The wake effect shall degrade RF signals.

To minimise this effect, the turbines are usually spaced between five to nine rotor diameters, in dominant wind direction, and between three to five diameters, in the perpendicular direction, Figure 2.7 [Cast11]. A more equidistant spacing is possible in the absence of a dominant wind direction, but in both cases the terrain is also taken into consideration.



Figure 2.7 - Wind turbine siting in a wind farm and its wake effect (adapted from [IWAG12]).

Besides that, and Table 2.1, it is necessary to assess the DVOR service volume in order to determine whether a wind farm may impinge upon it or not, potentially creating regions of diminished signal strength. If the wind turbines impinge upon the lower bounds of all three of the SSVs, they may potentially cast shadows of little to no signal strength behind them. The DVOR system performance may thus be degraded at the lower bounds of the SSVs [Rais12].

2.3.2 Interference Effects on VOR

Wind farms in the vicinity of airports or aeronautical navigation systems may cause different effects affecting RF linking performance the aeronautical navigation depends on, due to wave reflection by its components (blades, tower, rotor...). In this sense, it is pertinent to insert the RCS, which is a classical scheme used to characterise a target, as a wind turbine, from the transmitter's perspective, which acts as a radar, for the determination of the maximum range and visibility, considering that the RCS is defined explicitly for a plane wave excitation [GrBM09].

The blades rotate at a random velocity, and the consequent disturbances are also random, the nacelle and rotor turn according to the wind direction, and pitch control makes the blades turn along its longitudinal axis to vary the blade area that faces the wind. These three different movements of the turbine cause significant variability with time in the degradation effects [VFGA11]. The degradation mechanisms that may occur in the presence of wind farms are of different nature, and they are related to the structure and working regimes of the turbines:

- Reflection or Scattering;
- Shadow effect;
- Electromagnetic interference effects.

First and foremost, the reflected and scattered signals are generated by the components of the wind turbine, mainly by the metallic mast, blades of rotor and the nacelle. These reflected signals, occurring in the movable parts of the wind generators, are Doppler shifted due to the blade rotation. The Doppler Effect depends on the rotation angular speed, the blade length and the rotor orientation with respect to the transmitter and receiver locations [VFGA11], and the maximum may be determined by:

$$f_{Dbla[Hz]} = \frac{\pi \cdot D_{[m]} \cdot \omega_{rot[rps]}}{\lambda_{[m]}} \quad (2.2)$$

where:

- f_{Dbla} : frequency deviation for wind turbine's blades;
- D : diameter of rotor blades.

When an electromagnetic signal impinges upon a wind turbine, its energy is scattered depending on the angle of incidence, Figure 2.8. Since the nacelle and blades of a wind turbine are typically not stationary, it is not likely that the angle at which the signal is reflected stays the same over time.

A ray may be directly reflected at an aircraft, where the reflected ray meets with the direct ray. Conversely, a signal sent from the aircraft that is in communication with the DVOR ground beacon may reflect off a wind turbine towards the DVOR antenna, where they meet with the direct signal. If the timing of the arrival of the two signals is negligible (in case of a long distance of communication and a low angle of inclination for the direct ray), the signals of the two rays can interfere destructively, essentially creating a very low signal.

Figure 2.9 depicts if a wind turbine is within the Fresnel zone of a direct signal. In this scenario, the electromagnetic energy reflected by the wind turbine may combine destructively at the receiver,

creating a null that causes a loss of communication. This is a critical situation that may leave a pilot without distance and bearing information.

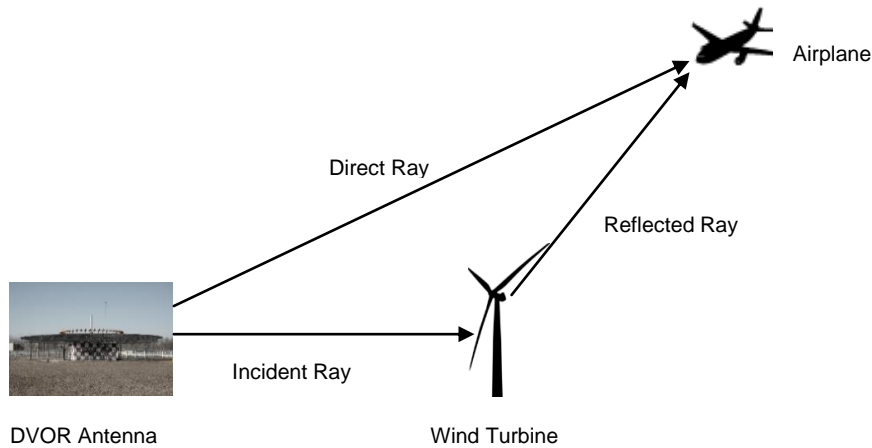


Figure 2.8 - Reflection/Scattered.

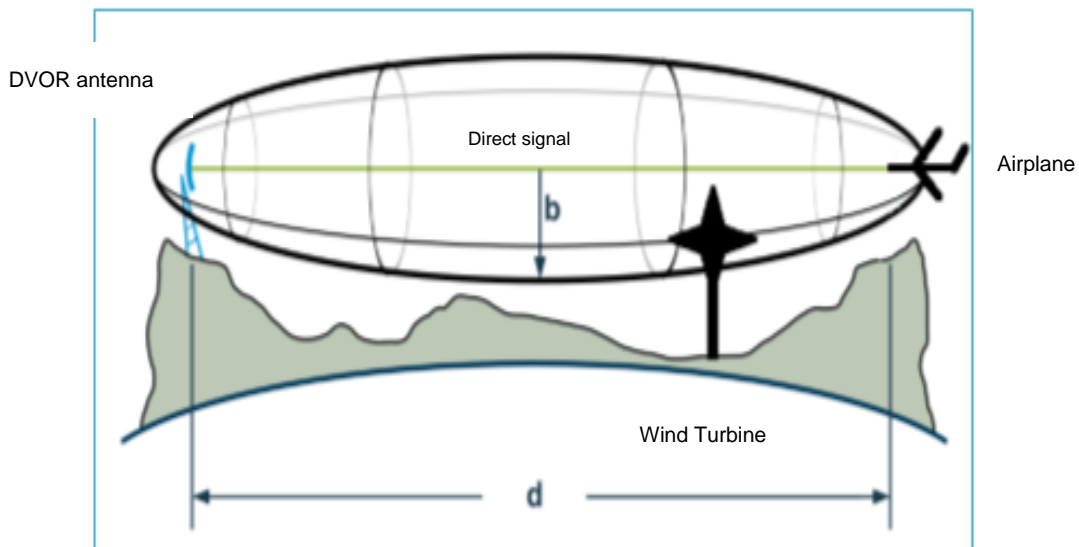


Figure 2.9 - Second Fresnel zone obstructed by wind turbine (adapted from [Rais12]).

Besides wind turbines, elevated terrain may also lead to reflections within the Fresnel zone, producing a signal of weakened or no energy. So, it is necessary to consider a gap, corresponding to the distance between the top of the obstacle and Fresnel's ellipsoid direct radius, i.e., the former is higher than the ellipsoid's radius ensuring the second Fresnel zone should be completely clear of obstacles [Rais12].

As previously mentioned, a wind turbine is a larger metallic structure that has the potential to block electromagnetic waves. The waves will hit the object and be scattered in all directions, including directly back at the sending antenna. The result is an area of potentially weakened signal behind the wind turbine. Figure 2.10 portrays the horizontal and vertical shadow regions created by a single wind turbine; understandably, a wind farm will potentially create a much greater horizontal shadow, while the vertical shadow will stay roughly the same given uniform turbine heights.

Such shadow regions of diminished signal strength may prevent a signal from reaching its destination

or may lower the power of the signal to a level such that the receiver does not detect its presence. And so, the shadow region affects both in- and outbound signals for a DVOR ground beacon; that is, a signal to be received by the DVOR antenna is affected as much as a signal being transmitted by the antenna, though the extent of the shadow length and height might vary. The extent of the shadow region is directly correlated with clutter dimensions close to the DVOR antenna. A higher tower will cast a greater shadow.

Shadow regions and their heights are relevant in a DVOR interference study, because a DVOR antenna can have an effective operating range up to 200 nmi, as previously mentioned in Subsection 2.1.1. To be effective at such a distance, the antenna pattern must have high gain at vertical angles near and slightly above horizontal [Rais12].

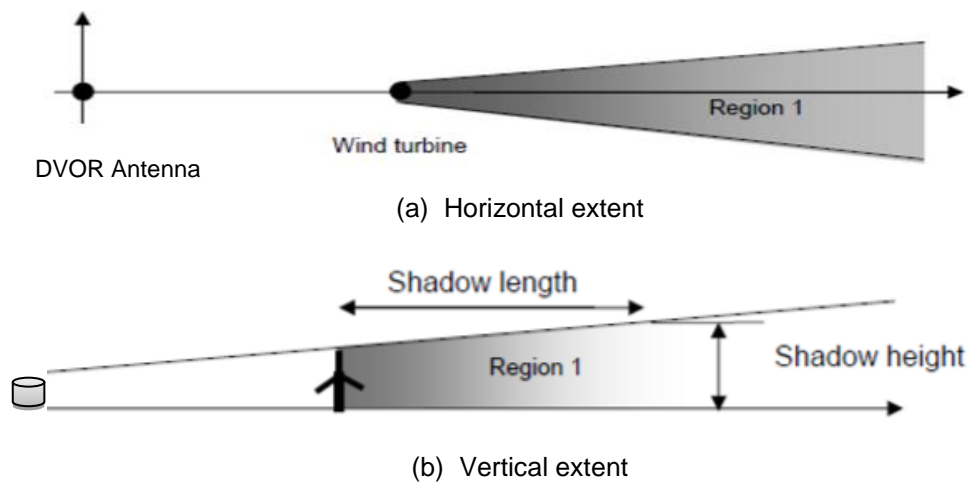


Figure 2.10 - Shadow region (adapted from [Rais12]).

In addition to the aforementioned degradation mechanisms, the installation of wind turbines in the vicinity of a DVOR may act as a potential source of electromagnetic interference effects to the performance of this system. The said interference may be originated by the rotation of the blades of the turbines.

The analysis of the impact of blades' movements on the DVOR system is carried out by the comparison between both the direct DVOR signal and the DVOR signal scattered by the wind turbine that reach an aircraft (in the Figure 2.8, the reflected signal corresponds to the signal scattered by the wind turbine), considering that the amount of scattered energy that reaches an airborne receiver is rather dependent on speed and direction of wind [Rais12]. The analytical procedures employed in the above study are logical extensions of those found acceptable [FAAu86] in the case of the static scatterers produced by a wind turbine [Seng84].

2.4 State of The Art

The assessment of wind turbines and wind farms impact on aeronautical navigation systems, namely

the disturbances caused on RF signal, have been studied and researched worldwide, giving rise to papers and technical documents stating conclusions and results obtained. The importance of this studies has risen since the end of the 1980s, when Sengupta in [Seng84] concludes the possibility to minimise the disturbances caused by a wind turbine or wind farm through the proper siting of turbines, regarding aeronautical navigation systems. This conclusion results of theoretical research and laboratory tests on the effects of electromagnetic interference caused by HAWTs and VAWTs. Besides that, and based on information disclosed by FAA, on static scatterers, Sengupta realised the interference when the wind turbine blades are rotating causes less disturbance than when the blades are stationary. Therefore, it follows that the siting of a wind turbine can be carried out according to the standard guidelines defined in FAA's handbook, VOR/VORTAC Siting Criteria [FAAu86].

Most researches in this scope focus mainly on the wind turbines and farms locations relative to aeronautical navigation aid. Nonetheless, Odunaiya [Odun06], besides considering the distance between turbines in a wind farm and VOR systems, carried out countless tests for different orbital flights and radial flights, supported on a model (Ohio University Navigation and Landing Performance Prediction Model) based on the theory of physical optics. Odunaiya results show that at low orbital flight, wind turbines will degrade the performance of the VOR system to levels that may be unacceptable. Regarding modelled radials, it was concluded that the studied system operates at acceptable levels. Besides that, the modelling analysis has shown that wind farms have significant effects on VOR performance, even when these wind farms are located several miles away from the VOR. As the number of wind turbines grows, the potential for the large wind farm to affect a navigation system also increases. Finally, the author declared that the siting criteria applied to a single turbine cannot be the same to study a wind farm with several turbines.

[MoFS08] is a paper revealing the methodology used and results obtained in wind turbine effects analysis on VOR system performance. In this paper, Morlass, Fares and Souny developed an electromagnetic CAD model for rotor blades based on a dielectric structure. In a first step, the dielectric blade model is compared to the metal one in terms of RCS, so that the dielectric rotor blade causes less scattering, because it is characterised by the far field scattering matrix obtained by method of moment. Subsequently, from the comparison between the impact of a three-blade rotor and the wind turbine's metal tower, they concluded that the blade effects are negligible compared to the tower effects at weak elevation directions where the tower's scattered field is maximum. On the other hand, besides the model developed by the rotor blades, they studied the impact caused by the growing number of turbines, in a wind farm, and by the distance to the VOR station. The authors concluded that the Doppler VOR seems to be a good solution to prevent VOR system from multipath.

In [ArHG09], a real environment study is performed on the main disturbances wind turbines may cause on general radio communications. Firstly, there is a detailed theoretical assessment of the main interference mechanisms due to wind turbines close to a generic antenna. Then, these mechanisms are framed within radio communications and the study case. Finally, some strategies are present, recommended by Kordia, to lessen the disturbances from wind turbines close to radio communication systems. These strategies are fixed linking services (relocating the radio transmission site of the

effected service or the turbine in question so that the first Fresnel zone is unobstructed) and other wide area coverage services (relocating the turbine in question to meet the minimum separation distance requirement). In another real environment study, [Rais12], the analysis of the impact Riviera wind farm is performed on the neighbour aeronautical navigation systems. The author used countless equations to calculate the exclusion zones limits around air radiocommunication system, for three different situations:

- Guidance for nav aids' siting in the FAA's National Airspace System.
- Minimum Safe Altitudes.
- Lower Bounds of SSVs.

The results obtained through the above mentioned equations were compared to the results from the ATDI Software applied to each one of the three above cases, which allowed to reach the results concordance.

Other assessments focus on the numeric comparison between the height of the wind turbine, located near the TACAN system (a combined and more accurate version of the VOR and DME systems) and the lower bounds SSVs, as well as the comparison between the different shadow heights, caused by the wind turbines, and the different flight altitudes for the aircraft based on the first Fresnel ellipsoid height. Finally, it was also studied electromagnetic interference effects caused by the turbines on the aeronautical navigation systems, which findings agree with the conclusions in [Seng84], that is, the interference from rotating wind turbine is less troublesome than that of a stationary one.

The software tool (with a description of its main functions and structure) to analyse the impact of wind farms in radiocommunication systems is proposed in [VFGA11]. This software allows, through several models and algorithms, to calculate the degradation potential on several radiocommunication services types, by assessing the degradation introduced by a wind farms close to any of the study systems in the paper.

Chapter 3

Model Development and Implementation

This chapter provides a description of the models used to develop the final simulator for a generic scenario, in MatLab, as well as an explanation related to the implementation of the detailed models and an assessment of it in the simulator.

3.1 Exclusion Regions Criteria

This section describes a detailed analysis related to the DVOR siting criteria, which are used in the determination of shadow height, flight altitude, and exclusion zones. These models are used for obtaining the results in a later section.

3.1.1 DVOR Interference Zone

The study of the interference effects caused by the presence of wind turbines in the vicinity of a DVOR must determine whether these turbines could be located within a restricted area or would interfere on protected airspace [Rais12].

In [ICAO09], the Building Restricted Area (BRA) is defined as “a volume where buildings have the potential to cause unacceptable interference to the signal-in-space in the service volume of Communication, Navigation, and Surveillance (CNS) facilities for All Weather Operations (AWO)”. Figure 3.1 portrays BRA for omnidirectional facilities, where the cylinder is referenced to the ground terrain and the cone to a horizontal plane, and the DVOR specific values for the variables on the figure are presented in the Table 3.1. This volume provides the case protection for navigational aids, namely DVOR.

It should be stressed that the radius, j , and height, h , of the second cylinder, present in both the figure and the table, are considered only in case of nearby wind turbines in the analysed scenario.

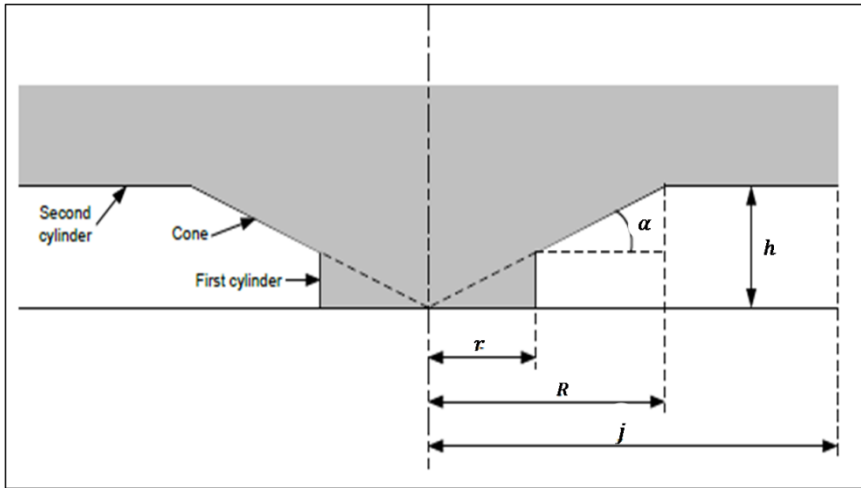


Figure 3.1 - Definition of BRA in side elevation view (adapted from [ICAO09]).

The radius, R , of the cone is limited to 3 km, provided wind turbines are present. A second much wider cylinder, at a height of 52 m AGL, is added for further protection, and this cylinder extends to 15 km from the navigational aid antenna [Rais12].

In the above conditions, the impact of wind turbines on the DVOR should be assessed within a radius

of 15 km from the ground beacon, and a more detailed assessment in this zone should be executed for any turbine which:

- lies within 600 m;
- infringe a 1° slope from the centre of the antenna at ground level up to 3 km;
- infringe a 52 m horizontal surface from a distance between 3 km to 15 km.

Table 3.1 - BRA parameter values (adapted from [ICAO09]).

Type of Navigation System	$r_{[m]}$	$\alpha_{[^\circ]}$	$R_{[km]}$	$j_{[km]}$	$h_{[m]}$	Origin of Cone and Axis of Cylinders
DVOR	600	1	3	15	52	Centre of antenna system at ground level

Besides that, where the terrain cannot be considered to be flat, all turbines beyond the 15 km radius should be assessed or the BRA should be adapted to this terrain.

The approval of wind turbines planned or existing that may cause interference effects on navigation aids is based on a two-step process, in which Step 1 should be an expedient evaluation and Step 2 should involve a detailed analysis, Figure 3.2.

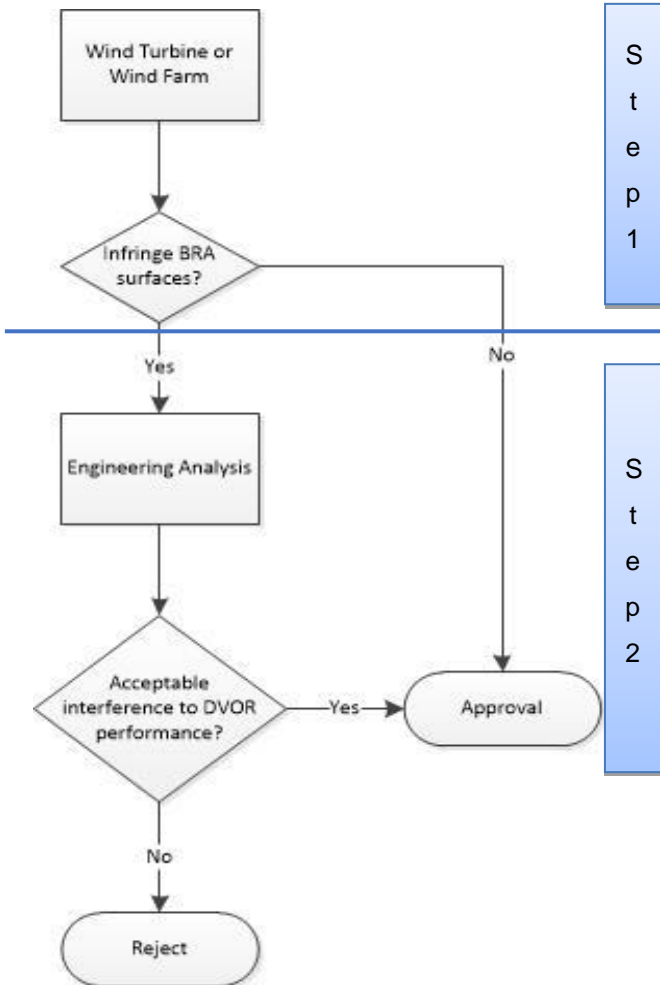


Figure 3.2 - Guidance process (adapted from [ICAO09]).

During a turbine’s planning stage, or during the assessment stage of an existing one, the first issue

comprehends checking whether this building infringe the BRA surfaces based on the analysis of Figure 3.1 and the values of Table 3.1. If it is built outside of BRA surfaces, then the process is terminated and the turbine under study is approved. Otherwise, it is necessary to perform an additional engineering analysis and in-depth study of the different degradation mechanisms caused by the presence of the wind turbines, mentioned in the Section 2.3. Finally, it is determined if the interference effects of wind turbines are acceptable or not for the nearby navigational aids, and the building is approved or rejected, respectively [ICAO09].

In the sequence of the previous detailed analysis related to the restricted area, it should be considered other DVOR siting criterion, mentioned in [FAAu86]. The mentioned criterion states that “no structures should be permitted within 1 000 feet of the antenna... All structures that are partly or entirely metallic shall subtend vertical angles of 1.2° or less, measured from ground elevation at the antenna site”.

The first restriction imposes that the proposed turbines should not infringe upon the lower bounds of the three SSVs (Table 2.1), as the failure to observe this may originate regions of diminished or no signal strength as a consequence of shadow regions created behind the turbines. On the other hand, the second restriction is applied to a worst case scenario, where both the DVOR antenna and the wind turbine are assumed to be at 0 m AGL, and in which flat Earth with no obstructions is assumed, Figure 3.3.

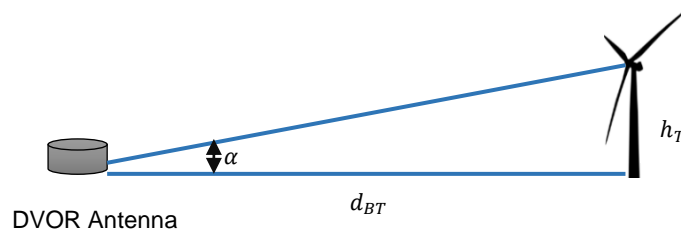


Figure 3.3 - Subtended angle by wind turbine.

According to configuration in Figure 3.3, the subtend vertical angle can be calculated by [Rais12]:

$$\alpha_{[^\circ]} = \tan^{-1} \left(\frac{h_T[m]}{d_{BT}[m]} \right) \quad (3.1)$$

where:

- α : subtend vertical angle;
- h_T : wind turbine's height;
- d_{BT} : distance from the DVOR beacon to the wind turbine.

3.1.2 Shadow Height and Flight Altitude Determination

According to the detailed study on wind turbines location compared to the VOR siting criteria and the theoretical description in Subsection 2.3.2, regarding interference effects of wind turbines on DVORs, one must perform an analysis of the main mathematical concepts of the said effects. The main information presented in this subsection is based on [Rais12].

- Shadow height calculation.
- Fresnel zone clearance analysis.

The shadow height calculation is just the consideration of the geometry of the turbine and the VOR transmitter taking some relevant characteristics into account:

- ✓ maximum height of the wind turbine;
- ✓ Earth curvature;
- ✓ Earth radius.

The fact that electromagnetic waves do not propagate in a straight line above Earth, its curvature, is taken into consideration, and one assumes the equivalent Earth's radius instead of its physical one. Hence, a factor K , which is the average refractive index of Earth and takes the typical value of 4/3, must be applied to calculate the central angle [Bore10] and [Sale02b]. So, the equivalent Earth's radius is given by:

$$r_{eq[\text{km}]} = Kr_o[\text{km}] \quad (3.2)$$

where:

- r_o : Earth radius (approximately 6 370 km [Sale02b]).

Figure 3.4 shows the principle of shadow height calculations and the involved parameters, assuming that all heights above the effective radius of the Earth are above mean sea level. So, according to this, one considers the worst case scenario, that is, the wind turbine near the DVOR beacon, thus, the one most likely to cast the tallest shadow. So, first the angle β is calculated to determine the angle between the vertical axis of the DVOR beacon's highest point and the top of the wind turbine, given by the following expression (derived from the Law of Cosines, detailed in the Appendix B):

$$\beta_{[^\circ]} = \cos^{-1} \left(\frac{(d_{BT[m]})^2 + (h_{Beq[m]})^2 - (h_{Teq[m]})^2}{2(d_{BT[m]})(h_{B[m]} + r_{eq[m]})} \right) \quad (3.3)$$

where:

$$h_{Beq[m]} = h_{B[m]} + r_{eq[m]} \quad (3.4)$$

$$h_{Teq[m]} = h_{T[m]} + r_{eq[m]} \quad (3.5)$$

- h_B : DVOR beacon's height.

From the result of (3.3) to a specific scenario, one determines the angle of the top of the nearest wind turbine above horizontal with respect to the antenna, seen from the top of the DVOR beacon, and the mentioned angle is obtained through $\beta_{[^\circ]} - 90^\circ$.

The final step is to determine the expression that allows one to calculate numerically the shadow height created by the wind turbine. This expression is obtained, as (3.3), via the Law of Cosines. So, once again, supported by Figure 3.4, the following expression gives the shadow height, h_S :

$$h_{S[m]} = \sqrt{(h_{Beq[m]})^2 + (d'_{[m]})^2 - 2(h_{B[m]} + r_{eq[m]})(d'_{[m]}) \cos \beta_{[^\circ]} - r_{eq[m]}} \quad (3.6)$$

where:

$$d'_{[m]} = d_{BT[m]} + d_{TP[m]} \quad (3.7)$$

All the steps effected to find (3.6), as well as its justification are detailed in Appendix B.

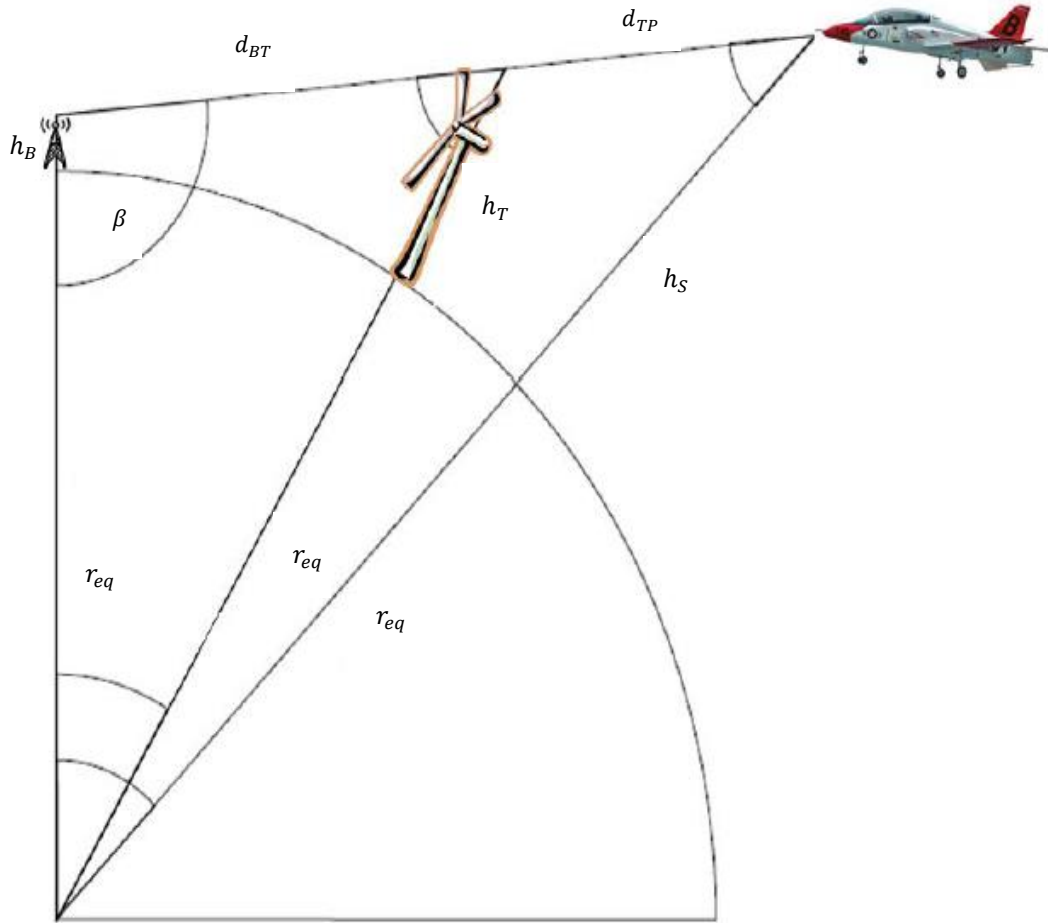


Figure 3.4 - Shadow height cast by the wind turbine diagram (adapted from [Rais12]).

Concerning the analysis of Fresnel zone's clearance, as within the second Fresnel zone occurs the maximum phase cancelling effect (a null creation), the power contained in this zone of an electromagnetic signal is a critical situation, and it is important to impose a clearance between a direct ray and a possible reflected one to minimise the potential for the creation of a null. The analysis of the Fresnel zone clearance evaluates the extra amount of clearance that must be above the previous calculated shadow zone, which is necessary to avoid the obstruction of the complete first Fresnel zone of a direct signal by a wind turbine, thus, allowing the maximum amount of energy to reach the receiver. Figure 3.5 portrays the comparison between the shadow height and the flight altitude required for Fresnel zone's clearance without considering Earth curvature.

The objective is to calculate the flight altitude required for first Fresnel zone's clearance, and, for this, it is necessary to include the calculation of the radius of Fresnel zone in the expressions that characterise the scenario in Figure 3.5. The radius of the n^{th} Fresnel zone is given by:

$$r_{ne[m]} = \sqrt{\frac{n\lambda_{[m]}d_{BT[m]}d_{TP[m]}}{d_{BT[m]} + d_{TP[m]}}} \quad (3.8)$$

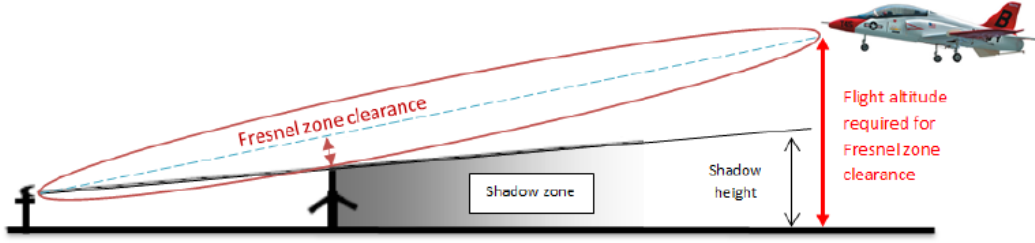


Figure 3.5 - Fresnel zone clearance diagram (extracted from [Rais12]).

Considering only the first Fresnel ellipsoid and particularising (3.8) to $n=1$, the minimum flight altitude of an aircraft is determined by:

$$h_{F[m]} = \sqrt{(h_{Beq[m]})^2 + (d_{TP[m]})(d'_{[m]} + (d''_{[m]}))((h_{Teeq[m]})^2 - (h_{Beq[m]})^2)} - r_{eq[m]} \quad (3.9)$$

where:

$$d''_{[m]} = \frac{d_{BT[m]} + d_{TP[m]}}{d_{BT[m]}} \quad (3.10)$$

$$h_{Teeq[m]} = h_{T[m]} + r_{eq[m]} + r_{1e[m]} \quad (3.11)$$

- r_{1e} : radius of the first Fresnel zone;
- h_F : flight altitude for the first Fresnel zone clearance;
- d_{TP} : distance from the wind turbine to an aircraft.

All the steps taken to obtain (3.8) and (3.9), as well as their explanation are presented, in detail, in Appendix B.

The comparison between (3.6) and (3.9) discloses that the flight altitude for first Fresnel ellipsoid is higher than the turbine shadow height, and this is a necessary situation for the aircraft to maintain a safe route above the shadow casted by the wind turbine. This clear increase occurs due to the inclusion of the radius of Fresnel ellipsoid in the second expression.

3.1.3 Exclusion Regions Determination

To complement the previous detailed theoretical analysis about siting criteria for DVOR beacons, exclusion regions around DVORs are determined and the main information presented in this subsection is based on [Rais12]. The exclusion zones free of wind turbines establishment depend on the criterion that is deemed most critical in the maintenance of flight safety in DVORs area:

- Exclusion zone based on FAA Order 6820.10.
- Exclusion zone based on Flight Levels (FL).
- Exclusion zone based on the Standard Service Volumes.

A restrictive exclusion region is laid forth in [FAAU86], which refers that the wind turbine tower should subtend an angle smaller or equal to 1.2° with respect to the DVOR beacon, measured from ground level at the ground site.

Considering that, usually, the ground may not be considered flat and its elevations vary with location

and azimuth, to determine the minimum distance between a DVOR beacon and a wind turbine, so that this distance obeys to the said criterion, a spherical Earth should be assumed. So, the Earth dip should be considered, Figure 3.6, and the respective equation is:

$$h_{dip[m]} = \left(\frac{d_{BTmin[m]}}{5829} \right)^2 \quad (3.12)$$

The minimum distance between a ground beacon and a turbine that imposes the exclusion zone based on the study siting criterion is determined by (3.12), and a modified version of (3.1) based on Figure 3.6.

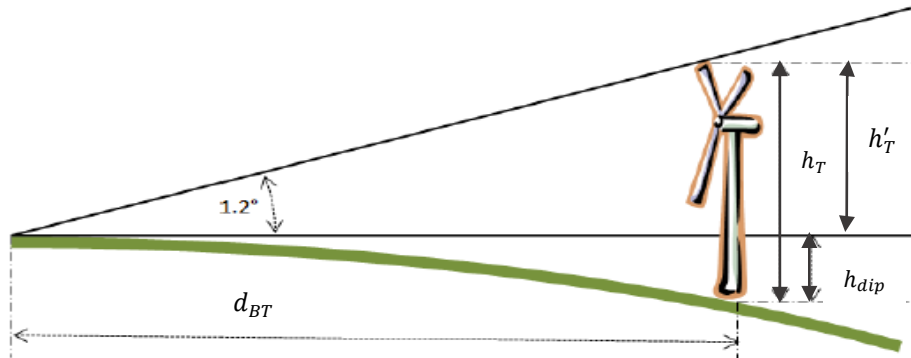


Figure 3.6 - Earth dip's effect on distance between DVOR antenna and wind turbine (adapted from [Rais12]).

According to the previous paragraph, the following equation is applied to calculate the boundary distance of the exclusion zone between a DVOR beacon and a wind turbine:

$$d_{BTmin[m]} = \frac{h'_T[m]}{\tan 1.2^\circ} \quad (3.13)$$

where:

- h'_T : equivalent wind turbine's height.

In (3.13), the variable corresponding to the equivalent height of a wind turbine is used due to the Earth curvature, being explained in detail in Appendix C.

Another possible exclusion region is based on communication without interference in relevant FLs, which defines the altitude in hundreds of feet. So, the exclusion zone is calculated for each of the different study FLs, presented in Table 3.2 [NAV12c].

In this sense, and taking the several FLs into account, the expression that solves the minimum distance is a new version of the one previously created, (3.9), however, the total distance between the DVOR beacon and aircraft is considered, instead of the distance between the wind turbine and aircraft. Thus, a worst case scenario is assumed, in which an aircraft is located a few nautical miles from the DVOR beacon:

$$\frac{-(h'_{Teq[m]})^2 + (h_{Beq[m]})^2 + (d_{BT[m]})^2}{d_{BT[m]}} + \frac{(h_{Feq[m]})^2 - (h_{Beq[m]})^2 - (d_T[m])^2}{d_T[m]} = 0 \quad (3.14)$$

where:

$$h'_{Teeq[m]} = h_{T[m]} + r_{eq[m]} + r'_{1e[m]} \quad (3.15)$$

$$h_{Feq[m]} = h_{F[m]} + r_{eq[m]} \quad (3.16)$$

- d_T : total distance from the DVOR beacon to an aircraft;
- r'_{1e} : radius of the first Fresnel zone for $d_{TP} = d_T - d_{BT}$.

With (3.14) set to zero, and all but one of the variables known, the minimum distance between a DVOR beacon and a wind turbine, d_{BT} , is solved for. The detailed explanation on how to obtain the solution is given in Appendix C.

Table 3.2 - Flight levels (in [NAV12c]).

Flight Level	Flight Altitude [ft]	Description
FL 55	5 500	Minimum flight altitude controlled outside the Terminal Manoeuvring Areas (TMAs)
FL 150	15 000	Intermediate flight altitude
FL 450	45 000	Maximum flight altitude controlled to “regular” aircrafts

The exclusion regions for wind turbines may also be determined for the lower bounds of the SSVs discussed earlier, which are defined in Table 2.1. The lower bounds of these service volumes allow for safe communication with aircrafts at 1 000 ft AGL at distances of 25 nmi (for the Terminal SSV) and 40 nmi (for the Low and High Altitude SSVs) from the DVOR. Therefore, the boundary distance of exclusion zone based on lower bounds of SSVs is calculated from (3.14).

In the case of a minimum distance between DVOR and wind turbine being calculated, such that the lower bound of the Low and High Altitude SSVs is unaffected, then, the result places the turbines out of LoS.

3.2 Wind Turbines Modelling

This section presents a detailed description of the wind turbines modelling, namely an analysis of the RCS of the tower, and the diffraction caused by the blades of an exemplary wind turbine. Also, it presents a study about Carrier-to-Interference Ratio (CIR) between the received power of the direct ray and the interfering power through the power calculation for different situations.

3.2.1 Tower RCS Model

In wind turbines tower’s modelling, it is fundamental to detail the RCS concept adequate to the target of the DVOR beacon under study, that is, wind turbines. In this sense, and as a first step, the characterisation of a target will be applied to an isolated wind turbine, and afterwards this will be expanded for a full wind farm, composed of several turbines.

The standard definition of the RCS, which is given by the equation below, assumes that a distance is

asymptotic infinite. This assumption implies a plane wave excitation, or a far field approximation, therefore, the RCS is a far field quantity such as the gain of an antenna [GrBM09].

$$\sigma_{[m^2]} = \lim_{R \rightarrow \infty} \left[4\pi R^2_{[m^2]} \frac{|E^s|^2}{|E^i|^2} \right] \quad (3.17)$$

where:

- E^s : scattered complex field strength;
- E^i : incident complex field strength;
- R : range.

It is worthwhile to notice that the RCS depends on the total squared scattered electric field of the total object (wind turbine). According to the general RCS definition and the limit condition of (3.17), the infinite distance may be replaced approximately by the standard far field condition $d > d_{min}$, which assumes the minimum valid distance to be the larger antennas' far zone given by:

$$d_{min[m]} = \frac{2d_{amax[m]}^2}{\lambda_{[m]}} \quad (3.18)$$

where:

- d_{amax} : largest dimension of the antennas.

Otherwise, significant phase errors occur, because the antennas are not in the far field [Sale02a] and [GrBM11].

The tower of a wind turbine is modelled as a set of small cylindrical sections, Figure 3.7, inasmuch as its size ensures that a far field approximation for each one can be used. So, the near field RCS can be calculated whereas the effective scattering centre for each section is known, considering that each section is assumed as a point scattered positioned at the centre the relevant section. The model is based on [RaBr07a] and [RaBr07b].

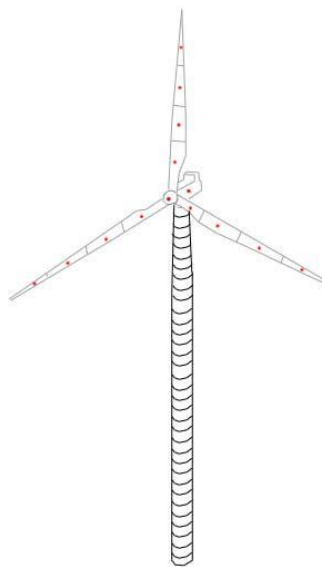


Figure 3.7 - Segmented tower geometry (extracted from [RaBr07a]).

Figure 3.8 presents two different perspectives of analysis of the tower of a wind turbine. In this sense, φ_1 corresponds to the angle of the incident ray, from the DVOR antenna, in the study section, and φ_2 is the reflection angle of the ray from the wind turbine to the aircraft. Both angles are in the vertical plane, as shown in Figure 3.8 (b). Besides that, angle θ corresponds to the one between the incident ray on the wind turbine and the reflected ray to the aircraft, and it is in the horizontal plane, as Figure 3.8 (a) shows. For the above mentioned angles, Figure 3.8, the reference scattered point is in the centre of the section.

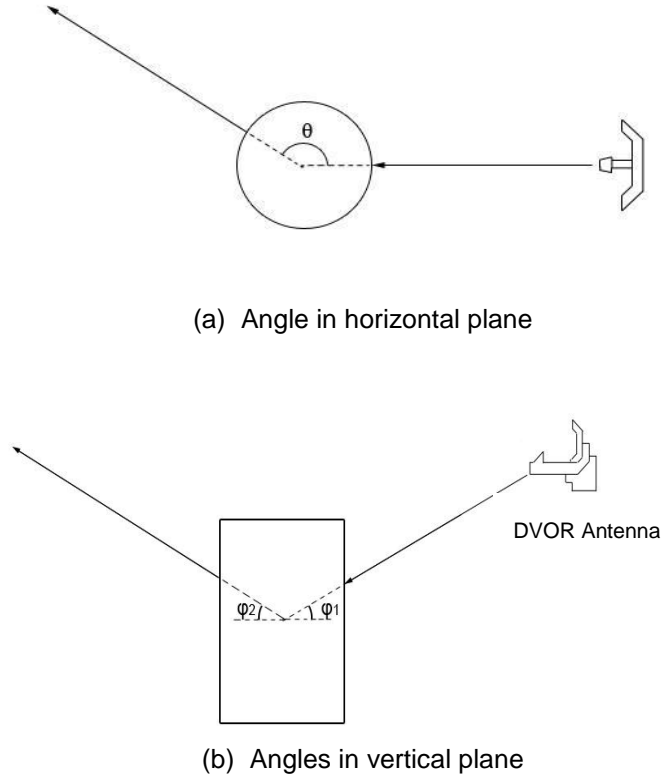


Figure 3.8 - Bi-static RCS layout (adapted from [RaBr07b]).

In the modelling of the tower, an analysis of bi-static RCS prediction is required, which is used to predict the appearance of ghost targets on the account of multiple reflection issues. The bi-static RCS determination of each section is achieved through standard simplified physical optics far field RCS approximations of a cylinder, and taking the different layouts of the tower into account, shown Figure 3.8. So, the expression is given by:

$$\sigma_b[m^2] = k_{[rad/m]} r_a[m] h_{[m^2]}^2 (\cos \varphi_{div[rad]} \cos(\theta_{[rad]}/2)) \text{sinc}^2 \left(\frac{k_{[rad/m]} h_{[m]}}{2} (\sin \varphi_{sum[rad]}) \right) \quad (3.19)$$

where:

$$\sin \varphi_{sum[rad]} = \sin \varphi_1[rad] + \sin \varphi_2[rad] \quad (3.20)$$

$$\cos \varphi_{div[rad]} = \cos^2(\varphi_2[rad]) / \cos \varphi_1[rad] \quad (3.21)$$

$$k_{[rad/m]} = 2\pi / \lambda_{[m]} \quad (3.22)$$

$$r_a[m] = \frac{r_{max[m]} + r_{min[m]}}{2} \quad (3.23)$$

- k : wavenumber;
- r_a : average radius of section;
- h : tower's height;
- θ : bi-static scattering angle;
- φ_n : incidence angle;
- r_{max} : maximum radius of the tower;
- r_{min} : minimum radius of the tower.

The radius of section included in (3.19), and given by (3.23) corresponds to the mean value, due to the conic shape of the tower, which means that the tower top has a lower radius (minimum radius) than the base (maximum radius). This situation gives rise to an error, due to the fact that the received power from the DVOR beacon is different at the top and bottom of the wind turbine. The aforesaid approximation can be used considering that the RCS of the tower is directly proportional to the radius of the tower support.

In the analysis of a wind farm, it is necessary to calculate the RCS for each single turbine via the model above, considering that all turbines may be of different dimensions. Later, one calculates the influence of each turbine on the received power in the aircraft, which is transmitted by the DVOR beacon and is reflected or scattered by them.

3.2.2 Blades Model

The influence of the blades of turbines on the scattered signal is modelled by the law of edge diffraction, in which diffracted rays lie on planes normal to the edge when incident rays are normal to the edge. Furthermore, for simplicity, it is assumed that the ray is in a homogeneous medium, so that it is a straight line [Kell62].

The signal emitted by the DVOR antenna reaches one of the edges of one blade (orange segment in Figure 3.9), and is diffracted by it to the aircraft. This propagation phenomenon depends on the position of the DVOR antenna and the aircraft with regard to the wind turbine position, which corresponds to the location of reference. Besides that, the diffraction coefficient depends on the angles between the DVOR beacon and the wind turbine, and also the aircraft and the wind turbine. So, the diffraction coefficient for one edge, D_e , of a blade is given by [Kell62]:

$$D_e[\sqrt{m}] = -\frac{e^{i\pi/4}}{2(2\pi k_{[rad/m]})^{1/2} \sin \beta_e[rad]} \left[\sec \frac{1}{2}(\theta_d[rad] - \alpha_d[rad]) + \csc \frac{1}{2}(\theta_d[rad] + \alpha_d[rad]) \right] \quad (3.24)$$

where:

- β_e : angle between the incident ray and the edge;
- θ_d : angle between the diffracted ray and the normal to the blade;
- α_d : angle between the incident ray and the normal to the blade.

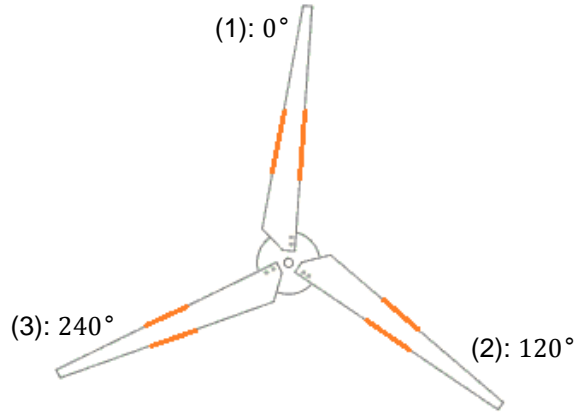


Figure 3.9 - Blades scheme (adapted from [Elec13]).

Considering that the DVOR antenna operates in the [108, 118] MHz range, the corresponding wavelength is approximately 2.6 m. Additionally, the blades length is approximately 15 to 20 m (that is, the blades length is much larger than the wavelength), hence, it can be assumed that the blades length is infinite and both its edges are parallel. In conclusion, for one blade composed of two edges, as shown in Figure 3.9, the diffraction coefficient, D_i , is obtained by:

$$D_{i[\sqrt{m}]} = 2|D_{e[\sqrt{m}]}| \quad (3.25)$$

The determination of this coefficient for the three blades of a wind turbine and for different rotation angles both of the blades as the rotor's blades is detailed in Annex E.

3.2.3 Power Calculation

The total received power reaching the aircraft corresponds to the power from the direct signal in free space and the interfering power due to the presence of a wind farm. This assessment is applied to each study scenario, which is composed of a transmitter (DVOR beacon), a wind turbine, and a receiver (aircraft).

Consequently, the received power, P_r , from the direct signal in the radio link between the DVOR beacon and the aircraft, can be calculated by [Figa12a]:

$$P_{r[W]} = \frac{P_{t[W]} G_t G_r \lambda_{[m]}^2}{(4\pi)^2 d_T^2 [m^2]} \quad (3.26)$$

where:

- P_t : transmitted power;
- G_t : gain of the transmitting antenna (detailed in Appendix D);
- G_r : gain of the receiving antenna.

Following the above, and in order to complete the assessment, the total interfering power, P_{rt} , is calculated by adding all the received powers from each i^{th} turbine, for the signal that reaches the tower and the signal diffracted by the blades, this power being calculated by:

$$P_{rt[W]} = \sum_{i=1}^{N_t} P_{ri[W]} \quad (3.27)$$

where:

$$P_{ri[W]} = P_{riRCS[W]} + P_{riD[W]} \quad (3.28)$$

- P_{ri} : received power for an i^{th} wind turbine;
- N_t : number of wind turbines in a wind farm;
- P_{riRCS} : received power for the signal reflected by the tower;
- P_{riD} : received power for the signal diffracted by the blades.

Considering this is the worst case scenario, the analysis of each one is effectively based on the sum of powers and not the sum of fields.

In (3.28), the received power for the signal that is reflected by the tower of an i^{th} turbine is determined considering its RCS, being obtained from the radar equation. So, the aforesaid power is given by [Figa12a]:

$$P_{riRCS[W]} = \frac{P_{t[W]} G_t G_r \lambda_{[m^2]}^2 \sigma_{bi[m^2]} F_{BT}^2 F_{TP}^2}{(4\pi)^3 d_{BTi[m^2]}^2 d_{TPi[m^2]}^2} \quad (3.29)$$

where:

- F_{BT} : terrain induced attenuation factor between the DVOR beacon and the wind turbine;
- F_{TP} : terrain induced attenuation factor between the wind turbine and the aircraft.

Considering the worst case analysis, in (3.29), the terrain induced factor is the same for the DVOR beacon and the turbine link, as well as for the turbine and aircraft link, being $F_{BT} = F_{TP} = 1$ [Bore10].

Besides the power in (3.29), as mentioned previously, also the signal diffracted by the blades of the turbine is required for the calculation of the interfering power. In this context, for the far field, this power is determined from the diffracted field equation given by [Elet13]:

$$|u_{e[V/m]}| = |u_{i[V/m]}| |D_{i[\sqrt{m}]}| \sqrt{\frac{r_b[m]}{r_p[m](r_p[m] + r_b[m])}} \quad (3.30)$$

where:

- u_e : diffracted field;
- u_i : incident field;
- r_b : distance to the blade;
- r_p : distance to the aircraft.

Therefore, the determination of the power for the diffracted signal takes the relationship between the power and the total field into account, being calculated by:

$$P_{riD[W]} = \frac{P_{t[W]} G_t G_r \lambda_{[m^2]}^2}{(4\pi)^2 d_{BTi[m^2]}^2} |D_{i[\sqrt{m}]}|^2 \frac{d_{BTi[m]}}{d_{TPi[m]}(d_{TPi[m]} + d_{BTi[m]})} \quad (3.31)$$

The most critical situation occurs in the radio link in LoS, and in the absence of obstructions between a turbine and an aircraft (corresponding to d_{TP}), because the receiver is not in a fix point, that is, the aircraft's position varies in time. This problem does not occur in the radio link between the DVOR beacon and the turbine (corresponding to d_{BT}). Consequently, in the first scenario, to ensure that the transmitter and receiver are in a far field distance (assumption previously mentioned in the beginning of the subsection), it is necessary to verify the case where the aircraft is closer to the turbine and the case where the aircraft is more distant, that is, the worst and best cases. This assessment is possible through an analysis of the flight routes (Section 3.3) for each scenario under study.

To complement the study related to the received powers in the aircraft, and in the case of existing obstacles in the terrain, it is required to calculate the additional loss that is introduced by them. In this calculation, a real obstacle is modelled by an ideal obstacle, which is, in general, of infinite length, in the normal direction to the propagation, and of negligible thickness, that is, a blade obstacle, or of finite thickness and round with constant curvature, that is, a cylindrical obstacle.

The Knife-Edge model is used in the calculation of the losses introduced by one obstacle, L_{ob} . This model should be used when its dimensions are much larger than the wavelength. The ideal case assumes that the obstacle is shaped by a semi plane normal to the propagation direction. So, it is possible to characterise it by a dimensionless parameter given by [Corr13a]:

$$v = \pm \bar{x}_{[m]} \sqrt{\frac{2d_{BT[m]}}{\lambda_{[m]}d_{BO[m]}d_{OT[m]}}} \quad (3.32)$$

where:

- d_{BO} : distance from DVOR beacon to the obstacle;
- d_{OT} : distance from obstacle to the wind turbine;
- \bar{x} : obstacle height above (positive signal) or below (negative signal) of the direct ray between the transmitting and receiving antennas.

The v parameter is positive if the obstacle is above the direct ray between the terminals, and negative if the obstacle is below. Usually, for $v \leq -0.8$ one considers $L_{ob}(v) \approx 0$ dB, and for $v > -0.8$, the value of the additional losses can be approximated by [Corr13a]:

$$L_{ob[\text{dB}]}(v) = 6.4 + 20 \log \left(v + \sqrt{v^2 + 1} \right) \quad (3.33)$$

If there are several obstacles, then the model used will be the Deygout model [Akka09].

Finally, the total interfering power should consider the losses introduced by an obstacle, if any. So, by considering the mentioned losses in (3.29) and (3.31), the first equation is:

$$P_{riRCS[W]} = \frac{P_{t[W]} G_t G_r \lambda_{[m]}^2 \sigma_{bi[m^2]} 1}{(4\pi)^3 d_{BTi[m^2]}^2 d_{TPi[m^2]}^2 L_{ob}} \quad (3.34)$$

where:

$$L_{ob} = 10^{L_{ob[\text{dB}]} / 10} \quad (3.35)$$

- L_{ob} : losses introduced by an obstacle, in linear units;

and (3.31) is as follows:

$$P_{riD[W]} = \frac{P_{t[W]} G_t G_r \lambda_{[m^2]}^2}{(4\pi)^2 d_{BTi[m^2]}^2} |D_{i[\sqrt{m}]}|^2 \frac{d_{BTi[m]}}{d_{TPi[m]}(d_{TPi[m]} + d_{BTi[m]})} \frac{1}{L_{ob}} \quad (3.36)$$

In a scenario in which the radio link must cross a sizeable extension of water between the DVOR antenna and the wind turbine, Figure 3.10, an analysis different from the previous one is required for the determination of the interfering power received by the aircraft.

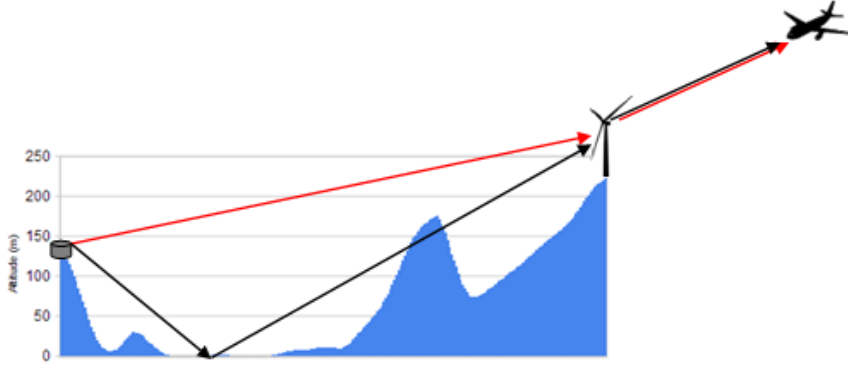


Figure 3.10 - Scenario with water.

In Figure 3.10, the power received in the aircraft of the signal represented by the red ray is determined by (3.34) and (3.36). The power of the signal pictured in black is determined taking the presence of the sea water extension into account. In this sense, in the presence of sea water (between the transmitter and the turbine), the signal in the radio link that reaches the turbine is reflected in the specular point in water, x_e , being given by [Sale02a]:

$$x_{e[km]} = \frac{h_{t[m]}}{h_{t[m]} + h_{r[m]}} d_{BT[km]} \quad (3.37)$$

where:

$$h_{t[m]} = h_{B[m]} + h'_{terrain[m]} \quad (3.38)$$

$$h_{r[m]} = h_{T[m]} + h''_{terrain[m]} \quad (3.39)$$

- $h'_{terrain}$: height of the terrain in the position of the DVOR antenna;
- $h''_{terrain}$: height of the terrain in the position of the wind turbine.

As a result, the received power for the signal reflected by the tower, in a scenario with sea water, can be calculated by:

$$P_{riRCS[W]} = \frac{P_{t[W]} G_t G_r \lambda_{[m^2]}^2 \sigma_{bi[m^2]}}{(4\pi)^3 (d_{BxeTi[m]})^2 d_{TPi[m^2]}^2} \frac{1}{L_{ob}} |\Gamma|^2 \quad (3.40)$$

where:

$$d_{BxeTi[m]} = d_{Bxe[m]} + d_{xeTi[m]} \quad (3.41)$$

- d_{Bxe} : distance between the DVOR beacon and the specular point;
- d_{xeTi} : distance between the specular point and the i^{th} wind turbine;

- $|\Gamma|$: reflection coefficient for sea water.

The received power for the signal diffracted by the blades, in the same scenario, is given by:

$$P_{riD[W]} = \frac{P_{t[W]} G_t G_r \lambda_{[m^2]}^2}{(4\pi)^2 (d_{BxeTi[m]})^2} |D_{i[\sqrt{m}]}|^2 \frac{d_{BxeTi[m]}}{d_{TPi[m]} (d_{TPi[m]} + d_{BxeTi[m]})} \frac{1}{L_{ob}} |\Gamma|^2 \quad (3.42)$$

Because the DVOR antennas under study are of the Alford Loop type (circular array), their polarisation is horizontal, and for high incidence angles the reflection coefficient in (3.40) and (3.42) is $|\Gamma| \approx 1$ [Figa12b].

The main objective of the detailed analysis undertaken is to determine CIR, represented by (C/I) , between the received powers of the direct signal and the interfering one, given by (3.43). Finally, one has to compare the calculated CIR with the typical value of CIR for the receiver, which corresponds to a minimum value acceptable, a threshold, $(C/I)_{min}$.

$$(C/I) = \frac{P_{r[W]}}{P_{rt[W]}} \quad (3.43)$$

Due to the comparison above, two different situations can occur:

- ✓ $(C/I) > (C/I)_{min}$: desirable situation, that is, good communication;
- ✓ $(C/I) < (C/I)_{min}$: there is interference in the receiver, because the power of interfering signals is higher than the direct signal one. Therefore, there is no communication in the worst case.

Only the interfering powers received by the aircraft, that is the received power of the signal reflected by the tower or the received power of the signal diffracted by the blades of the turbine, which satisfy the condition below, are taken into account in the CIR calculation.

$$P_{ri[dBm]} > P_{N[dBm]} \quad (3.44)$$

So, the average noise power, P_N , can be calculated by [Corr13b]:

$$P_{N[dBm]} = -174 + 10 \log(\Delta f_{[Hz]}) + F_{[dB]} \quad (3.45)$$

where:

- Δf : bandwidth;
- F : noise figure of the receiver equipment.

The bandwidth of the DVOR beacon is obtained from the analysis of its frequency spectrum. Therefore, according to Figure 2.3, the signal bandwidth, considering the subcarrier in $\pm 9\,960$ Hz with a deviation of ± 480 Hz, is $\Delta f_{[Hz]} = 20400$ Hz.

3.3 Flight Routes

This section introduces the methodology to be used in the simulator for the different possible aircraft positions calculation, in order to know its specific location in single points, and in route. The information presented in the section is based, mainly, on [Pint11].

In the definition of the aircraft routes a rhumb line is considered that takes the aircraft from one point to another, crossing the multiple meridians with a constant angle, being named loxodrome [Alex04]. The mentioned points are named checkpoints, which ensure that the aircraft is on course, and although both checkpoints and the angles are changing, the latter are equal when they are between two contiguous checkpoints. Besides that, each airspace route is defined by a specific identification, name, and FL.

The angles represented in all air navigation maps are the magnetic North, which are the ones that the navigation equipment measures, these angles being different from the true North that corresponds to the theoretical angle used in models. So, the loxodrome angle (angle that defines the loxodrome), which is the true North, is not the angle in the mentioned maps, and the relation between the magnetic and true angle is the following:

$$\alpha_{dec}[\text{rad}] = \alpha_{mag}[\text{rad}] - \alpha_{true}[\text{rad}] \quad (3.46)$$

where:

- α_{true} : true angle (loxodrome angle) of the route;
- α_{mag} : magnetic angle of the route;
- α_{dec} : declination angle in relation to West.

The length of the rhumb line, d_{path} , between two points ($i = A; B$) and the respective loxodrome angle are defined by the following equations [Alex04]:

$$d_{path}[\text{nmi}] = r_o[\text{nmi}] |L_B[\text{rad}] - L_A[\text{rad}]| |\sec \alpha_{true}[\text{rad}]| \quad (3.47)$$

$$\alpha_{true}[\text{rad}] = \text{arccot} \left(\frac{\sum L_B[\text{rad}] - \sum L_A[\text{rad}]}{\lambda_B[\text{rad}] - \lambda_A[\text{rad}]} \right) \quad (3.48)$$

where:

$$\sum L_i[\text{rad}] = \ln \left(\tan \left(\frac{\pi}{4} + \frac{L_i[\text{rad}]}{2} \right) \right) \quad (3.49)$$

- $\sum L_i$: vertical spacing of the parallel of latitude in point i ;
- L_i : parallel of latitude in point i ;
- λ_i : longitude in point i .

The true angle is calculated from (3.48) and (3.49). In this way, any declination angle can be obtained from (3.46), using the true angle and the magnetic angle given by the air navigation maps.

The longitude, in (3.48), which is defined as East-West coordinate, is negative and when using trigonometric functions it is necessary to take into account that there are two possible solutions. Besides this, there is a limit case, which occurs for an aircraft that travels from one checkpoint to

another always in the same parallel of latitude, which means $L_A = L_B = L$ and, from (3.48), α_{true} equal to $\pi/2$ or $3\pi/2$. Consequently, in this situation, instead of (3.47), and because $L_B - L_A = 0$, one uses the following equation:

$$d_{path[nmi]} = r_{o[nmi]} \frac{\lambda_B[\text{rad}] - \lambda_A[\text{rad}]}{\sec L[\text{rad}]} \quad (3.50)$$

In (3.50), and for a spherical Earth, $\sec L$ denotes the local stretching factor at parallel of latitude L . If an aircraft travels in the equator, this equation is equal to (3.47) for an angle of 0° or 180° [Alex04].

Unlike single points, every other test types have to define a certain number of points in the path, so that the number of test points for each path must be taken into consideration. Thus, the coordinates of the path separated by a given interval are:

$$d_{inter[nmi]} = \frac{d_{path[nmi]}}{N_{points} - 1} \quad (3.51)$$

$$L_i[\text{rad}] = L_{initial}[\text{rad}] + \frac{d_{inter[nmi]}}{r_{o[nmi]} \times |\sec \alpha_{true}[\text{rad}]|} \times (i + 1) \quad (3.52)$$

$$\lambda_i[\text{rad}] = \lambda_{initial}[\text{rad}] - \frac{\sum L_i[\text{rad}] - \sum L_{initial}[\text{rad}]}{\cot \alpha_{true}[\text{rad}]} \quad (3.53)$$

in which:

- d_{inter} : distance between fixed intervals;
- N_{points} : number of points to test in the path;
- i : current position (if $i = 0$ is the initial position and if $i = N_{points} - 1$ is the final position).

In the above analysis, it should be noticed that the referred latitudes and longitudes may be positive or negative according to the aircraft position. So, if the aircraft is in the North hemisphere the latitude is positive, and if it is relative to the East the longitude is also positive.

3.4 Implementation in a Simulator

In this section, one describes the main structure of the simulator developed entirely within the framework of this Thesis, which computes the CIR for some possible aircraft positions. Also, the auxiliary functions and input files, which allowed one to implement the simulator in Matlab, are depicted.

In order to develop the simulator, three of the models from Section 3.2 were implemented: the tower RCS model, the blades model, and the Knife-edge/Deygout model. The first two concern the modelling of each turbine, namely for the tower and the blades, being auxiliary functions, whereas the last of these three models estimates the losses introduced by an obstacle, being implemented in the main function. Besides these auxiliary functions, other three were implemented:

- GainVOR: This function calculates the gain of the transmitting antenna based on the turbine's and aircraft's positions;
- Routes: This function calculates the aircraft coordinates in route, through the input file with specific positions of the aircraft, with the expressions presented in Section 3.3.

Hence, aided by all auxiliary functions and the simulator (main function), a MatLab script determines the CIR for each study scenario, based on the total received and interfering powers obtained by the simulator. In this regard, the script comprises of specific input parameters needed to run the simulator and of three input files, in a .txt format, which are:

- Name.txt;
- DataName.txt;
- RouteName.txt.

Name.txt contains, for each point in the distance between the DVOR beacon and the turbine, the height of the terrain, thus, this file is structured into two columns: one for the several points of the distance and the other for the terrain's height. These data are obtained by [ScGo13]. DataName.txt contains, in one column, the latitude, longitude in decimal degrees and height (including the height of the terrain) of the DVOR and in the other column the same information for the turbine. Finally, RouteName.txt is composed of two columns corresponding to the latitude and longitude of the aircraft in decimal degrees, and three rows, in which the first one corresponds to the initial point of the route, the second one to the position of the DVOR in the route, and the latter to the final point of the study route.

For this simulator, several simulation parameters, which are also input parameters, can be modified depending on the scenario under analysis, such as:

- Terrain profile;
- Flight route of the aircraft;
- h_B : Height of the DVOR beacon;
- h_T : Height of the wind turbine;
- f : Frequency;
- P_t : Transmitted power;
- h : Height of the tower;
- G_t : Gain of the transmitting antenna;
- FL to study.

The structure of the simulator is depicted in Figure 3.11, in which is notorious the split into two different groups: structure of the simulator, in orange, and data flow needed for the simulator, in green and blue.

The blue block, as its name indicates, allows designing the terrain profile, including the first Fresnel ellipsoid, which depends on the scenario under study, with the Name.txt file as the input parameter required for this purpose, as well as the height of the DVOR beacon and the wind turbine, and the

frequency. The resulting profile is one of the simulation parameters of the simulator structure group.

In the simulation itself, first of all, it is verified if the terrain has an extension of sea water or not, in order to perform a proper analysis according to the study scenario. Afterwards, the losses introduced by an obstacle are estimated through the model presented in Subsection 3.2.3. Together with the aid of the parameters resulting from the auxiliary scripts, the received (from the direct signal) and interfering (from the reflected/diffracted signal) powers are determined. Finally, the CIR of the link for the case under study is estimated in the auxiliary script. So, the inputs of the simulator are the terrain profile, the points to define the flight route, the height of the wind turbine, of the tower and of the DVOR beacon, the frequency, the transmitting power, and the FL to study.

The block “Aircraft’s routes” gives the user the several positions of the aircraft in the study route, in spherical coordinates, from a file with three specific points (the initial point of the route, the DVOR point and the final one). For this function, the input parameters are the points to define the flight route under study and the FL to analyse.

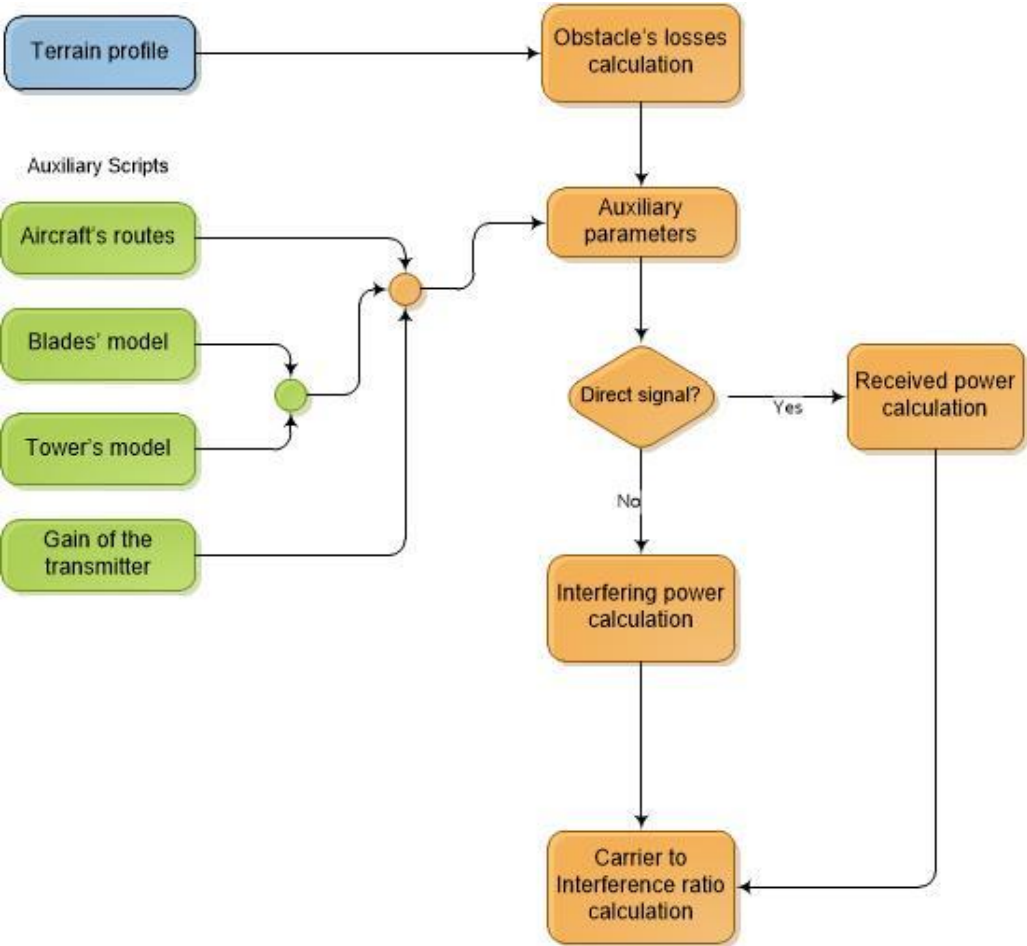


Figure 3.11 - General structure of the simulator.

The auxiliary function “Blades’ model” estimates the maximum and minimum diffraction coefficient of each blade for different rotation angles and of the rotor, and for the dominant wind direction, taking into consideration the position of the aircraft in route obtained by the function “Aircraft’s routes”, whereas the auxiliary function “Tower’s model” estimates the RCS for the tower of the turbine under

study. Therefore, the main input parameters of these functions are the points to define the flight route for the aircraft and the frequency. Besides this, for these functions, the position of the aircraft determined by the function “Aircraft’s routes” is required, and function “Tower’s model” needs to have the height of the tower of the wind turbine.

Finally, the auxiliary function “Gain of the transmitter” determines the gain of the transmitting antenna in the direction of the turbine (in the case of the diffracted/reflected signal) and the aircraft (in the case of the direct signal), depending of the scenario under analysis; for this function, the input parameters are the azimuth and elevation of the turbine and the aircraft.

3.5 Simulator Assessment

In this section, the simulator developed and described in Section 3.4, is assessed to validate the implemented models and the generated output. Therefore, extreme cases were simulated, such as scenarios with and without water, in order to compare the results obtained, and to conclude that the simulator works according to the models.

First, in order to verify whether the simulator is working as anticipated, a simple scenario is tested, with a DVOR beacon installed in Porto Santo, a wind farm composed of two wind turbines and located approximately 4 km from the transmitter, and one flight route defined randomly to the FL150, as portrayed in Figure 3.12. In the defined flight route (line in red) the aircraft moves in the direction from South-West (SW) to North-East (NE), and the wind farm is in line with the aircraft route and with the DVOR, which is installed at 19.88 km from the initial point of the flight route. For the selected FL, the DVOR has a maximum range of approximately 74.08 km, in order to guarantee the safe communication with an aircraft that is between 1 000 ft and 18 000 ft, Table 2.1.



Figure 3.12 - Scenario for the DVOR in Porto Santo.

In a first instance, the simulator calculates the losses introduced by the terrain for both wind turbines, when its orography causes obstacles to the propagation of the signal transmitted by the beacon. In this sense, Figure 3.13 portrays the profile of the terrain, as well as the first Fresnel ellipsoid, for the nearest wind turbine of the beacon, in which an obstacle inside of the ellipsoid that is obstructing the direct ray between the beacon and the turbine is noticeable. For the farthest turbine, the figure obtained by the simulator is similar to the previous one, notwithstanding the height of the obstacle between the beacon and the farthest turbine is higher than the height of the obstacle for the situation in the figure.

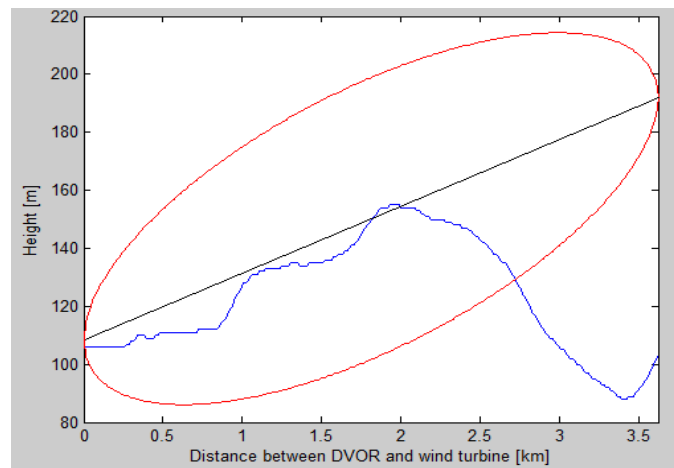


Figure 3.13 - Terrain profile and Fresnel ellipsoid for the Porto Santo scenario.

Based on the losses due to the presence of obstacles, Figure 3.14 depicted the received power of the direct signal, P_r , the interfering power of the signal reflected by the tower, $P_{rRCS, far}$ and $P_{rRCS, near}$, for the farthest and nearest wind turbines, respectively, and the interfering power for the maximum diffraction coefficient of the signal diffracted by the blades, $P_{rD, far}$ and $P_{rD, near}$, for the farthest and nearest wind turbines, respectively, all the powers introduced in Subsection 3.2.3. In order to get a comparison between the power of the direct signal and the interfering ones, and to ascertain the influence of the turbine on the signal, the sensitivity of the receiver, $P_{r, min}$, is also presented in Figure 3.14.

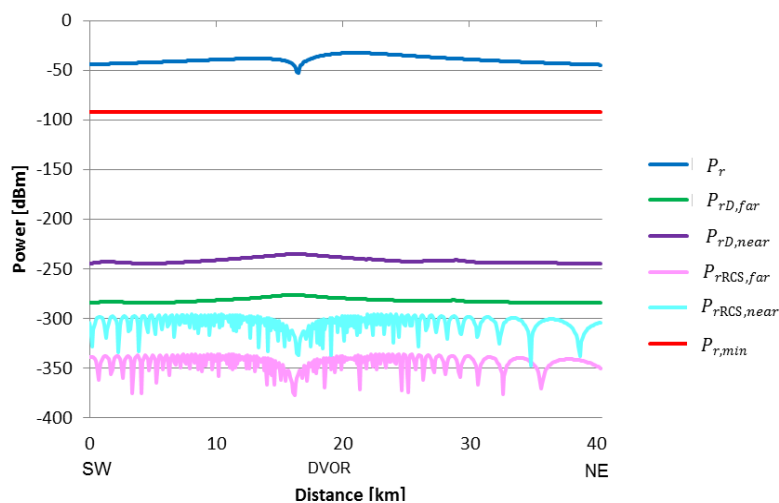


Figure 3.14 - Received and interfering powers in the Porto Santo Island scenario.

From the analysis of Figure 3.14, it is noticeable that the power of the direct signal received by the aircraft is higher than the interfering powers caused by the presence of two turbines. This situation occurs due to the fact that the signal transmitted by the DVOR beacon and reflected or diffracted by the turbines is attenuated by the orography of the terrain, originating values of interfering power very small compared to the sensitivity of the receiver. Another important aspect to emphasise is related with the values of the received power of the direct signal. The transmitted power is approximately -13 dBm, so, as is presented in Figure 3.14 the simulator determines properly the aforesaid power, considering that its values are around -45 dBm and lower than the transmitted power. This decreasing of the received power in comparison with the transmitted one is due to the fact that the power of the signal reflected/diffracted by the structures of the wind turbine gives rise to an interfering power that causes an attenuation of the power of the direct signal. So, the transmitted power should be much higher than the received power of the direct signal.

The interfering powers due to the signal reflected by the tower for both farthest and nearest turbines is much lower than the thermal noise, which is approximately -174 dBm/Hz for a 50 Ω system at room temperature [Sale02c]; its depiction in Figure 3.14 aims at demonstrating that, for the several defined scenarios, the developed simulator calculates all the discussed powers, even if their values are neglected.

Subsequently, based on the interfering power for the maximum diffraction coefficient of the blades and for the maximum diffraction coefficient in the prevailing wind direction, the simulator determines the CIR along the flight route, as shown in Figure 3.15. In this case, giving the fact that the interfering power of the signal reflected by the tower is rather small, the determination of the CIR takes into account only the interfering power of the signal diffracted by the blades. Therefore, following the analysis of the powers, both determined CIRs, one based on the interfering power for the maximum diffraction coefficient, $CIR_{D,max}$, and another based on the interfering power for the maximum diffraction coefficient in the prevailing wind direction, $CIR_{D,NW}$, are much higher than the minimum acceptable value, CIR_{min} .

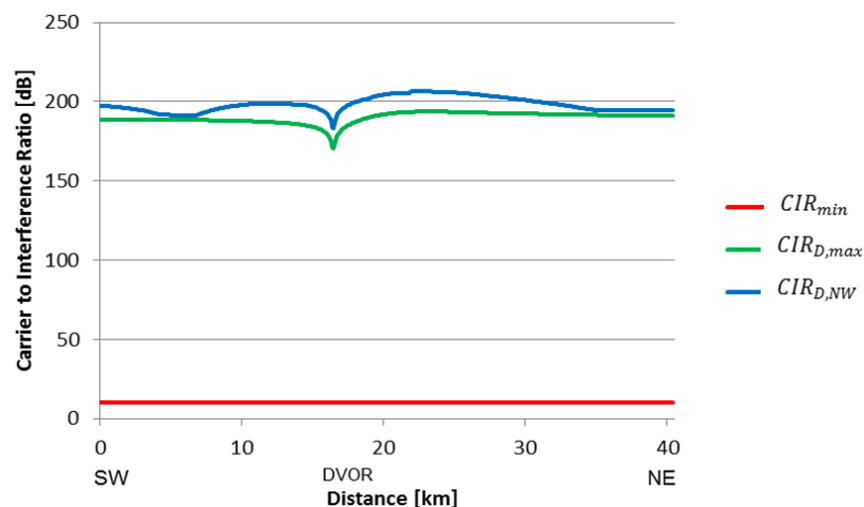


Figure 3.15 - Carrier to Interference Ratio in the Porto Santo Island scenario.

So, as expected, the wind turbines do not cause interference problems in the received signal by the aircraft along of the defined flight route.

Subsequently, a scenario with a sizeable extension of sea water between the DVOR beacon and the wind turbines located at approximately 5 km from the antenna is simulated, in order to guarantee that the simulator also works for whatsoever scenario under analysis, regardless of the type of the terrain. Besides this and as the previous scenario, one has selected one random flight route, with the same FL, in which the aircraft moves in the direction from SW to NE, and the wind farm is located in the left side of the DVOR, which is in line with the aircraft and is installed at 59.83 km from the initial point of the flight route. This scenario is portrayed in Figure 3.16.



Figure 3.16 - Scenario for the DVOR in Horta.

In this case, it is required to separate the total path between the DVOR beacon and the turbines into two distinct paths, and to analyse both separately. Thus, the first path to analyse is between the DVOR beacon and the specular point in which occurs the reflection of the signal, and the second path is between the specular point and the wind turbines.

In Figure 3.17, one presents the profile of the terrain for the scenario under study and for the nearest wind turbine, in which is notorious the two aforesaid paths, and for each one the direct ray and the first Fresnel ellipsoid, as well as the obstacles that obstruct the latter. For the farthest wind turbine, the profile of the terrain is similar to the previous one, considering that for the scenario defined by the farthest wind turbine the height of the obstacle is lower than the height of the obstacles introduced in the scenario defined by the nearest wind turbine. So, the losses introduced by the obstacle in the scenario defined by the farthest wind turbine are lower than the losses introduced in the other scenario.

Based on the profile of the terrain, the losses introduced by the obstacles are calculated for the scenario defined by both wind turbines, and then the simulator determines the power of the direct

signal received by the aircraft, as well as the interfering power of the signal reflected and diffracted by the tower and the blades, respectively.

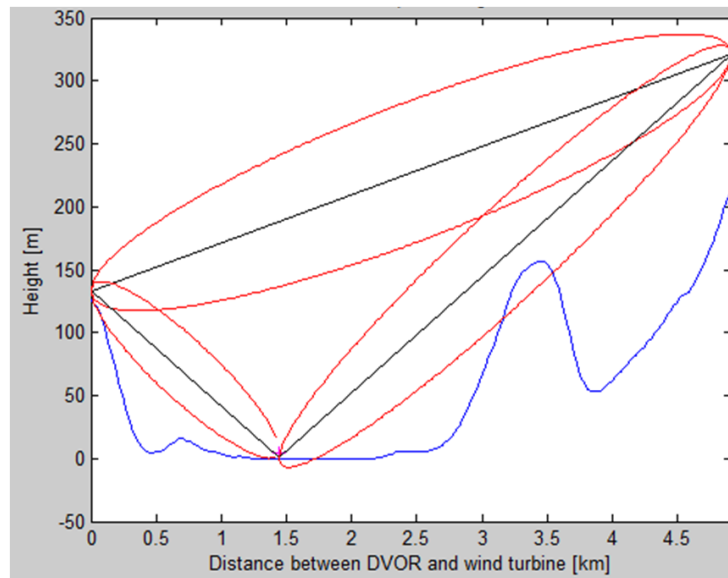


Figure 3.17 - Terrain profile and Fresnel ellipsoid for the Porto Santo scenario.

The output of the simulator for the determination of the powers is shown in Figure 3.18, and considering that the introduced losses are lower for the second scenario, for the farthest wind turbine the interfering power both the signal reflected by the tower, $P_{rRCS, far}$, as the signal diffracted by the blades, $P_{rD, far}$, is higher than the interfering power determined for the nearest wind turbine ($P_{rRCS, near}$ for the reflected signal and $P_{rD, near}$ for the diffracted signal), and both cases are lower than the sensitivity of the receiver, $P_{r, min}$. Also, the power of the direct signal, P_r , received by the aircraft is presented in the figure, and as for the first scenario in test, this received power is lower than the transmitted power.

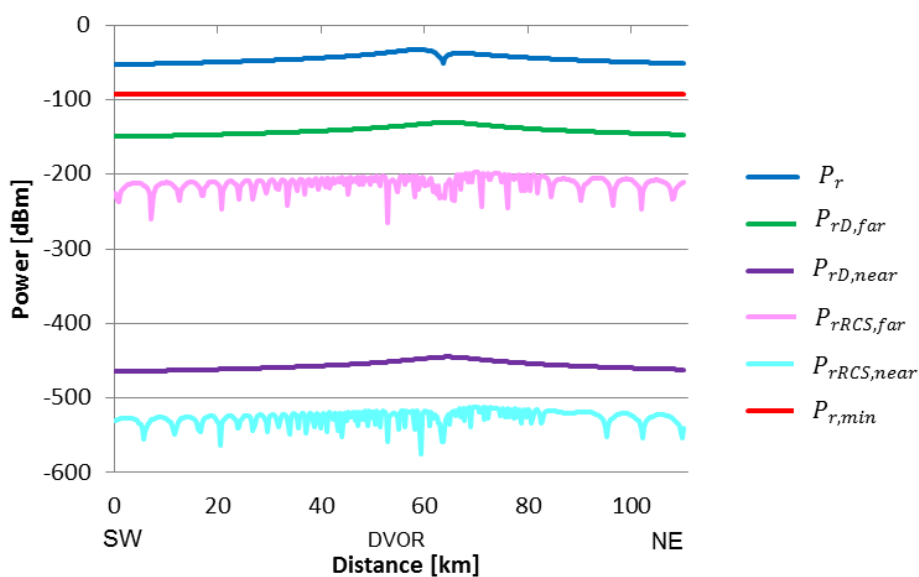


Figure 3.18 – Received and interfering powers in the Horta Island scenario.

Afterwards, with the aid of the received and interfering powers, one has determined the CIR for the

maximum diffraction coefficient, $CIR_{D,max}$, and for the maximum coefficient in the dominant wind direction, $CIR_{D,NW}$, Figure 3.19. In this scenario, as expected, the turbines do not cause interference problems on the DVOR beacon, considering that the determined CIRs are above the minimum acceptable value, CIR_{min} , as shown in Figure 3.19.

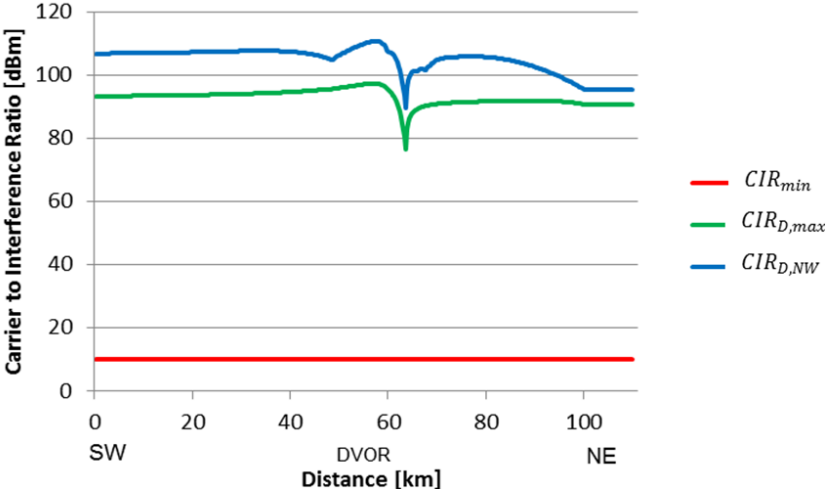


Figure 3.19 - Carrier to Interference Ratio in the Horta Island scenario.

Therefore, from the results obtained for the two different test scenarios (Porto Santo Island and Horta, Faial Island), in which the turbines are located at a distance roughly similar in both cases, one can conclude that the simulator is working according to the studied models, for both type of terrains (with and without the influence of sea water).

Chapter 4

Results and Data Analysis

In this chapter, different study scenarios are defined from the aeronautical navigation systems location and the wind turbines generators close by, and, based on a developed simulator, results are provided and analysed. In a final stage, the exclusion regions obtained from the previous analysis are defined.

4.1 Scenarios Definition

In this section, one presents the several scenarios, defined by a DVOR beacon and a wind farm in its vicinity, to be analysed, and it is also presented the several flight routes to consider in the simulations in order to define the test positions of the aircraft on the selected flight route, as discussed in Section 3.3.

NAV Portugal has several VOR systems all over the country, Azores and Madeira included, thereby strategically positioned in order to allow NAV to fully execute its air traffic control mission, as well as to ensure air traffic safety.

Considering that the communication with VOR systems is permanent from the moment the aircraft receives take off authorisation, the location (longitude and latitude coordinates) of each system should be indicated to the pilot and to the regional air traffic control centre, in order to ensure the aircraft's free and safe route to its final destination. Also, each of these systems was designed to operate at a certain frequency and transmit a certain power, Table 4.1, which allows defining the operating features of each CVOR or DVORs.

Table 4.1 - Characteristics of CVOR and DVORs located in Portugal (in [NAV12c]).

Site	Type	$f_{[MHz]}$	Lat _[DD°MM'SS,SS'']	Long _[DD°MM'SS,SS'']	$P_{[W]}$
Santa Maria	CVOR	113.7	36°57'46.68"	-25° 9'59.04"	50
Espichel	DVOR	112.5	38°25'27.19"	-9°11'8.92"	50
Fátima	DVOR	113.5	39°39'56.48"	-8°29'33.60"	50
Faro	DVOR	112.8	37° 0'48.60"	-7°58'30.23"	70
Flores	DVOR	113.3	39°27'12.93"	-31°12'37.81"	50
Funchal	DVOR	112.2	32°44'49.69"	-16°42'19.62"	50
Horta	DVOR	112.7	38°31'10.09"	-28°37'23.58"	50
Lisbon	DVOR	114.8	38°53'15.86"	-9° 9'45.81"	70
Nisa	DVOR	115.5	39°33'52.81"	-7°54'52.51"	50
Ponta Delgada	DVOR	114.5	37°50'46.15"	-25°45'30.64"	50
Porto Santo	DVOR	114.9	33° 5'25.36"	-16°21'2.31"	50
Porto	DVOR	114.1	41°16'22.83"	-8°41'15.98"	50
Sagres	DVOR	113.9	37° 5'1.55"	-8°56'47.29"	80
Viseu	DVOR	113.1	40°43'24.42"	-7°53'8.99"	50

Being fundamental to identify every possible scenario, to define later the exclusion regions in Section 4.3, based on the analysis done in Section 4.2, it is necessary to know the location (longitude and latitude coordinates) of every wind farm on the whole Portuguese territory, islands included (Appendix A). Considering that only wind turbines up to a maximum distance of 15 km [ICAO09] will cause interference in the aeronautical navigation systems, Figure 4.1 to Figure 4.3 show only the

generators (blue tag) that satisfy this specification. Also the CVOR and DVORs are tagged (yellow tag) in the map, as a reference to the wind turbines generators representation.



Figure 4.1 - DVOR and wind turbines location in Madeira Archipelago.



Figure 4.2 - CVOR or DVOR and wind turbines location in Azores Archipelago.

In a total of 14 aeronautical navigation aids, presented in Table 4.1, only 8 are located in areas prone to disturbance due to the presence of wind turbines in a radius up to 15 km from the beacon location, as the previous figures portray. The number of wind turbines that may create interference problems

depends on the scenario under analysis, this information being presented in Table 4.2.



Figure 4.3 - DVOR and wind turbines location in mainland Portugal.

Considering the above, each scenario to be studied is composed of a CVOR or DVOR beacon, a wind farm and an aircraft in route. Thus, a total of 7 DVOR beacons and 1 CVOR beacon, that is 8 beacons in total, 27 wind turbines, located at different distances from the DVOR, and 18 different routes were analysed. For the established scenarios, the receiver (aircraft) is characterised by a sensitivity of -92 dBm, an antenna with a receiving gain of 2 dB and a minimum CIR of 10 dB [NAV12c].

As the aim of this Thesis is to estimate the minimum distance from which the wind turbine may be located in order to prevent disturbance in the CVOR and DVOR beacons, for the defined scenarios it is required to assess the influence of the nearest (the worst case) and farthest (the better case) turbine to the beacon. In this sense, in Table 4.2, besides the information mentioned previously, one also presents the minimum and maximum distances of a turbine in the wind farm, as well as the name of the wind farm located in the vicinity of each CVOR or DVOR beacon.

In order to accomplish this analysis, each of the scenarios is simulated for a specific route and for two different FLs, the maximum (FL450) and minimum (FL55), being presented in Table 3.2. The

simulation of the scenarios to different FLs enables to assess the possible influence of the variation of the FL together with the variation of the location of the wind turbines.

Table 4.2 - Characterisation of each scenario.

Site (CVOR or DVOR)	Wind farm	Number of wind turbine	Nearest [km]	Farthest [km]
Santa Maria	Figueiral	3	3.4	3.7
Fátima	Pias Longas	11	8.8	12.6
Flores	Boca da Vereda	2	4.2	4.4
Horta	Salão	6	4.9	5.2
Lisbon	Arruda	3	8.8	9.6
	Sobral	10	8.8	11.2
	Almargem do Bispo	11	4.1	10.6
	Bolores	9	5.9	7.9
	Fanhões	9	1.2	2
Nisa	Serra da Lage	6	9.1	10
	Serra da Amêndoa	14	10.1	12.3
	Zimbreira	1	7.7	
Porto Santo	Cabeço do Carvalho	3	3.6	3.8
Sagres	Barão de S. João	13	13	14.8

Following the previous definition of the scenarios, it was defined the flight routes to study for each scenario, and in order to facilitate the assessment of the simulations results, the several scenarios are divided according to the territorial units for statistics of Portugal, which in this case are: Lisbon Region, Centre and Algarve Regions, and Madeira and Azores Autonomous Regions.

4.1.1 Lisbon Region Scenario

The simulation of the Lisbon scenario requires the definition of the test positions of the aircraft for the flight routes that pass through the DVOR beacon. So, Figure 4.4 portrays the two selected routes to simulate this scenario.

These two routes, route UN870 and route Y207, are selected in order to overlie all the possibilities of aircraft approach to the location of the DVOR beacon in Lisbon, as well as the passage by the beacon. In the former, the aircraft flies in the direction from SW to NE and in the latter the aircraft flies in the direction from NE to SW.

The coordinates displayed in Figure 4.4, and in every airspace chart, starts by the direction (North (N) / South (S) or East (E) / West (W)) and then degrees, minutes and seconds separate by a space; however, the coordinates are converted to decimal ones, to include in the input file of the developed simulator, as shown in Table F.1.

For each of these two flight routes, as well as for the remaining routes of the other scenarios under

test, in the simulations the routes are limited to a range of 60 km from the position of the DVOR, for each section of the flight routes, regardless of the total distance travelled by the aircraft.

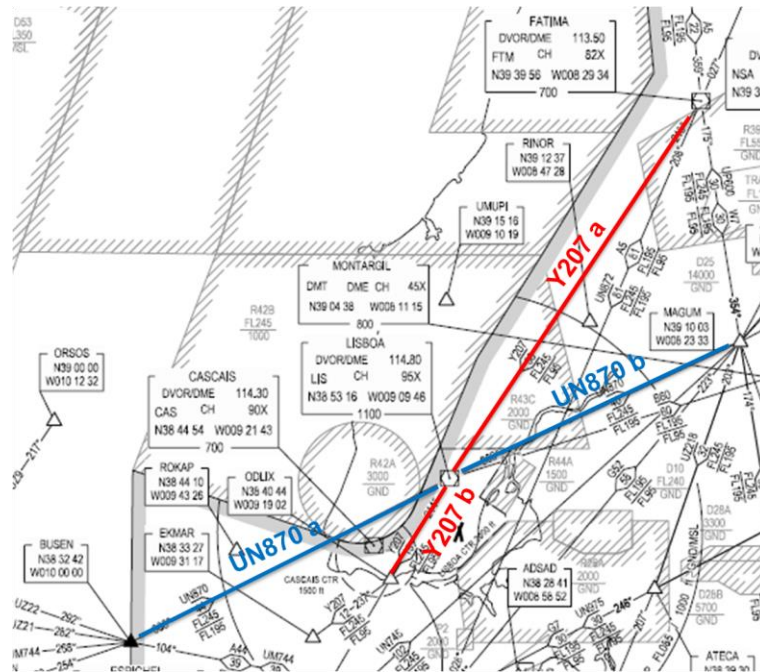


Figure 4.4 - Flight routes for the Lisbon scenario (adapted from [NAV12c]).

4.1.2 Centre and Algarve Regions Scenarios

In the Centre region, one has assessed the scenarios of Fátima and Nisa DVOR beacons. The performed analysis is similar to the one accomplished for the scenarios defined in Lisbon region.

The simulation of the Fátima scenario requires the selection of the flight routes that pass through the corresponding DVOR beacon, in order to define the test points of the aircraft in the selected routes. So, the input file with the initial and final positions of each section of the routes is presented in Table F.2, based on the flight routes portrayed in Figure 4.5. The three flight routes, route A5, route UN870 and route UP600, that were selected comprise different possibilities of direction of flight around the location of the DVOR beacon installed in Fátima, as well as the wind farm to study in this scenario.

In the three flight routes, routes A5, UN872 and UP600, the aircraft flies in the direction from North-West (NW) to SW, in the direction from NE to SW and in the direction from SE to NW, respectively. These different possibilities enable to assess the influence of the wind turbines in the beacon for distinct positions of the aircraft.

Finally, to conclude the assessment of the scenarios in the Centre region, the choice of the flight routes for the Nisa scenario is required. Thus, Figure 4.6 depicts the two selected flight routes, and the corresponding initial and final latitude and longitude of each section of each of the two routes are presented in Table F.3. For this scenario, in the selected routes, routes G52 and R72, the aircraft flies in the direction from SW to NE and in the direction from S to N, respectively.

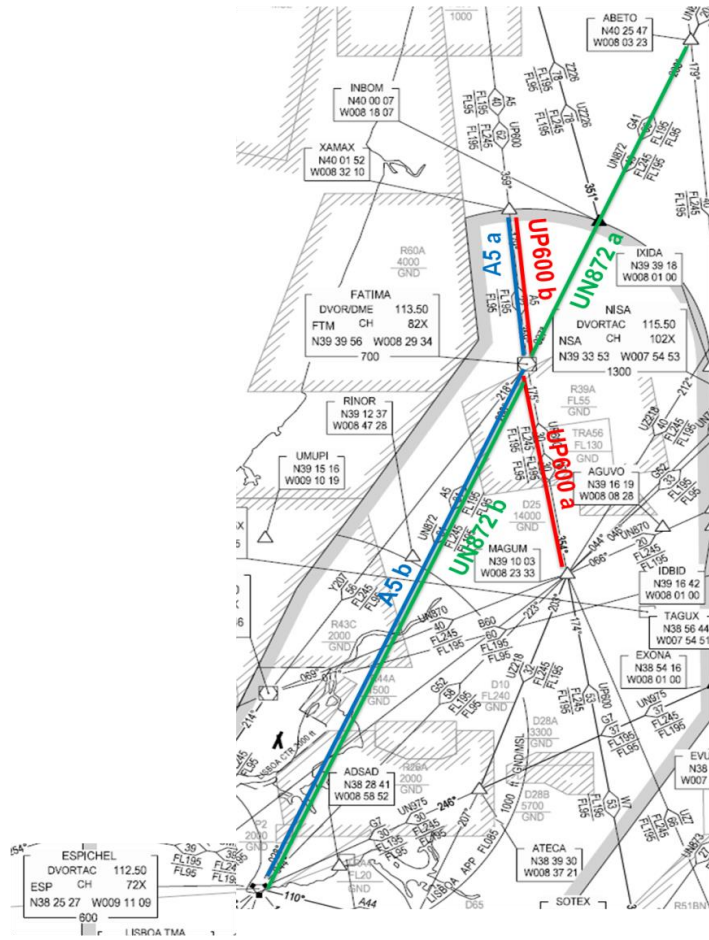


Figure 4.5 - Flight routes for Fátima scenario (adapted from [NAV12c]).



Figure 4.6 - Flight routes for Nisa scenario (adapted from [NAV12c]).

In mainland Portugal, the last scenario to analyse is the DVOR beacon located in Sagres. So, the flight route used to test the referred scenario is depicted in Figure 4.7, and the corresponding coordinates of the initial and final points of each section are presented in Table F.4.

In the flight route in which the aircrafts are controlled by the DVOR beacon of Sagres, the ‘holding’ in the vertical of the beacon (the grey box) can be made between the FL100 and FL140. So, for this specific scenario, only these FLs were tested in the simulations.

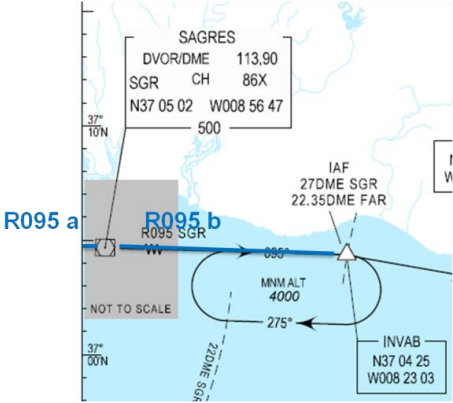


Figure 4.7 - Flight routes for Sagres scenario (adapted from [NAV12c]).

4.1.3 Autonomous Regions Scenarios

In addition to the previous study, and to conclude the analysis of all the scenarios defined in Section 4.1, the archipelagos of Madeira and Azores are taken into account, and the results obtained by the simulator are assessed.

In Porto Santo island, three flight routes were selected to simulate different positions of the aircraft relative to the wind farm and the DVOR beacon location. The chosen flight routes are portrayed in Figure 4.8, and the coordinates of the initial and final point of each section are presented in Table F.5.

For this scenario, in the routes UQ11 and R1, the aircraft flies in the direction from SW to NE, and in the route B18, the aircraft flies in the direction from SE to NE.

In the Azores archipelago, one studied three islands (Flores, Horta and Santa Maria island), and for each one different flight routes were selected. So, Figure 4.9 portrays the several routes for each of the islands, and Table F.6 presents the input test points.

In the Flores scenario, the routes H141 and H142 have the same second section, because the other sections of the flight routes lie in the Lajes military control area. The same situation occurs for routes H131 and H132 in the Horta scenario. Besides this, for the DVOR beacon of Flores, the selection of the routes takes into consideration the location of the wind farm and the beacon relative to the position of the aircraft in the selected routes. For the Santa Maria scenario, the flight routes were defined in order to overlie all the possibilities of aircraft approach to the location of the CVOR beacon, as well as the passage by the beacon.

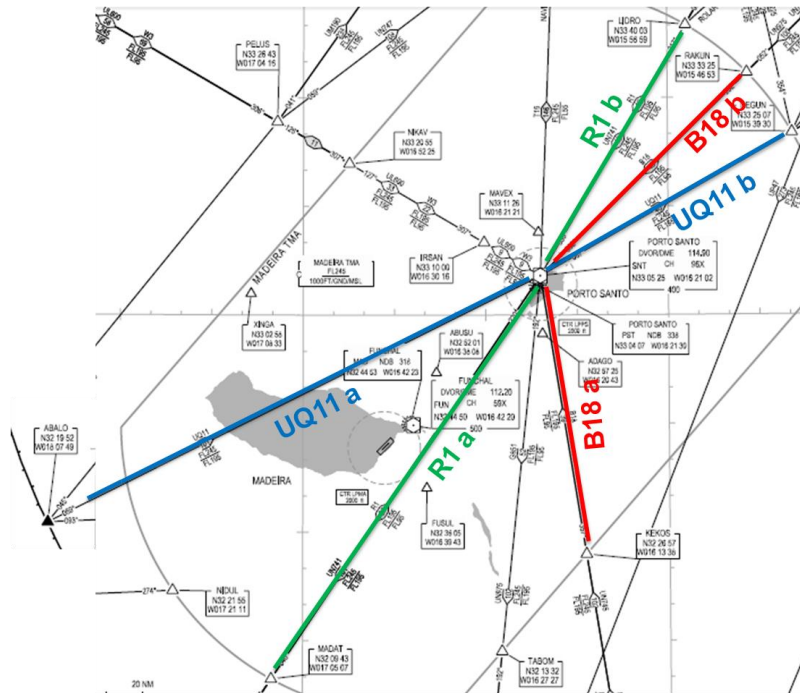


Figure 4.8 - Flight routes for Porto Santo scenario (adapted from [NAV12c]).

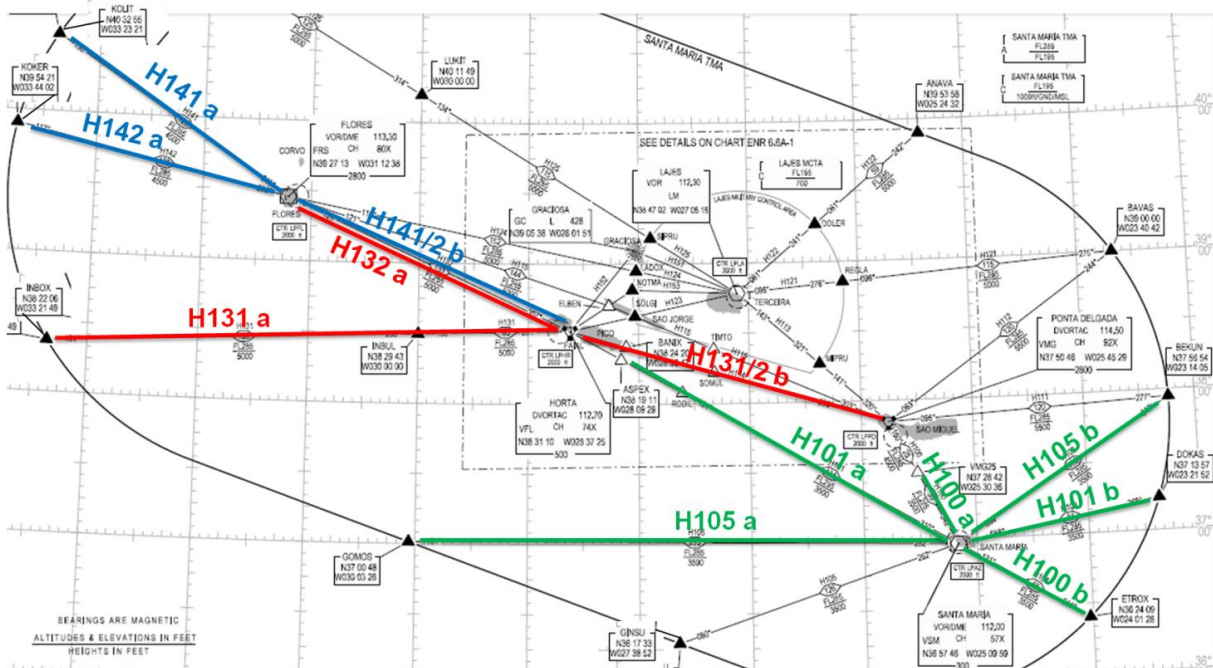


Figure 4.9 - Flight routes for Flores, Horta and Santa Maria scenarios (adapted from [NAV12c]).

4.2 Simulator Results and Analysis

In this section, for each defined scenario, one presents an analysis of the impact of the wind turbines in the aeronautical navigation aids based on the results obtained for the power of the signals that

reaches the aircraft and the comparison between the CIR of the system under study and the typical value of CIR along the flight route.

As explained in Section 3.2, the assessment of the turbines influence in the CVOR and DVOR beacons depends on the wind turbine modelling, mainly the blades model. The tower model is neglected, since on the flight route the interfering power due to the signal that is reflected by the tower is much less than both the sensitivity of the receiver and the noise power, as depicted in the figures of the Section 3.5.

From the aforesaid assessment, one obtained the interference distance, that is, the distance at which there are problems of communication between the CVOR or DVOR beacons under analysis, and the aircraft due to the presence of a wind farm in the vicinity of the transmitter, which originates a received power of the diffracted signal higher than the received power of the direct one, and consequently values of CIR in a certain range less than 10 dB.

4.2.1 Lisbon Region Scenario

In the simulation of the Lisbon region scenario, the diffraction coefficient for the signal diffracted by the blades is determined in order to determine the interfering power received by the aircraft. Hence, for the DVOR in Lisbon and Sobral wind farm, one took the flight route Y207, the FL55 and considering the farthest wind turbine of the beacon, Figure 4.10 showing the variation of the diffraction coefficient for the rotation of the blades' rotor, in the horizontal plane, and Figure 4.11 the variation for the rotation of the blades, in the vertical plane.

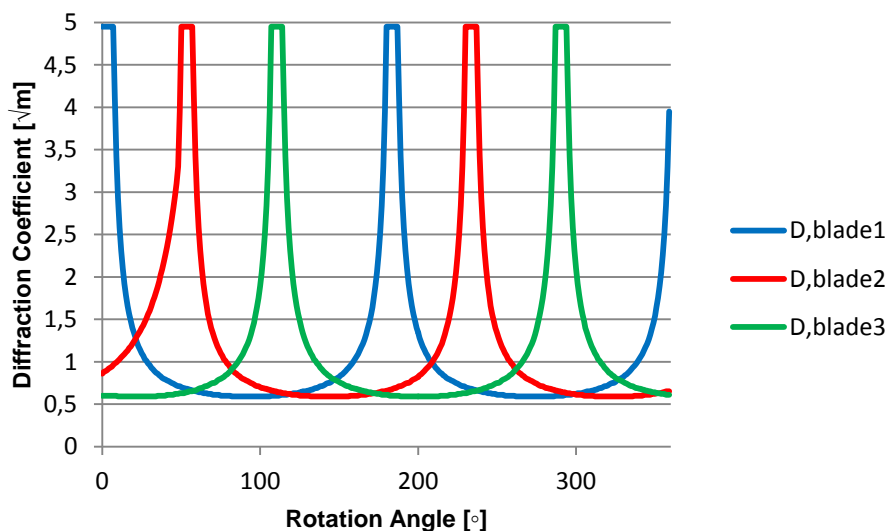


Figure 4.10 - Variation of the diffraction coefficient for the rotation of the blades' rotor.

In both Figure 4.10 and Figure 4.11, it is noticeable the periodic behaviour of the diffraction coefficient with the variation of the rotation angles for each blade, taking into consideration that each one is 120° from the others, hence, the verified difference between the representation of the coefficient for each blade. Furthermore, in Figure 4.10 the differences in the values of the diffraction coefficient

between the blade 1 and blades 2 and 3 is due to the variation of the azimuth of the aircraft on the selected flight route relative to the position of the wind turbine.

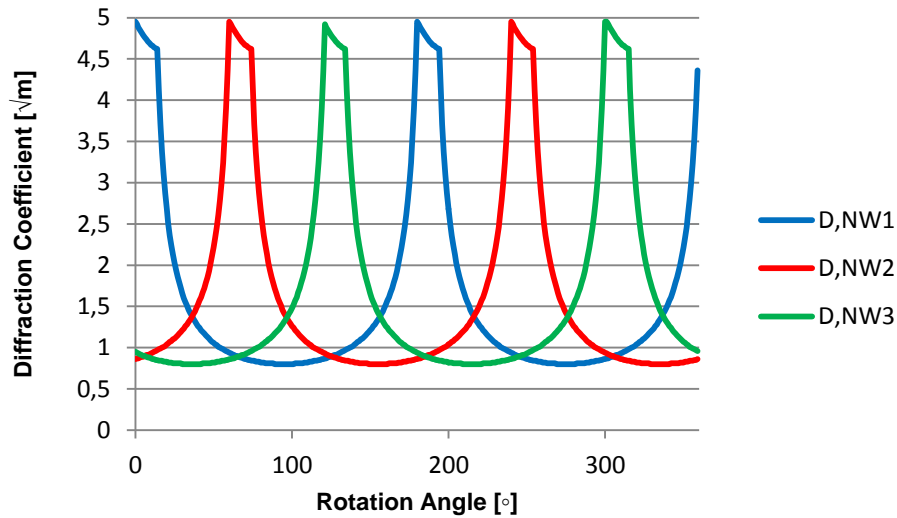


Figure 4.11 - Variation of the diffraction coefficient for the rotation of the blades.

The output of the simulator gives the received power of the direct signal and the interfering power calculated for the nearest and farthest wind turbine of the Sobral wind farm. Figure 4.12 presents the comparison between the sensitivity of the receiver and the most significant powers received by the aircraft, that is, the power of the direct signal and the power of the signal diffracted by the blades for the maximum diffraction coefficient.

In this case, as well as in the following one, the interfering power for the minimum diffraction coefficient of each of the three blades, and the minimum diffraction coefficient for the prevailing wind direction, that are less than the sensitivity of the receiver and the thermal noise are neglected, as they will not contribute to the determination of the CIR.

The two received powers for the nearest and the farthest wind turbines are the ones portrayed in Figure 4.12, in which $P_{rD, far}$ corresponds to the interfering power for the farthest wind turbine case, $P_{rD, near}$ to the interfering power for the nearest one, and P_r corresponds to the case of the received power of the direct signal.

In Figure 4.12, and for the route under analysis, the aircraft flies in the direction from NE to SW and in the instant that it passes by the location of the DVOR beacon, the wind turbine, which influence in the signal is being considered, is on the right of the aircraft. The DVOR beacon is located 103 km from the starting point of the route, and the wind turbine is 11.2 km from the beacon. So, it is noticeable that the interfering powers, both for the nearest turbine, $P_{rD, near}$, as for the farthest turbine, $P_{rD, far}$, increases when the distance between the aircraft and the beacon decreases, and the opposite occurs when the distance increases. Besides this, the interfering powers have maximum values in the region around the beacon and the turbine; however, along the flight, for the route even in this critical region, these powers are lower than the sensitivity of the receiver. And, the received power of the direct signal is lower than the transmitted one, since the values of the first are around -52 dBm and -20 dBm, the

latter is approximately -11 dBm.

In the aforesaid zone, the received power of the direct signal has minimum and maximum values due to the radiation pattern of the transmitting antenna in the vertical plane, which is similar to the dipole one.

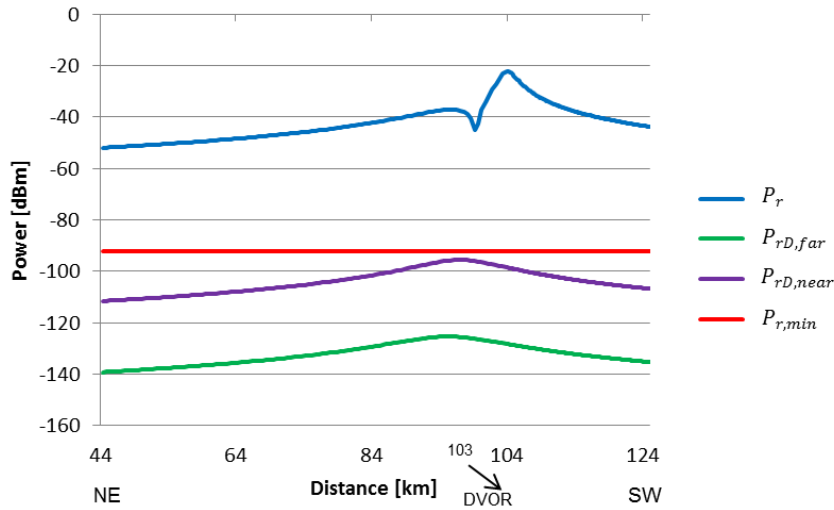


Figure 4.12 - Received and interfering powers for Lisbon scenario and Sobral wind farm.

Finally, to complete the assessment of the Lisbon scenario for the Sobral wind farm, the CIR for the maximum interfering power of the blades, $CIR_{D,max}$, and for the wind dominant direction, $CIR_{D,NW}$, is depicted in Figure 4.13, as well as the minimum CIR, CIR_{min} .

In the prevailing wind direction, the CIR is considerably greater than the minimum value. This is due to the fact that the interfering power for the diffraction coefficient of the prevailing wind direction, which is negligible, compared to the power of direct signal, as discussed before. As a consequence of the interfering power for the blades being lower than the sensitivity, the corresponding CIR for the system is significantly larger than the minimum acceptable CIR. Thus, it is concluded that the presence of the wind turbines in this scenario does not influence the DVOR beacon.

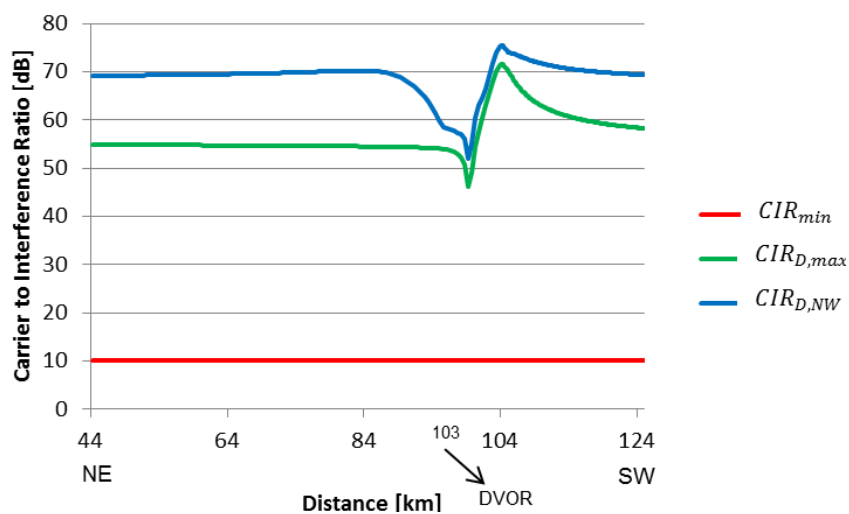


Figure 4.13 - Carrier to Interference Ratio for Lisbon scenario and Sobral wind farm.

In the analysis of the results given by the simulations, the most significant results are the ones obtained for the maximum diffraction coefficient and not for the coefficient in the dominant wind direction. This situation is due to the fact that during the operation of the wind turbines, the probability of the blades being oriented in the prevailing wind direction is small compared to the probability of the latter being oriented in other direction.

From the analysis of the simulator results obtained for the several wind farms installed in the vicinity of the Lisbon DVOR beacon, one can conclude that none of the wind farms creates interference problems in the signal transmitted by the beacon and received by the aircraft that it is in communication with it during the selected flight routes. Thereby, verified the absence of interference due to the orography of the terrain between the DVOR beacon and the wind turbines, which forms obstacles to the propagation of the signal and introduces high losses, there is a signal attenuation that is reached by the blades of the turbines and that would originate an interfering power received by the aircraft. So, any of the two FLs can be flown by the aircraft in both of the two selected flight routes under analysis.

4.2.2 Centre and Algarve Regions Scenarios

From the analysis of the results obtained from the several simulation of the scenario composed of the Fátima DVOR beacon and the Pias Longas wind farm for the three flight routes depicted in Figure 4.5 and the two FLs under study, one can conclude that the wind farm installed in the vicinity of the DVOR beacon in Fátima does not cause interference in the signal transmitted by the DVOR and received by the aircraft in the flight routes under study, as one can state based on the results given by the simulator. Thereby, both FLs under study can be indicated to aircrafts flying in the three aforesaid flight routes.

The absence of interference distance in this scenario is related to the fact that, in the zone between the DVOR beacon and the wind turbines, the orography of the terrain introduces significant losses in the signal diffracted by the blades. Thus, the interfering signal received by the aircraft has lower power compared to the power of the direct signal between the beacon and the aircraft. Consequently, the CIR for this situation is higher than the reference one.

In Nisa, in the vicinity of the DVOR beacon three wind farms are installed in different locations. Thus, the simulations were performed for the three farms, the two routes and the FLs under study, and the output of the simulator gives the results shown in Table 4.3. This table shows the interference distance, d_{int} , that is, the distance in which the CIR of the system is less than the minimum one, for the selected flight routes and FLs, and one makes made the distinction between the maximum diffraction coefficient for the rotation angles, D_{max} , and the diffraction coefficient for the dominant wind direction, D_{NW} , as the interfering power has different values for each case, thereby implying different results for the CIR.

The main difference between the scenarios defined by each of the three wind farms is related to the orography of the terrain due to the location of each one relative to the DVOR beacon position.

Therefore, in the scenario defined by the Serra da Lage wind farm, as well as in the one defined by the Zimbreira wind farm, in the region between the beacon and the wind turbines the profile of the terrain creates obstacles to the propagation of the signal, and introduces significant losses in it, leading to a situation similar to the Lisbon and Fátima scenarios concerning the powers and CIR.

Table 4.3 - Interference distance for Nisa DVOR beacon.

Site	Wind farm	Route name	$d_{int}[\text{km}]$			
			FL55		FL450	
			D_{max}	D_{NW}	D_{max}	D_{NW}
Nisa	Serra da Amêndoa	G52	0.61	0	0.91	0.61
		R72	0.69	0	1.73	1.04
	Serra da Lage	G52	0	0	0	0
		R72	0	0	0	0
	Zimbreira	G52	0	0	0	0
		R72	0	0	0	0

In the scenarios defined by the Serra da Amêndoa wind farm, considering that the farm is on the top of a hill, it is in LoS with the DVOR beacon. Thereby, the signal diffracted by the blades creates significant interfering power, which is received by the aircraft, besides the power of the direct signal. As a consequence, the CIR obtained for this scenario is lower than the minimum one, and then one can conclude that there is interference in the DVOR beacon created by the presence of wind turbines.

Following the above, Figure 4.14 shows the received power of the direct signal and the interfering power of the diffracted signal for the maximum diffraction coefficient of each wind turbine, for the scenario aforesaid and the flight route G52 and FL55. In this flight route, the aircraft moves in the direction from SW to NE, as shown in Figure 4.6, and the DVOR beacon is located at 59.70 km from the initial point of the route.

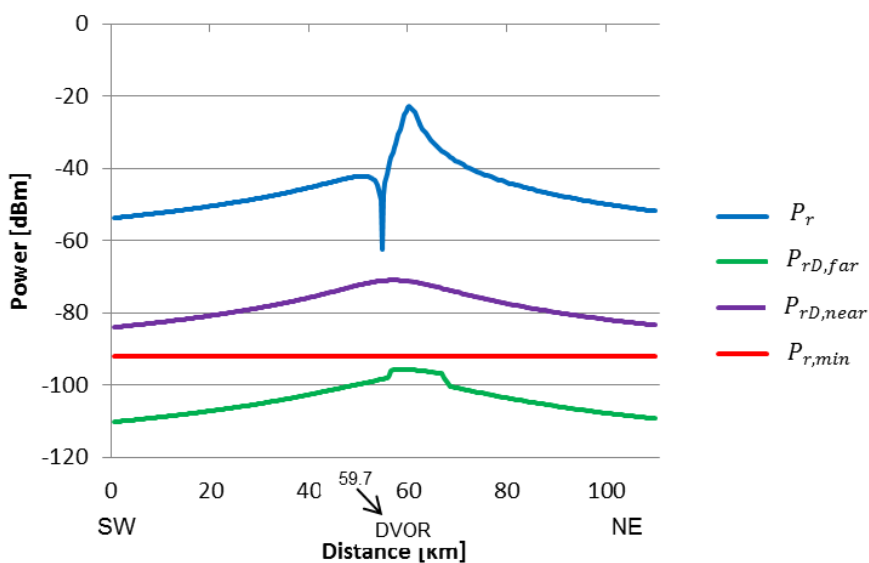


Figure 4.14 – Received and interfering powers for Nisa scenario and Serra da Amêndoa wind farm.

In Figure 4.14, it is noticeable that the interfering power determined for the nearest wind turbine,

$P_{rD, near}$, is higher than the interfering power determined for the farthest one, $P_{rD, far}$, and the sensitivity of the receiver, $P_{r, min}$. This situation occurs due to the fact that in the path between the DVOR beacon and the farthest turbine there is an obstacle that introduces losses in the signal, originating an interfering power lower than the interfering power obtained for a path where there are no obstacles.

Based on the received power of the direct signal and the interfering power determined for each wind turbine, the CIR for the maximum diffraction coefficient of the blades and for the maximum diffraction coefficient in the dominant wind direction were calculated, being depicted in Figure 4.15.

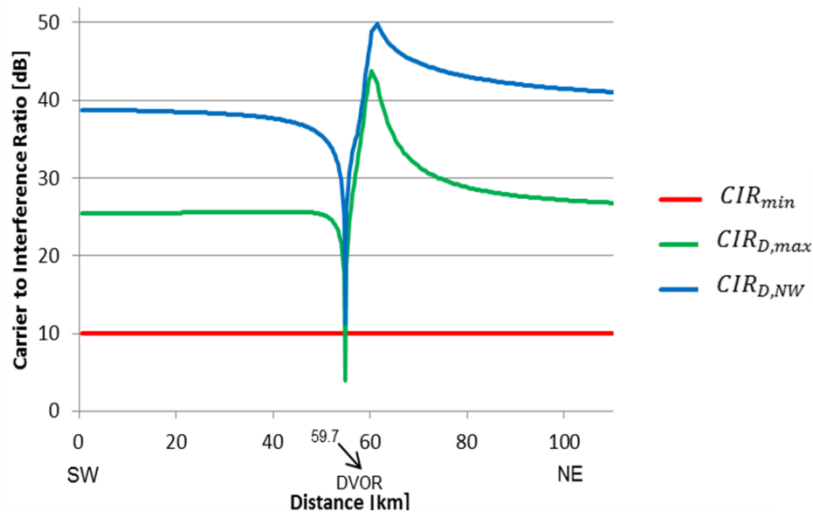


Figure 4.15 - Carrier to Interference Ratio for Nisa scenario and Serra da Amândoa wind farm.

At first sight, from Figure 4.15, one can conclude that, for the flight route and FL under analysis, the wind farm causes interference problems in the signal transmitted by the DVOR beacon. The critical situation occurs for the maximum diffraction coefficient of the blades, whereas the respective CIR, $CIR_{D,max}$, is lower than the minimum acceptable value, CIR_{min} , near to the location of the beacon, as opposed to the CIR obtained for prevailing wind direction, $CIR_{D,NW}$, which is higher than the minimum value.

For the remaining scenarios, defined by the Serra da Amândoa wind farm, the analysis is similar to the one carried out for the aforesaid scenario.

From the analysis of the results presented in Table 4.3, one concludes that for Serra da Lage and Zimbreira wind farms, both FLs can be used by the aircraft on the flight routes under study, considering that the wind turbines do not cause interference on the signal transmitted by the DVOR and received by the aircraft. However, for the case of the Serra da Amândoa wind farm, the FL55 is the one that should be flown on the both tested routes, in order to reduce the interference distance due to the presence of the referred wind farm, because in FL450 the interference distance is higher both for the maximum diffraction coefficient and for the diffraction coefficient in the prevailing wind direction than the interference distance obtained for FL55, that is, the maximum FL is a worst case compared to the minimum FL. In the higher FL, the wind turbines cause more interference problems in the DVOR beacons due to the fact that the gain of the transmitting antenna is lower for this level than for the FL55, that is, for the increasing of the distance between the aircraft and the DVOR beacon, as

well as between the aircraft and the wind turbine, it is verified a decreasing of the gain of the transmitting antenna, and consequently, an increasing of the interference distance caused by the wind turbines, for higher FLs, in the same flight route.

In addition, for the same flight route, and different FLs, the interference distance due to the interfering power for signal diffracted by the blades for the diffraction coefficient in the prevailing winds direction is lower than the interference distance for the interfering power for the maximum diffraction coefficient. This occurs because the prevailing wind direction is the optimum case compared to the others directions of the blades.

Finally, from the analysis of the results given by the output of the simulator for the Sagres scenario and the defined flight route, it is noticeable that the wind farm installed in the vicinity of the DVOR beacon, does not affect the signal transmitted by the navigation aid. This situation is related to the fact that the wind turbines under study are installed almost at 15 km from the beacon, as well as the fact that the losses introduced by the terrain are high, which creates an attenuation of the signal diffracted by the blades and a low interfering power. Consequently, the CIR determined for this case is higher than the minimum value, and one can conclude that the presence of this wind farm does not cause interference problems in the propagation of the signal between the beacon and the aircraft. In the subsequent analysis of the simulator results, for this specific case, both the minimum and the maximum FLs are appropriated for the aircraft flying routes.

4.2.3 Autonomous Regions Scenarios

In the Madeira archipelago, for the Porto Santo scenario, for each of the three defined flight routes and the two different FLs, one can conclude that the wind farm under study does not cause interference problems in the propagation of the signal received by the aircraft, when it flies in the flight routes in the Figure 4.8. This situation occurs due to the fact of the direct ray between the DVOR beacon and the wind turbines under study are practically obstructed by the terrain, which leads to the cancellation of the signal between the beacon and the wind turbines. Thus, the power of the signal diffracted by the blades is neglected, compared to the value of the sensitivity of the receiver, implying the increasing of the CIR for the maximum interfering power of the blades, and for the wind dominant direction. Hence, the aircraft can fly on the defined flight routes in both FLs.

Finally, for the Azores archipelago, in the three scenarios under analysis (Flores, Horta and Santa Maria), the wind farms of each one in the vicinity of the corresponding CVOR (in the case of the Santa Maria scenario) or DVOR beacon (in the case of the Flores and Horta scenarios), do not have influence on it. Once again, this situation, for all the scenarios, is due to the fact that the direct ray between the CVOR or DVOR beacon and the wind turbines is obstructed by the terrain, and the obstacles introduce losses in the diffracted signal. Furthermore, for the Horta scenario, in the radio link between the DVOR beacon and the corresponding wind farm, the terrain is composed of a sizeable extension of sea water, which contributes to the attenuation of the diffracted signal. Thus, verified for the Porto Santo scenario, the power of the signal diffracted by the blades is neglected, and the CIR increases to values higher than the value of reference. So, from the results of the simulator output,

one can conclude that for the three aforesaid scenarios, the aircraft can fly in any one of the FLs under study, for the several flight routes tested.

In conclusion, the difference between the several simulated scenarios is related to the orography of the terrain between the location of the DVOR beacon and the location of the farthest and nearest wind turbines. In most scenarios, the terrain creates obstacles to the propagation of the signal transmitted by the DVOR beacon that reaches the structures of the wind turbines, and consequently these obstacles introduce losses in the signal, which originates a decreasing of the power reflected/diffracted by the blades and a decreasing of the interference problems caused by the wind turbines installed in the vicinity of the beacon. In some scenarios occurs the total obstruction of the signal that reaches the turbines creating a negligible interfering power, and consequently a situation without interference problems due to the presence of the wind turbines.

In simulations of the scenarios under study, it was verified that none of the wind turbines impinge upon the BRA, because the terrain profile between the DVOR beacon and the wind turbines presents roughness, and in some locations of the path, the terrain causes an obstacle to the propagation of the signal leading to a cancellation of the influence of the turbines in the DVOR beacon. Besides this, in the case of the Nisa scenario, in which the Serra da Amêndoa wind farm is causing interference problems in the DVOR beacon, based on the distance between the turbines and the beacon and its height, one can conclude that the subtend angle of the turbine is lower than the angles imposed by the BRA. So, also in this case, the turbines do not impinge upon the BRA.

The current location of the wind farms in each one of the simulated scenarios do not cause interference with exception of the scenario defined by the DVOR beacon in Nisa and the Serra da Amêndoa wind farm.

4.3 Exclusion Regions Definition

In this section, exclusion regions are defined, based on the analysis of the results from Section 4.2 on the scenarios defined in Section 4.1. Afterwards, one determines exclusion regions with the aid of the expressions presented in Subsection 3.1.3.

To conclude the definition of the exclusion regions for the DVOR under study, the results of both analyses are compared, in order to establish a boundary distance of the exclusion region around the DVOR of the scenario under study, and within which a wind farm cannot be installed.

The boundary distance of the exclusion region in a specific scenario is based on the interference distance obtained from the simulations, in Section 4.2, for each of the established scenarios. This safety zone is determined by simulations performed for different locations of the nearest wind turbine of the beacon until finding the optimum distance in which the wind turbine does not influence the DVOR beacon.

The minimum acceptable distance between the DVOR beacon and the wind turbines was calculated for the nearest wind turbine, whereas the definition of the boundary of the exclusion zone for this wind turbine guarantees that the farthest one as well as the others are also at a certain safety distance from the DVOR, and the presence of the wind farm under study does not cause interference problems in the corresponding aeronautical aid.

In addition, the simulations were carried out for different locations of the wind turbines, with increments of 100 m in the distance between the beacon and the turbine, in order to observe the reduction of the interference distance until there is no interference. The results obtained by the several simulations for the determination of the boundary distance of the exclusion regions around the DVOR beacon under analysis are presented in Table 4.4.

In the Nisa scenario defined by the Serra da Amêndoa wind farm, the establishment of the boundary distance of the exclusion regions for the FL55 route G52, as well as for the FL450 in both routes, is achieved in the second increment of the initial distance between the DVOR beacon and the nearest wind turbine, that is, after two simulations for a new terrain profile in which the nearest wind turbine should be relocated at 200 m relative to the initial position. This relocation of the position of the wind turbine enables to establish that its presence does not influence the signal transmitted by the beacon, and that would be diffracted by the blades. In this final position, the LoS between the beacon and the turbine is obstructed by the terrain, which introduces significant losses in the diffracted signal, decreasing the interfering power and, consequently, increasing the CIR to values higher than the minimum one.

In contrast to previous situation, for the other scenario defined by the Serra da Amêndoa wind farm, that is, for the FL55 route R72, only one increment in the initial position of the wind turbine under analysis is performed. For this scenario, the nearest turbines should be at 100 m from its initial location.

In conclusion, in this scenario, for both FLs and both flight routes, the relocation of the wind turbines to a 200 m from the initial position guarantees that in all situations the wind turbines do not cause interference problems in the DVOR beacon; at 100 m from its positions of installation, defined for FL55 and route R72, in the remaining scenarios there can be interference problems. These results obtained for the minimum acceptable distance between the DVOR beacon and the wind turbines are presented in Table 4.4.

Table 4.4 - Boundary distance of the exclusion zone for the simulations.

FL	Site	Wind farm	Route name	$d_{BTmin}[\text{km}]$
FL55	Nisa	Serra da Amêndoa	G52	10.3
			R72	10.2
FL450	Nisa	Serra da Amêndoa	G52	10.3
			R72	10.3

The difference on the results for the minimum acceptable distance between the nearest wind turbine and the beacon is related to the fact that, in each route and FL, the aircraft is in different positions

relative to the wind turbine under test.

In route, if the aircraft is in the shadow area created by the wind turbine, then it is not possible to establish communication between the DVOR beacon and the receiver. This situation occurs when the FL is less than h_s . Thus, in an analysis of the wind turbines influence in the aeronautical navigation aids, it is required to determine the shadow height behind the turbine along the flight route of the aircraft, through (3.6), in order to verify if the aircraft is in this zone or not.

The determination of the shadow height is done for the FL55, since by ensuring that the aircraft along of the route is above of the shadow zone for the minimum FL, then at higher FLs there is the same situation. Therefore, for the scenarios where interference problems were identify, and for the flight routes of each one, by solving (3.6) one concludes that along of the flight route the aircraft is always above the shadow height created by the wind turbines.

In view of the foregoing, the exclusion regions around the DVOR beacon location are determined by the equations of Subsection 3.1.3, to compare the boundary distance of the exclusion zones acquired from the simulations with the distances obtained using the criteria discussed in the referred subsection.

The first criterion to consider enables to determine the exclusion region based on the FAA Order 6820.10, in which it is assumed that the wind turbines in the vicinity of the DVOR beacon will subtend vertical angles of approximately 1.2° . This criterion depends only on the height of the wind turbine under analysis, and the obtained results for the boundary distance are shown in Table 4.5.

Subsequently, the second criterion determines the safety regions around the DVOR beacon based on the minimum and maximum (maximum cruising level) FLs presented in Table 3.2, and one assumes a worst case scenario, that is, a scenario in which the aircraft is flying near the DVOR beacon, therefore, the total distance between the DVOR beacon and the aircraft to consider is 25 nmi.

Finally, the third criterion is based on the SSVs for the DVOR systems. In this regard, the flight altitude to use in (3.14) is FL10, that is, the approach flight altitude for an aircraft, considering that it is required to guarantee that the installed wind turbines does not impinge upon the lower bounds of the SSVs (worst case scenario), as discussed in Subsection 3.1.3. So, for this analysis, from Table 2.1 the possible ranges of the DVOR beacon in the FL to consider are 25 nmi for the lower bound of the Terminal SSV and 40 nmi for the lower bound of the Low and High Altitude SSVs. These ranges in (3.14) correspond to the distance between the DVOR beacon and the aircraft, that is, the total distance.

The boundary distances of the safety regions around the DVOR beacon determined for each one of the defined scenarios in which interference is noticeable, due to the presence of a wind farm, and from each one of the discussed criteria are presented in Table 4.5.

In Table 4.2, the distance in which the nearest and farthest wind turbines are located relative to the DVOR beacon is presented. For the scenario under analysis in this section, the distance between the beacon and the location of the nearest wind turbine is higher than the boundary distance obtained by the three criteria, which at first sight could mean that the turbines are not causing interference

problems in the signal. Nevertheless, the fact that the wind turbines are installed on the top of hill, in which the height of the terrain is higher than the height of the site where the beacon is installed, coupled with the fact that the turbines are in LoS with the DVOR beacon, provides the propagation of the diffracted signal by the blades of the turbines, and it originates an interfering power in the receiver.

In addition, for the range of 25 nmi and for increasing FLs (comparing between the SSVs and FLs criteria), the minimum acceptable distance between the DVOR beacon and the nearest wind turbine decreases, due to the fact that the distance between the beacon and the aircraft increases, as expected by the analysis of the (3.14), and the other parameters remain constant. Nonetheless, for FL10 and for the increasing range of the DVOR beacon, the boundary distance defined around the beacon increases. Once again, this result was expected from the analysis of the expression that allows one to determine the minimum distance between an aeronautical aid and a wind turbine.

In conclusion, a comparison is required between the boundary distances of the exclusion regions presented in Table 4.4 and the boundary distances in Table 4.5.

The boundary distances obtained by theoretical expressions are more stringent than the ones obtained by the simulation of different distances between the DVOR beacon and the wind turbines, since the former considers, among other parameters, assumptions and FLs, the FL that is used by the aircrafts on approach to a runway, and the latter is determined taking only the distance between the beacon and the nearest wind turbine into account. Nevertheless, except for the SSVs criterion, the boundary distances of the exclusion regions obtained by both analyses are according to the theoretical value, which establish that the safety distance is defined to a radius of 15 km from the beacon, as discussed in Subsection 3.1.1.

Table 4.5 - Boundary distance of the exclusion zone for the three criteria.

Site	Wind farm	$d_{BTmin}[km]$				
		FAA Order	FLs		SSVs (FL10)	
			FL55	FL450	25 nmi	40 nmi
Nisa	Serra da Amêndoa	5.20	3.09	0.353	21	45

In addition, the difference noticeable in the results of both analyses is due to the fact that the first determines the boundaries for a fix distance between the beacon and the aircraft, and the latter determines the boundary distances for the flight route under test, that is, for the distance between the DVOR beacon and the aircraft, which varies along the route. However, both analyses depend on the FLs, the height of the wind turbines, and the range of the DVOR beacon under study.

Chapter 5

Conclusions

In this chapter, the main conclusions of this thesis are pointed out, summarising a discussion and a critical analysis of the results obtained, as well as referring some aspects to be developed in future work.

The main objective of this Thesis was to assess the influence of wind turbines in VOR aeronautical navigation aids that are installed in Portugal (mainland and archipelagos), and to define exclusion regions around their location. These aims were accomplished mainly through the development and implementation of tower RCS and blades models, which enable the modelling of the wind turbines, and to assess its impact on the transmitted signal by the aeronautical aid, and subsequently through simulations, to define the aforesaid exclusion regions.

Chapter 2 is focused on four different subjects: the fundamental aspects of aeronautical navigation systems, the characterisation of wind turbines generators, the main effects of wind turbines on aeronautical aids, and a brief state of the art. The first section includes the basic aspects of aeronautical aids, more specifically their main features, operation mode and radio interface, focusing DVOR systems, given that these systems are the ones installed in Portugal. The wind turbines generators section concerns the fundamental aspects to consider about their features and includes a brief description of their operation mode. The section about the effects of turbines on DVOR beacons includes an introduction to the problem of the wind turbines installed in the vicinity of DVORs, as well as their main interference effects on the aforesaid systems. Finally, the state of the art is an overview about the most relevant works developed on this area, in the sense of the different approaches to the resolution of the problem of wind turbines near aeronautical navigation aids.

In Chapter 3, the Knife-edge/Deygout, the tower and the blades models were developed in order to determine the scenarios where wind turbines cause interference problems on the DVOR beacon, and to estimate the boundary distances of the exclusion regions around these systems. The Knife-edge/Deygout model is used, based on the profile of the terrain surrounding the scenario under study, as well as on the height of the DVOR beacon and on the height of the wind turbine, which enables to estimate the possible losses introduced by the terrain when it constitutes an obstacle to the propagation of the transmitted signal. For the tower RCS and the blades models, the position of the DVOR beacon and the wind turbine, and the flight route of the aircraft were required for the modelling of the wind turbines and to estimate the interfering power caused by them. Besides this, and to complete the models to implement, in the case of a scenario composed of sea water, one developed an analysis taking the reflection coefficient of the signal in the water into consideration. These models were implemented in a MatLab function, in which through an auxiliary script, containing the location of file with the profile of the terrain, the file with the specific location of the DVOR beacon and the wind turbine, and the file with the initial and final positions of the aircraft for the desired flight route, as well as the determination of the tower RCS and the diffraction coefficients of the blades, and also the input parameters required for the simulations, as the frequency, the wind turbines' height and tower's height, the DVOR beacon's height and the transmitted power, is able to execute the main function and to determine the powers received by the aircraft along of the flight route and the CIR of the system under analysis. This main function leads to the output results independently of the type of the terrain under analysis.

Chapter 3 also includes some specific criteria to estimate exclusion regions through solving simple equations, which enable to determine the shadow height created by a wind turbine in order to assess

the position of the aircraft along the flight route regarding the height of the turbine, and finally to estimate the boundary distances of the exclusion regions. As these models are developed and implemented with simple expressions, they do not have a simulator.

In the final simulator, several input parameters can be changed according to the scenario under assessment. The user can decide the location of the wind turbines, as well as its main features, and as a consequence the profile of the terrain between the DVOR beacon and the wind turbines will be different. Besides, also the features of the DVOR beacon are different according to the beacon under consideration.

Finally, a last model was developed and implemented in order to define the flight route and to determine the coordinates of the aircraft from an initial and final points, for each section that compose the route. In this model, the user can choose the points of departure and arrival of each section for an aircraft, as well as the FL to be flown by it on the route defined through the model implemented in the simulator.

In Chapter 4, the analysis of all simulations results and of the intermediate calculations given by the several criteria was shown. In order to achieve the objective of the aforesaid chapter, the definition of a scenario to study was required. In general, for each DVOR beacon, one defined the wind farms installed in its vicinity and that could be causing interference problems. Subsequently, a more detailed definition was carried out, in which one made a distinction between the wind farms, in the locations where there are more than one. This detailed definition allowed one to establish all possible scenarios with different locations of the wind farms, to analyse the influence of the wind turbines on the signal transmitted by the DVOR beacon.

By assessing the results of Chapter 4, the overall conclusions from this work can be separated into two categories, the boundary distances of the exclusion regions and the FLs for each flight route. The conclusions regarding the boundary distances estimated to define the exclusions regions around the DVOR beacons are divided into two analyses: the boundary distances obtained by the simulator and the distances obtained from the criteria discussed in Chapter 3.

From the results given by the simulator, only the DVOR beacon in Nisa presents interference problems due to the presence of the wind farm of the Serra da Amêndoa, considering that in all other scenarios the terrain obstructs the radio link between the beacon and the turbine, leading to a decreasing of the interfering power and an increasing of the CIR. From the simulator results, one can conclude that in a specific scenario the decreasing of the interfering power leads to an increasing of the CIR of the system, considering that the power of the direct signal is the same independently of the FL for a particular route, and independently of the flight route to a particular FL.

In the estimation of the boundary distances through the simulator, the work is divided into three steps: to estimate the interference distance for the scenario, to relocate the wind turbines, and then to determine the minimum acceptable distance within which the wind turbines can be installed. The interference distance caused by the wind turbines depends on the FL and the flight route used by the aircraft, with the worst case verified for FL450 and both flight routes, in which the interference distance

is 0.91 km near to the DVOR beacon for the route G52, and for the route R72 the wind turbines are causing an interference distance of 1.73 km, contrary to the values of the interference distance obtained for the FL55. Besides this, the interference distance determined based on the prevailing wind direction, for the worst case (FL450), is 0.61 km and 1.04 km, for routes G52 and R72, respectively, which corresponds to an interference distance lower than the previous one.

Based on these results, the conclusions that one can achieve for the estimation of the boundary distances of exclusion regions, through the simulator, are the following:

- For the route G52 and both FLs, the minimum distance acceptable for the installation of the wind turbine is 10.3 km from the location of the DVOR beacon, in order to guarantee that the wind turbines are in Non-Line-of-Sight (NLoS) with the beacon, leading to a weak diffracted signal. The same result is applied to the FL450 and flight route R72.
- In the flight route R72 and FL55, the boundary distance to ensure between the nearest wind turbine and the beacon is 10.2 km.

Regarding the estimation of the minimum acceptable distances through the several criteria, the study is split into two different parts: to analyse the variation of the boundary distance with the variation of the FL for a constant range of the DVOR beacon, and to analyse the behaviour of the boundary distance with the variation of the range for a constant FL. From this study, one can conclude that the boundary distances of exclusion regions decrease with the increase of the FL for a constant range. And, for a constant FL and the increase of the range of the DVOR beacon, boundary distances increase. A detailed analysis of each of the above conclusions is:

- For the criterion based on the FAA Order 6820.10, the exclusion zone around the DVOR beacon is defined up to a distance of 5.02 km from its location. This criterion is less strict than the other two, since it considers only the height of the wind turbine, the position of the aircraft relative to the beacon and to the turbine being irrelevant.
- The criterion based on the FLs considers a range of the DVOR beacon at 25 nmi, and takes into account the position of the aircraft, in addition to the height of the wind turbine. For FL55, the boundary of the exclusion region is 3.09 km and for the FL450 it is 0.353 km. These results have been estimated for a fixed total distance between the beacon and the aircraft, which is assumed to be the range of the beacon.
- The last criterion, which is based on the lower bounds of the SSVs, is used to estimate the boundary distances to FL10, and two different ranges of the beacon. For the range of 25 nmi the boundary distance of the exclusion zone around the beacon is 21 km, and for the range of 40 nmi it is 45 km. The results estimated by this criterion constitute a worst case scenario, considering that the DVOR beacons are used for the aircraft in route and not on approach to the runway, which corresponds to the FL under analysis.

By the analysis of the height of the shadow behind the wind turbines, one conclude that the aircraft is always above the referred height, and consequently it is in LoS with the DVOR beacon in the study flight routes and for both FLs.

The developed simulator proves to be a powerful tool in the estimation and analysis of the interference distance caused by a wind turbine in the scenarios under study. However, it was necessary to consider some approximations in the models implemented. For the case of a scenario composed of sea water, in the study of the reflections on the water, it was assumed that the angles of incidence of the reflected ray on the water were high, and consequently the value assumed for the reflection coefficient was an approximation. For the model of the tower and the blades it was assumed that the aircraft was in far field zone all along the flight route, even when the aircraft is over the turbine.

For future work, first of all, one suggests an improvement of the simulator in its limitations, described in the previous paragraph in order to get more accurate results. In addition, detailed analyses of the terrain surround to the DVOR beacon and the location of the wind turbines should be performed, in order to verify the most suitable locations to the installation of the wind turbines that cause interference problems on the DVOR beacons, so that the terrain obstructs the signal that would be diffracted by the blades. Moreover, it would be interesting to simulate the defined scenarios for the FL150, and not only for the maximum and minimum FLs, and to analyse the variation of the interference distance, as well as the variation of the range of the exclusion zones, for the three FLs. The study could be extended to the remaining turbines of the wind farms, and not just taking the nearest and farthest wind turbines.

All in all, hopefully, the work developed in this Thesis is of value to an air navigation service provider, enabling to a deeper knowledge on how to evaluate the performance of the systems under analysis.

Annex A

Usage of Wind Generators in Portugal

This Appendix contains information on wind farms installed in Portugal.

In this Appendix, the Table A.1 to Table A.5 include information on wind generators location, regarding its position on the ground (longitude and latitude coordinates). This data were gathered from Official documents sent to the Municipal entities in 2009 and made available by NAV Portugal, E.P.E. This information, subsequently, shall be considered to implement the developed model.

Table A.1 - Wind generators' usage in Lisbon district (in [WFiP12] and [NAV12c]).

Municipality	Lat _[DD°MM'SS.SS'']	Long _[DD°MM'SS.SS'']
Arruda	38°58'25.01"	-9°10'10.62"
	38°58'12.69"	-9°10'22.07"
	38°58'18.52"	-9°10'35.42"
Sintra Almargem do Bispo	38°50'38.60"	-9°15'59.81"
	38°50'28.87"	-9°16'2.84"
	38°50'21.26"	-9°16'3.77"
	38°53'0.67"	-9°12'34.76"
	38°52'58.50"	-9°12'44.27"
	38°53'12.65"	-9°12'49.84"
	38°52'48.59"	-9°13'23.61"
	38°52'46.75"	-9°13'32.64"
	38°52'48.68"	-9°13'4.00"
	38°52'16.90"	-9°13'13.10"
	38°52'28.29"	-9°13'30.64"
Loures		
Bolores	38°51'41.12"	-9°14'18.17"
	38°51'35.76"	-9°14'25.81"
	38°51'27.96"	-9°14'35.00"
	38°51'22.47"	-9°14'43.67"
	38°51'46.45"	-9°14'7.76"
	38°51'48.00"	-9°13'48.67"
	38°51'41.29"	-9°13'44.85"
	38°51'32.66"	-9°13'37.51"
	38°51'38.33"	-9°13'19.60"
Fanhões	38°53'47.05"	-9° 9'11.32"
	38°53'45.75"	-9° 8'59.63"
	38°53'41.52"	-9° 8'50.55"
	38°53'26.90"	-9° 8'58.07"
	38°53'23.39"	-9° 8'42.27"
	38°53'8.15"	-9° 8'22.29"
	38°52'50.89"	-9° 8'34.31"
	38°52'48.85"	-9° 8'40.94"
	38°52'38.97"	-9° 8'44.01"

Table A.1 (cont.) - Wind generators' usage in Lisbon district (in [WFiP12] and [NAV12c]).

Sobral	38°59'17.70"	-9°10'33.72"
	38°59'8.53"	-9°10'25.85"
	38°59'0.73"	-9°10'27.59"
	38°58'58.67"	-9°10'15.01"
	38°58'50.39"	-9°10'24.58"
	38°58'43.91"	-9°10'35.94"
	38°58'18.58"	-9°10'35.22"
	38°58'12.99"	-9°10'21.86"
	38°58'1.56"	-9°10'17.11"
	38°58'1.73"	-9°10'34.05"

Table A.2 - Wind generators' usage in Santarém district (in [NAV12c]).

Municipality	<i>Lat</i> _[DD°MM'SS.SS'']	<i>Long</i> _[DD°MM'SS.SS'']
Ourém	39°34'39.76"	-8°35'8.26"
Pias Longas	39°34'46.38"	-8°35'4.70"
	39°34'57.95"	-8°35'0.28"
	39°35'3.36"	-8°34'53.31"
	39°35'8.05"	-8°34'43.55"
	39°35'11.96"	-8°34'34.62"
	39°35'18.10"	-8°34'29.62"
	39°35'25.53"	-8°34'23.15"
	39°35'33.35"	-8°34'20.74"
	39°36'6.15"	-8°33'29.20"
	39°36'9.35"	-8°33'17.87"

Table A.3 - Wind generators' usage in Santarém district (in [NAV12c]).

Municipality	<i>Lat</i> _[DD°MM'SS.SS'']	<i>Long</i> _[DD°MM'SS.SS'']
Mação		
Serra da Lage	39°37'33.71"	-7°59'6.17"
	39°37'37.24"	-7°59'8.16"
	39°37'41.74"	-7°59'9.49"
	39°37'45.88"	-7°59'10.96"
	39°37'57.50"	-7°59'18.21"
	39°38'1.17"	-7°59'21.70"
Serra da Amêndoa	39°36'7.77"	-8° 1'21.05"
	39°36'12.96"	-8° 1'18.18"
	39°36'30.29"	-8° 1'33.73"
	39°36'32.79"	-8° 1'28.93"
	39°36'34.15"	-8° 1'22.08"

Table 4.3 (cont.) - Wind generators' usage in Santarém district (in [NAV12c]).

	39°36'55.33"	-8° 1'23.79"
	39°37'5.57"	-8° 1'29.24"
	39°37'12.07"	-8° 1'35.17"
	39°37'16.92"	-8° 1'38.13"
	39°37'21.91"	-8° 1'42.77"
	39°37'26.77"	-8° 1'47.96"
	39°37'30.16"	-8° 1'52.32"
	39°37'33.97"	-8° 2'2.27"
	39°37'28.79"	-8° 2'5.04"
Zimbreira	39°34'12.01"	-7°49'32.14"

Table A.4 - Wind generators' usage in Faro district (in [WFiP12] and [NAVA12]).

Municipality	<i>Lat</i> _[DD°MM'SS.SS'']	<i>Long</i> _[DD°MM'SS.SS'']
Lagos	37° 8'16.77"	-8°48'58.20"
Barão de S. João	37° 8'26.59"	-8°48'58.48"
	37° 8'34.04"	-8°48'50.96"
	37° 8'48.88"	-8°48'53.08"
	37° 8'57.01"	-8°48'46.23"
	37° 9'3.50"	-8°48'37.04"
	37° 9'11.86"	-8°48'51.38"
	37° 9'20.54"	-8°49'11.38"
	37° 9'9.04"	-8°48'26.70"
	37° 9'16.91"	-8°48'20.23"
	37° 9'30.28"	-8°48'38.50"
	37° 9'23.37"	-8°48'47.24"
	37° 8'57.53"	-8°47'51.85"
	37° 9'10.03"	-8°47'41.73"
	37° 9'37.96"	-8°48'14.64"
	37° 9'28.00"	-8°48'18.00"
	37° 8'46.00"	-8°49'5.00"
	37° 8'46.59"	-8°49'5.79"
	37° 9'26.92"	-8°48'17.62"
	37° 8'58.12"	-8°47'36.19"
	37° 9'37.97"	-8°48'14.35"
37° 8'4.45"	-8°48'57.53"	

Table A.5 - Wind generators' usage in Azores and Madeira (in [WFiP12] and [NAVA12]).

Municipality	<i>Lat</i> _[DD°MM'SS.SS'']	<i>Long</i> _[DD°MM'SS.SS'']
Porto Santo	33° 3'32.93"	-16°21'43.19"
Cabeço do Carvalho	33° 3'31.06"	-16°21'48.69"
	33° 3'30.20"	-16°21'54.01"
Santa Maria	36°56'56.91"	-25° 7'44.83"
Figueiral	36°56'54.94"	-25° 7'51.55"
	36°56'53.04"	-25° 8'0.18"
Flores	39°25'21.50"	-31°10'56.87"
Boca da Vereda	39°25'14.73"	-31°10'52.03"
Horta	38°33'58.05"	-28°37'32.06"
Salão	38°33'56.95"	-28°37'26.61"
	38°33'55.55"	-28°37'24.11"
	38°33'53.55"	-28°37'20.76"
	38°33'51.53"	-28°37'18.63"
	38°33'48.96"	-28°37'17.07"

Annex B

Shadow Height and Flight Altitude Details

This Appendix provides a detailed explanation of the steps followed to achieve the results presented in the Subsection 3.1.2.

The present appendix aims to report in detail some concepts and mathematical procedures that are important to understand the expressions obtained in Chapter 3, Subsection 3.1.2, in particular related to the Law of Cosines and shadow height and flight altitude calculation.

- Law of Cosines:

The Law of Cosines is used for computing the angles when all three length sides of an oblique triangle (Figure B.1) are known or for computing one length side of a triangle when the other two and the opposite angle are known.

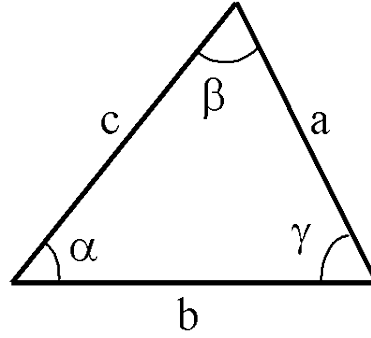


Figure B.1 - Generic oblique triangle (extracted from [Math13]).

Based on Figure B.1 and using the notation represented, the following equation indicates that the law says [Wolf13]:

$$b^2 = a^2 + c^2 - 2ac \cos \beta_{[^\circ]} \quad (\text{B.1})$$

The β angle is the one restrained between side of length a and c , and the opposite side has length b . So, to determine β based on (B.1) and solve it in order to the angle, the result is given by:

$$\beta_{[^\circ]} = \cos^{-1} \frac{a^2 + c^2 - b^2}{2ac} \quad (\text{B.2})$$

By adapting the first triangle (that includes the ground beacon and the wind turbine) on Figure 3.4 to the one of Figure B.1, the variables in (B.2) are the following:

$$a_{[m]} = d_{BT[m]} \quad (\text{B.3})$$

$$b_{[m]} = h_{T[m]} + r_{eq[m]} \quad (\text{B.4})$$

$$c_{[m]} = h_{B[m]} + r_{eq[m]} \quad (\text{B.5})$$

With all these variables, from (B.3) to (B.5), the unknown β angle is determined (equation (3.3)), and is used to further on shadow height calculation (equation (3.6)).

- Explanation of Shadow Height and Flight Altitude Calculation:

The computation of shadow height, h_s , cast by a wind turbine is derived from the presented Law of Cosines, starting from (B.1), and once again supported by Figure 3.4, namely the second triangle that includes the ground beacon and the airplane. So, the variables on (B.1) are:

$$a_{[m]} = d_{BT[m]} + d_{TP[m]} \quad (\text{B.6})$$

$$b_{[m]} = h_{S[m]} + r_{eq[m]} \quad (\text{B.7})$$

$$c_{[m]} = h_{B[m]} + r_{eq[m]} \quad (\text{B.8})$$

By substituting (B.6) with (B.8) in (B.1), and considering that the β angle is calculated by (3.3), the resulting equation is the following:

$$(h_{Seq[m]})^2 = (d'_{[m]})^2 + (h_{Beq[m]})^2 - 2(d'_{[m]})(h_{Beq[m]}) \cos \beta_{[^\circ]} \quad (B.9)$$

where:

$$h_{Seq[m]} = h_{S[m]} + r_{eq[m]} \quad (B.10)$$

$$d'_{[m]} = d_{BT[m]} + d_{TP[m]} \quad (B.11)$$

$$h_{Beq[m]} = h_{B[m]} + r_{eq[m]} \quad (B.12)$$

By algebraic manipulation of (B.9) the result is (3.6) that enables to calculate the shadow height in a generic scenario and for the worst case.

For the calculation of the minimum flight altitude, taking into account the shadow height cast by a wind turbine and the radius of Fresnel zone, (B.9) is used with an additional variable, which corresponds to the radius of the first Fresnel zone clearance obtained by (3.8) for $n=1$ and it is indicated by:

$$r_{1e[m]} = \sqrt{\frac{\lambda_{[m]} d_{BT[m]} d_{TP[m]}}{d_{BT[m]} + d_{TP[m]}}} \quad (B.13)$$

Thus, from the analysis of the first triangle of Figure 3.4, considering the influence of the above mentioned radius (Figure 3.5), and applying (B.1), the equation that represents this is the following:

$$(h_{Teeq[m]})^2 = (d_{BT[m]})^2 + (h_{Beq[m]})^2 - 2(d_{BT[m]})(h_{Beq[m]}) \cos \beta_{[^\circ]} \quad (B.14)$$

where:

$$h_{Teeq[m]} = h_{T[m]} + r_{eq[m]} + r_{1e[m]} \quad (B.15)$$

Solving (B.14) in order to reach $\cos \beta$, for the first triangle:

$$\cos \beta_{[^\circ]} = \frac{-(h_{Teeq[m]})^2 + (d_{BT[m]})^2 + (h_{Beq[m]})^2}{2(d_{BT[m]})(h_{Beq[m]})} \quad (B.16)$$

For the larger second triangle of Figure 3.4, the equation is similar to (B.9), in which the shadow height is substituted by the flight altitude, h_F , for an aircraft, and the equation is the following:

$$(h_{Feq[m]})^2 = (d'_{[m]})^2 + (h_{Beq[m]})^2 - 2(d'_{[m]})(h_{Beq[m]}) \cos \beta_{[^\circ]} \quad (B.17)$$

where:

$$h_{Feq[m]} = h_{F[m]} + r_{eq[m]} \quad (B.18)$$

Once again, the equation that is obtained when (B.17) is solved in order to the cosine of the angle is given by:

$$\cos \beta_{[^\circ]} = \frac{-(h_{Feq[m]})^2 + (d'_{[m]})^2 + (h_{Beq[m]})^2}{2(d'_{[m]})(h_{Beq[m]})} \quad (B.19)$$

Finally, making (B.16) equal to (B.19), and solving for h_F , the final equation (3.9) is obtained, enabling to compute the minimum flight altitude for an aircraft, in a generic scenario.

Annex C

Exclusion Zones Details

This Appendix provides a detailed explanation related to the followed steps to achieve the expressions presented in the Subsection 3.1.3.

This appendix details some mathematical procedures that enable to obtain the expressions presented in Chapter 3, Subsection 3.1.3, related to the exclusion zones.

- Exclusion zone based on FAA Order:

In the determination of the minimum distance between a DVOR beacon and a wind turbine, agreeing with the FAA Order, it is necessary to take into account that a wind turbine is on spherical Earth, that is, the Earth's dip effect was accounted for. Therefore, the considered wind turbine height is the equivalent one (Figure 3.6) which is given by:

$$h'_{T[m]} = h_{T[m]} - h_{dip[m]} \quad (C.1)$$

In (C.1), the Earth dip is obtained by (3.12).

- Exclusion zone based on Flight Levels:

To determine the exclusion region based on FL, the total distance between a DVOR beacon and an aircraft is considered, instead of the distance between a wind turbine and an aircraft. So, the total distance might be calculated by:

$$d_{T[m]} = d_{BT[m]} + d_{TP[m]} \quad (C.2)$$

In this case, the radius of the first Fresnel zone also considers the total distance indicated in (C.2), according to the following equation:

$$r'_{1e[m]} = \sqrt{\frac{\lambda_{[m]} d_{BT[m]} (d_{T[m]} - d_{BT[m]})}{d_{T[m]}}} \quad (C.3)$$

In this way, the equation that enables to calculate the minimum distance, based on FL, in a generic study scenario is reached by making the modified versions of (B.16) equal to (B.19) with some algebraic manipulation, and is the following:

$$\frac{-(h'_{Teq[m]})^2 + (d_{BT[m]})^2 + (h_{Beq[m]})^2}{(d_{BT[m]})} = \frac{-(h_{Feq[m]})^2 + (d_{T[m]})^2 + (h_{Beq[m]})^2}{(d_{T[m]})} \quad (C.4)$$

where:

$$h'_{Teq[m]} = h_{T[m]} + r_{eq[m]} + r'_{1e[m]} \quad (C.5)$$

$$h_{Beq[m]} = h_{B[m]} + r_{eq[m]} \quad (C.6)$$

$$h_{Feq[m]} = h_{F[m]} + r_{eq[m]} \quad (C.7)$$

Finally, by making the equation equal to zero the final equation (3.14) is obtained.

Annex D

Gain of the Transmitting Antenna

This Appendix presents a detailed explanation of the method used to obtain the gain of the transmitting antenna, including the equations employed for the calculation of the total gain, as well as the gain for the horizontal and vertical components.

The DVOR antenna under study is a circular array with 48 omnidirectional elements, with Alford Loop type antennas. Subsequently, to obtain the radiation pattern of the antenna a joint analysis of both horizontal and vertical patterns for the mentioned antenna is required.

There is a circular radiation pattern of each antenna of the array, in the horizontal component. So for the DVOR antenna, the normalised directional pattern in the horizontal plane is obtained by [Davi83]:

$$D_m(\varphi) = C_m j^m J_m(kr) e^{jm\varphi} + \sum_{q=1}^{\infty} C_m j^{-q} J_q(kr) e^{-jq\varphi} + \sum_{q=1}^{\infty} C_m j^q J_q(kr) e^{jq\varphi} \quad (D.1)$$

where:

$$C_m = \frac{1}{j^m J_m(kr)} \quad (D.2)$$

$$g = (n_t q - m) \quad (D.3)$$

$$h = (n_t q + m) \quad (D.4)$$

- C_m : excitation of m^{th} mode;
- $J_{m(kr)}$: Bessel function;
- kr : modulation index;
- r : radius of the array;
- n_t : total number of elements in the array;
- φ : angle between the beam direction and the wind turbine measured horizontally.

The m^{th} mode in (D.1) corresponds to the highest-order mode which can be excited at a reasonable strength, considering that those are also omnidirectional. Thus, the maximum order mode is $m \approx \pm(kr)$. Also, according to [NAV12d], the modulation index is specified as $kr = 16$. Hence, the radiation pattern for the horizontal plane is the one shown in Figure D.1.

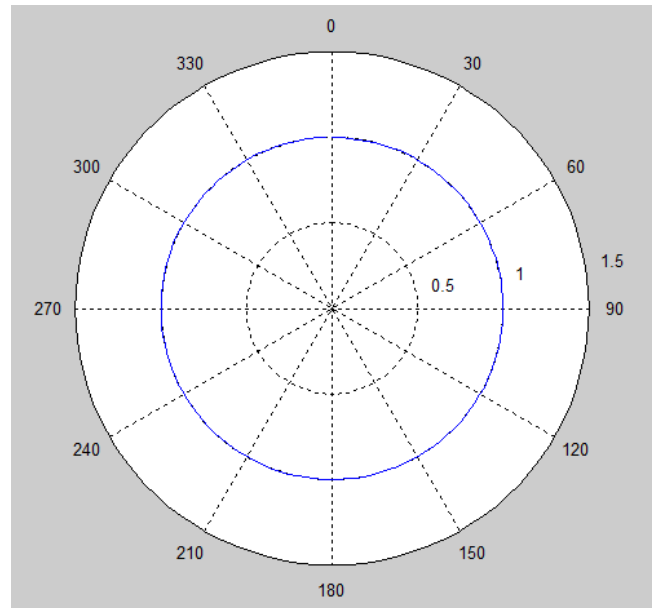


Figure D.1 - Horizontal pattern of a DVOR loop antenna.

On the other hand, the pattern for the vertical component of the DVOR antenna is depicted in Figure

D.2, and the corresponding gain, G_V , can be calculated by:

$$G_V(\theta_V) = |\sin(\theta_V)| \quad (D.5)$$

where:

- θ_V : angle between the beam direction and the wind turbine measured vertically.

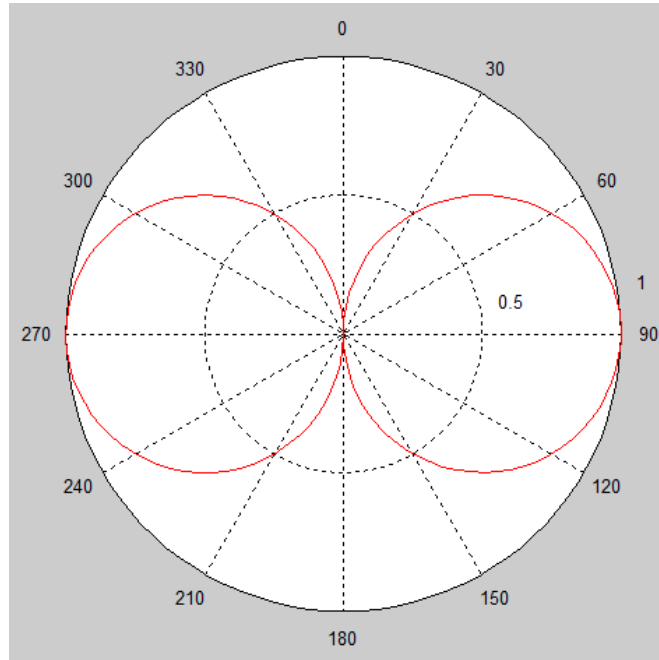


Figure D.2 - Vertical pattern of a DVOR loop antenna.

The gain of the transmitting antenna for a specific direction (θ_V, φ) of the receptor (wind turbine or aircraft, depending of the scenario under analysis) relative to the DVOR antenna is given by:

$$G_t(\theta_V, \varphi) = G_{max} \times G_H(\varphi) \times G_V(\theta_V) \quad (D.6)$$

where:

$$G_H(\varphi) = |D_m(\varphi)| \quad (D.7)$$

- G_H : gain of horizontal component;
- G_V : gain of vertical component;
- G_{max} : gain of the transmitting antenna in the maximum direction (in linear units).

In (D.6), and considering the circular array of 48 antennas, the maximum gain is, approximately, $G_{max \text{ [dB]}} = 7 \text{ dB [NAV12c]}$.

Annex E

Diffraction Coefficient Details

This appendix explains all the steps followed in the determination of the diffraction coefficient, by clarifying the concept of transformation of coordinates and matrixes rotation applied to the scenarios under study and allows to obtain the appropriated diffraction coefficient for each position of the blades and rotor, and for the dominant wind direction.

Each analysed scenario comprehends three points of study which are: position of the DVOR beacon, the wind turbine and the aircraft; where the initial coordinates are spherical (latitude, longitude, height), and the origin of the coordinates is at the centre of the Earth, for convention.

Given the fact that the axes need to be rotated, so that the origin of the axes is coincident with the turbine position, it is necessary to convert the spherical coordinates into Earth-Centred, Earth-Fixed (ECEF) coordinates that is a Cartesian coordinates (x, y, z) system. The stated transformation will be applied to the coordinates system of the DVOR antenna, the wind turbine and the aircraft.

In view of the foregoing, for any point i with (latitude, longitude, height) values, the corresponding (x_u, y_u, z_u) values are given by the following equations [Koks08]:

$$x_{u[m]} = \left(\frac{a_{[m]}}{\sqrt{\cos^2 \varphi_{i[\text{rad}]} + r_{axes} \sin^2 \varphi_{i[\text{rad}]}}} + h_{i[m]} \right) \cos \varphi_{i[\text{rad}]} \cos \lambda_{i[\text{rad}]} \quad (\text{E.1})$$

$$y_{u[m]} = \left(\frac{a_{[m]}}{\sqrt{\cos^2 \varphi_{i[\text{rad}]} + r_{axes} \sin^2 \varphi_{i[\text{rad}]}}} + h_{i[m]} \right) \cos \varphi_{i[\text{rad}]} \sin \lambda_{i[\text{rad}]} \quad (\text{E.2})$$

$$z_{u[m]} = \left(\frac{b_{[m]}}{\sqrt{r_{axes}^{-1} \cos^2 \varphi_{i[\text{rad}]} + \sin^2 \varphi_{i[\text{rad}]}}} + h_{i[m]} \right) \sin \varphi_{i[\text{rad}]} \quad (\text{E.3})$$

where:

$$r_{axes} = \left(\frac{b_{[m]}}{a_{[m]}} \right)^2 \quad (\text{E.4})$$

- a : length for semi-major axis;
- b : length for semi-minor axis;
- φ_i : latitude in point i ;
- λ_i : longitude in point i ;
- h_i : height of the point i (which is the addition of the terrain height to the height of the antenna or wind turbine).

The most common used shape for Earth in the above calculations is the oblate spheroid stated by the World Geodetic System 1984 standard (WGS-84), which has a circular cross section at any given latitude, and a constant elliptical cross section through any meridian, having identical axes lengths for all longitudes. So, by definition, these axes lengths in (E.1) to (E.4) are [Koks08]:

- Semi-major: $a = 6\,378\,137$ m;
- Semi-minor: $b = 6\,356\,752.3142$ m.

Afterwards, the DVOR and aircraft coordinates, and also its latitude and longitude, are adjusted to the coordinates system of the wind turbine, considering that this is defined as the reference centre of the system. So, the new coordinates for the DVOR and the aircraft are given by:

$$(x'_u, y'_u, z'_u) = (x_u, y_u, z_u) - (x_T, y_T, z_T) \quad (\text{E.5})$$

where:

- (x'_u, y'_u, z'_u) : new coordinates for the DVOR or the aircraft;
- (x_T, y_T, z_T) : coordinates for the wind turbine.

And, subsequently, a rotation about z axis and about x axis were taken in order to set the latitude and longitude of the transmitter and the receiver with regard to the wind turbine axes system. Therefore, the rotation about z is obtained by [DaFo09]:

$$\begin{bmatrix} x_2 \\ y_2 \\ z_2 \\ 1 \end{bmatrix} = \begin{bmatrix} \cos(\lambda_T[\text{rad}]) & 0 & -\sin(\lambda_T[\text{rad}]) & 0 \\ \sin(\lambda_T[\text{rad}]) & \cos(\lambda_T[\text{rad}]) & 0 & 0 \\ 0 & 0 & 1 & 0 \\ 0 & 0 & 0 & 1 \end{bmatrix} \begin{bmatrix} x'_u \\ y'_u \\ z'_u \\ 1 \end{bmatrix} \quad (\text{E.6})$$

where:

- λ_T : longitude of the wind turbine.

And, the rotation about x axis by [DaFo09]:

$$\begin{bmatrix} x_2 \\ y_2 \\ z_2 \\ 1 \end{bmatrix} = \begin{bmatrix} 1 & 0 & 0 & 0 \\ 0 & \cos(\theta_{[\text{rad}]}) & -\sin(\theta_{[\text{rad}]}) & 0 \\ 0 & \sin(\theta_{[\text{rad}]}) & \cos(\theta_{[\text{rad}]}) & 0 \\ 0 & 0 & 0 & 1 \end{bmatrix} \begin{bmatrix} x'_u \\ y'_u \\ z'_u \\ 1 \end{bmatrix} \quad (\text{E.7})$$

where:

$$\theta_{[\text{rad}]} = \frac{\pi}{2} - \varphi_T[\text{rad}] \quad (\text{E.8})$$

- φ_T : latitude of the wind turbine.

Hereupon, after converting the new Cartesian coordinates of the DVOR and the aircraft into spherical ones [Sphe13], with the equations below, the azimuth, φ , of each point under analysis is defined with the purpose of orientating the plane of rotation of the wind turbine blades to the DVOR position.

$$r_{u[\text{m}]} = \sqrt{x_{2[\text{m}^2]}^2 + y_{2[\text{m}^2]}^2 + z_{2[\text{m}^2]}^2} \quad (\text{E.9})$$

$$\theta_{u[\text{rad}]} = \arccos\left(\frac{z_{2[\text{m}]}}{r_{[\text{m}]}}\right) \quad (\text{E.10})$$

$$\varphi_{u[\text{rad}]} = \arctan\left(\frac{y_{2[\text{m}]}}{x_{2[\text{m}]}}\right) \quad (\text{E.11})$$

where:

- $\theta_u \in [0; 2\pi]$;
- $\varphi_u \in [0; \pi]$.

Once again, and in order to determine the diffraction coefficient for each blade, the coordinates calculated by (E.9) to (E.11) are converted into Cartesian ones, which two different rotations are applied. First, a rotation about x axis, by (E.7) and an angle $\theta = i * 2\pi/3 + \theta'$ with $i = 0; 1; 2$ and θ' between $[0; 2\pi/3]$, in order to estimate the several positions of the blades rotating in the vertical plane. Next, a rotation about z axis, through (E.6) with an angle between $[0; \pi]$, allows estimating the several

positions of the rotor of the blades.

Finally, after converting all the coordinates into spherical ones, the diffraction coefficient is determined by (3.25), for all the different positions of the blades.

Additionally, the diffraction coefficient is estimated for the dominant wind direction, taking into account that in Portugal the wind direction prevails from northwest (45° from the north) [MePi13]. So, in this direction the rotor of the blades is orientated with an angle $\varphi_{B[\text{rad}]} + \pi/4$ relative to the DVOR beacon position, more precisely relative to its azimuth, φ_B .

Annex F

Test Routes

In this appendix one presents the format of the input files to be used on the simulator and that contains the information about the flight routes for each one of the scenarios defined in Section 4.1.

All the selected flight routes for each scenario that are simulated are comprised by two sections, since the magnetic angle is different from one section to another, as discussed in Section 3.3, and the position of the DVOR is common to both of them, thereby in the input file is included the initial and final points of each section.

In the Lisbon scenario two flight routes were selected, and the corresponding input file for each one is shown in Table F.1. The number of test points to use in all simulations, and all the scenarios, is 200.

Table F.1 - Input files for Lisbon scenario.

Name	Initial		Final	
	Latitude [°]	Longitude [°]	Latitude [°]	Longitude [°]
RN870 a	38.64262	-9.98194	38.88778	-9.16278
RN870 b	38.88778	-9.16278	39.17372	-8.39395
Y207 a	39.66556	-8.49278	38.88778	-9.16278
Y207 b	38.88778	-9.16278	38.67889	-9.31722

For the Fátima scenario, Table F.2 presents the coordinates of the initial and final points of each section for the three flight routes, and that constitute the input file.

Table F.2 - Input files for Fátima scenario.

Name	Initial		Final	
	Latitude [°]	Longitude [°]	Latitude [°]	Longitude [°]
A5 a	40.03111	-8.53611	39.66556	-8.49278
A5 b	39.66556	-8.49278	38.42418	-9.18583
UP600 a	39.16750	-8.39250	39.66556	-8.49278
UP600 b	39.66556	-8.49278	40.03111	-8.53611
UN872 a	40.42972	-8.05639	39.66556	-8.49278
UN872 b	39.66556	-8.49278	38.42418	-9.18583

In the Nisa scenario two flight routes were selected that pass through the DVOR beacon, and the relevant geographical coordinates of each section are presented in Table F.3.

Table F.3 - Input files for Nisa scenario.

Name	Initial		Final	
	Latitude [°]	Longitude [°]	Latitude [°]	Longitude [°]
G52 a	39.16750	-8.39250	39.56472	-7.91454
G52 b	39.56472	-7.91454	40.32980	-7.09889
R72 a	38.94556	-7.91417	39.56472	-7.91472
R72 b	39.56472	-7.91472	40.72333	-7.88583

The final coordinates of the second section of each route (G52 b and R72 b) were defined through the Google maps, since the airspace chart of the Centre region does not include the final point of the referred sections.

The input file with the initial and final test coordinates of the selected flight route for the Sagres

scenario is presented in Table F.4. Anew, the initial coordinates of the first section of the route were defined with the aid of the Google maps.

Table F.4 - Input files for Sagres scenario.

Name	Initial		Final	
	Latitude [°]	Longitude [°]	Latitude [°]	Longitude [°]
R095 a	37.08511	-8.98898	37.08452	-8.94631
R095 b	37.08452	-8.94631	37.07641	-8.38466

In the Porto Santo island, the coordinates of the test points to include in the input file of the simulator are shown in Table F.5.

Table F.5 - Input files for Porto Santo scenario.

Name	Initial		Final	
	Latitude [°]	Longitude [°]	Latitude [°]	Longitude [°]
UQ11 a	32.33111	-18.13028	33.09028	-16.35056
UQ11 b	33.09028	-16.35056	33.41861	-15.65833
R1 a	32.16194	-17.08528	33.09028	-16.35056
R1 b	33.09028	-16.35056	33.66750	-15.94972
B18 a	32.44917	-16.22722	33.09028	-16.35056
B18 b	33.09028	-16.35056	33.55694	-15.78139

Finally, Table F.6 presents the coordinates of the test points of the input file, to use in the simulator, for the Flores, Horta and Santa Maria islands.

Table F.6 - Input files for Flores, Horta and Santa Maria scenario.

Site	Name	Initial		Final	
		Latitude [°]	Longitude [°]	Latitude [°]	Longitude [°]
Flores	H141 a	40.54861	-33.38917	39.45361	-31.21056
	H141 b	39.45361	-31.21056	38.51944	-28.62361
	H142 a	39.90583	-33.73389	39.45361	-31.21056
	H142 b	39.45361	-31.21056	38.51944	-28.62361
Horta	H131 a	38.36833	-33.36361	38.51944	-28.62361
	H131 b	38.51944	-28.62361	37.84611	-25.75806
	H132 a	39.45361	-31.21056	38.51944	-28.62361
	H132 b	38.51944	-28.62361	37.84611	-25.75806
Santa Maria	H101 a	38.31972	-28.15806	36.96278	-25.16639
	H101 b	36.96278	-25.16639	37.23250	-23.36444
	H105 a	36.29250	-27.64778	36.96278	-25.16639
	H105 b	36.96278	-25.16639	37.94833	-23.23472
	H100 a	37.47833	-25.51000	36.96278	-25.16639
	H100 b	36.96278	-25.16639	36.40250	-24.02444

References

- [Alex04] Alexander,J., “Loxodromes: A Rhumb Way to Go”, *Mathematics Magazine*, Vol. 77, No. 5, Dec. 2004, pp. 349-356.
- [ArHG09] Armstrong,J., Hill,J. and Gudsell,D., *Long Gully Wind Farm – Compatibility with Radio Services*, Appendix G – Radiocommunication Assessment, Windflow Technology Limited, Christchurch, New Zealand, Feb. 2009.
- [Akka09] Akkasli,C., *Methods for Path Loss Prediction*, Internal Report, Vaxjo University, Vaxjo, Sweden, 2009 (<http://lnu.diva-portal.org/smash/get/diva2:273839/FULLTEXT01.pdf>).
- [Bore10] Borely,M., *Guidelines on How to Assess the Potential Impact of Wind Turbines on Surveillance Sensors*, EUROCONTROL Guidelines, EUROCONTROL-GUID-130, European Organisation for the Safety of Air Navigation, Brussels, Belgium, June 2010.
- [Cast11] Castro,R., *An introduction to Renewable Energies: Wind, Photovoltaic, and Minihydroelectric* (in Portuguese), IST Press, Lisbon, Portugal, 2011.
- [Corr13a] Correia,L.M., *Propagation Models*, Lecture Notes of Mobile Communication Systems, Instituto Superior Técnico, Lisbon, Portugal, 2013.
- [Corr13b] Correia,L.M., *Cellular Design*, Lecture Notes of Mobile Communication Systems, Instituto Superior Técnico, Lisbon, Portugal, 2013.
- [DaFo09] Dam,V. and Foley, *3D Geometrical Transformations*, Lecture Notes, Brandeis University, Waltham, USA, June 2013 (http://www.cs.brandeis.edu/~cs155/Lecture_07.pdf).
- [Davi83] Davies,D.E.N, “Circular arrays”, in Rudge,A.W., Milne,K., Olver,A.D., Knight,P. (ed.), *The Handbook of Antenna Design – Volume 2*, Peter Peregrinus Ltd., London, UK, 1983.
- [Elec13] Electronic (in Portuguese), <http://www.electronica-pt.com/index.php/content/view/79/46/>, June 2013.
- [Elet13] Esposti,V.D., *Propagation and systems planning* (in Italian), Worksheet, Bologna University, Cesena, Italy, Sep. 2013 (<http://www.elettra2000.it/vdegliespsti/Esercizi%20Propagazione%20e%20Pianificazione%20LM/ExA2.pdf>).
- [Eoli13] Eólicas de Portugal (in Portuguese), http://www.eneop.pt/subcanais_n1.asp?id_subcanal_n1=189&id_canal=110, Sep. 2013.
- [FAAu86] Federal Aviation Authority, *VOR, VOR/DME and VORTAC Siting Criteria*, Internal Report, Order 6820.10, Federal Aviation Authority, SW Washington, D.C., USA, Apr. 1986.

- [Figa12a] Figanier,J., “Free Space Propagation”, in Fernandes,C.A. (ed.), *Aspects of Propagation in the Atmosphere* (in Portuguese), AEIST, Lisbon, Portugal, 2012.
- [Figa12b] Figanier,J., “Ground Reflection”, in Fernandes,C.A. (ed.), *Aspects of Propagation in the Atmosphere* (in Portuguese), AEIST, Lisbon, Portugal, 2012.
- [GrBM09] Greving,G., Biermann,W. and Mundt,R., “On the Relevance of the Measured or Calculated RCS for Objects on the Ground – Case Wind Turbines”, in *Proc. of EuCAP 2009 - 3rd European Conference on Antennas and Propagation*, Berlin, Germany, Mar. 2009.
- [GrBM11] Greving,G., Biermann,W. and Mundt,R., “The Radar Cross Section and Wind Turbines – Definition and Effects of the Ground and Finite Distances”, in *Proc. of IRS 2011 – International Radar Symposium*, Leipzig, Germany, Sep. 2011.
- [GWGT13] Goodman,C.M., Wilson,J., Gillanders,R., Tywoniuk,W. and Kim,W.W.Y., *The wind energy industry; A global perspective*, Internal Report, Independent Contracting, Southern Alberta, Canada, Sep. 2013 (<http://www.projectgoodman.com/2009/04/14/the-wind-energy-industry-a-global-perspective/>).
- [Hard13] Hard Cash (in Portuguese), <http://www.dinheirovivo.pt/Empresas/Artigo/CIECO243845.html>, Sep. 2013.
- [Hill04] Hill,Mc., “Air Navigation”, McGraw-Hill Professional Publishing, *McGraw-Hill Concise Encyclopedia of Science and Technology*, McGraw-Hill, New York, USA, 2004 (<http://www.answers.com/topic/doppler-vor>).
- [Hist13] History of Wind Energy (in Portuguese), <http://pedesenvolvimento.com/2009/07/15/historia-da-energia-eolica-e-suas-utilizacoes/>, Sep. 2013.
- [Hult08] Hultin,M., *DVOR 6512, Instruction Manual*, Northrop Grumman, Oslo, Norway, Nov. 2008.
- [ICAO09] International Civil Aviation Organization, *ICAO EUR Doc 015: European Guidance Material on Managing Building Restricted Areas*, Internal Report, ICAO, Montreal, Canada, Sep. 2009.
- [IWAG12] Industrial Wind Action Group, <http://www.windaction.org/pictures/25251>, Dec. 2012.
- [Kell62] Keller,J.B., “Geometrical Theory of Diffraction”, *Journal of the Optical Society of America*, Vol. 52, No. 2, Feb. 1962, pp. 116-130.
- [Koks08] Koks,D., *Using Rotations to Build Aerospace Coordinate Systems*, Electronic Warfare and Radar Division Systems Sciences Laboratory, DSTO-TN-0640, Australian Government – Department of Defense, Edinburgh, Australia, Aug. 2008.
- [Math13] Mathematics for Mechanics, <http://emweb.unl.edu/Math/mathweb/mathtoc.html>, Mar. 2013.

- [MePi13] Meteorology and Pigeon Racing (in Portuguese), <http://www.fpcolumbofilia.pt/meteo/main0613.htm>, July 2013.
- [MiCh10] Mishra,K.V. and Chandrasekar,V., “Signal Analysis and Modeling of Wind Turbine Clutter in Weather Radars”, in *Proc. of IGARSS 2010 - IEEE International, Geoscience and Remote Sensing Symposium*, Honolulu, USA, July 2010.
- [MoFS08] Morlaas,C., Fares,M. and Souny,B., “Wind Turbines Effects on VOR System Performance”, *IEEE Transactions on Aerospace and Electronic Systems*, Vol. 44, No. 4, Oct. 2008, pp. 1464-1476.
- [NAV12a] NAV Portugal, *VOR*, Internal Report, NAV Portugal, E.P.E, Portugal, Lisbon, Portugal, Nov. 2012.
- [NAV12b] NAV Portugal, *DVOR General Information - DVOR/VOR Principle*, Internal Report, NAV Portugal, E.P.E, Lisbon, Portugal, Nov. 2012.
- [NAV12c] NAV Portugal, Private communications, 2012.
- [NAV12d] NAV Portugal, *Manual VFR*, Public Report, Portuguese Aeronautical Information Service – NAV Portugal, Lisbon, Portugal, 2012 (www.NAV.pt/ais/).
- [NAVA12] NAV AIS, “Air Navigation Obstacles”, *VFR Manual*, Lisbon, Portugal, 2012 (<http://www.nav.pt/ais/VFRs/App2%20Obstacles.pdf>).
- [OAGR13] OAG Report, <http://www.greenaironline.com/news.php?viewStory=62>, Sep. 2013.
- [Odun06] Odunaiya,S.A., “Wind Farms and Their Effects on Radio Navigation Aids”, 14th *SIIV IFIS*, Toulouse, France, June 2006.
- [Pint11] Pinto,J.V.P.T, *Assessment and Design of Multilateration Telecommunication Systems installed in NAV Portugal*, EPE, M.Sc. Thesis, IST/TUL, Lisbon, Portugal, 2011.
- [Prin13] Principles of Navigation, http://www.pilotfriend.com/training/flight_training/nav/navigation.htm, Sep. 2013.
- [RaBr07a] Rashid,L.S. and Brown,A.K., “RCS and Radar Propagation Near Offshore Wind Farms”, in *Proc. of 2007 IEEE - Antennas and Propagation Society International Symposium*, Honolulu, USA, June 2007.
- [RaBr07b] Rashid,L.S. and Brown,A.K., “Impact Modelling of Wind Farms on Marine Navigation Radar”, in *Proc. of IET 2007 - International Conference on Radar Systems*, Edinburgh, UK, Oct. 2007.
- [Rais12] Rais,M., *Impact of Riviera Wind Farm on Tactical Air Navigation (TACAN) Beacon at Naval Air Station Kingsville*, Contract No. N68836-10-P-3103, CNIC, ATDI TACAN Study-NAS Kingsville, Washington, DC., USA, Dec. 2012.
- [Rene12] Renewables, http://www.greenrhinoenergy.com/renewable/wind/wind_technology.php, Nov. 2012.

- [Sale02a] Salema,C., “Propagation Elements”, in Calado,J.C.G. (ed.), *Radio Links* (in Portuguese), IST Press, Lisbon, Portugal, 2002.
- [Sale02b] Salema,C., “Spheric Earth”, in Calado,J.C.G. (ed.), *Radio Links* (in Portuguese), IST Press, Lisbon, Portugal, 2002.
- [Sale02c] Salema,C., “Analogical Hertzian Beams”, in Calado,J.C.G. (ed.), *Radio Links* (in Portuguese), IST Press, Lisbon, Portugal, 2002.
- [Sant12] VOR and DME, http://web.ist.utl.pt/carlos.santos/public/VOR_DME.pdf, Nov. 2012.
- [ScGo13] Script google,
<file:///C:/Users/Joana/Desktop/Dropbox/Simulator/Link%20data%20from%20Google%20maps.html>, 2013.
- [Seng84] Sengupta,D.L., “Electromagnetic Interference Effects of Wind Turbines”, *The Working Committee on EMI International Energy Association*, Copenhagen, Denmark, Aug. 1984.
- [Sphe13] Spherical Coordinates, <http://mathworld.wolfram.com/SphericalCoordinates.html>, July 2013.
- [ToWy07] Tooley,M. and Wyatt,D., “VHF omnidirectional range”, in Butterworth-Heinemann Ltd, *Aircraft Communications and Navigation Systems: Principles, Operation and Maintenance*, Helsevier, Burlington, USA, 2007.
- [VFGA11] Vega,D., Fernández,C., Grande,O., Angulo,I., Guerra,D., Wu,Y., Angueira,P. and Ordiales,J.L., “Software Tool for the Analysis of Potential Impact of Wind Farms on Radiocommunication Services”, in *Proc. of BMSB 201 - IEEE International Symposium on Broadband Multimedia Systems and Broadcasting*, Nuremberg, Germany, June 2011.
- [WFiP12] *Wind Farms in Portugal*, Internal Report, INEGI and APREN, Lisbon, Portugal, Dec. 2012 (http://e2p.inegi.up.pt/relatorios/Portugal_Parques_Eolicos_201212.pdf).
- [WiCo12] Wikimedia Commons, http://commons.wikimedia.org/wiki/File:D-VOR_PEK.JPG, Nov. 2012.
- [WiEn12] The Recycle Times, <http://therecycletimes.com/category/wind-energy/>, Nov. 2012.
- [WiTu13] Wind Turbines,
http://www.chemistryviews.org/details/ezone/1444481/How_Wind_Turbines_Work.html,
 Sep. 2013.
- [Wolf13] Wolfram MathWorld, <http://mathworld.wolfram.com/LawofCosines.html>, Mar. 2013.